UNIVERSITE ECOLOGIE BRETAGNE GEOSCIENCES LOIRE AGRONOMIE ALIMENTATION

UNIVERSITÉ DE NANTES

THESE DE DOCTORAT DE

L'UNIVERSITE DE NANTES
COMUE UNIVERSITE BRETAGNE LOIRE

ECOLE DOCTORALE N° 600
Ecole doctorale Ecologie, Géosciences, Agronomie et Alimentation
Spécialité : Sciences de l'aliment

Par
Hoang Thanh NGUYEN

Etude de la relation entre la digestion de triglycérides et la bioaccessibilité de micronutriments lipophiles en temps réel par microfluidique à gouttes

Thèse présentée et soutenue à Nantes, le 26-11-2018

Unité de recherche : Biopolymères Interactions Assemblages

Rapporteurs avant soutenance :

Mme Stéphanie DESCROIX	Directeur de recherche, CNRS, Institut Curie
Mme Maud CANSELL	Professeur des universités, ENSCBP

Composition du Jury :

Président :	Mme Marie-Caroline JULLIEN	Directeur de recherche, CNRS, ESPCI
Examinateurs :	Mr Jack LEGRAND	Professeur d'université, Université de Nantes
Dir. de thèse :	Mr Marc ANTON	Directeur de recherche, INRA
Co-dir. de thèse :	Mr Sébastien MARZE	Chargé de recherche, INRA

Invité(s)

Mme Mélanie MARQUIS	Ingénieur d'études, INRA

Table of contents

LIST OF ABBREVIATIONS

BC	beta-carotene
BS	bile salt
CMC	critical micellar concentration
DG	diglyceride
DHA	docosahexaenoic acid
DLS	dynamic light scattering
FA	fatty acid
FFJ	flow focusing junction
GIT	gastrointestinal tract
HOSO	high oleic sunflower seed oil
LC	long-chain
LMN	lipophilic micronutrients
LRAT	lecithin: retinol acyltransferase
LSCM	laser scanning confocal microscopy
MC	medium-chain
MG	monoglyceride
PDMS	polydimethylsiloxane
PL	phospholipid
PMMA	polymethylmethacrylate
PTFE	polytetrafluoroethylene
REH	retinyl ester hydrolase
RP	retinyl palmitate
SAXS	small angle X-ray scattering
SC	short-chain
SLS	static light scattering
TC	tricaprylin
TG	triglyceride
W/O	water to oil

1 INTRODUCTION

In daily diet, besides macronutrients (lipids, proteins, carbohydrates), human body also needs micronutrients (vitamins, carotenoids) which are essential in maintaining its normal functions. In particular, the good absorption of these lipophilic micronutrients is an important key to prevent chronic diseases, especially cardiovascular. However, this assimilation is less efficient than that of macronutrients. Moreover, it greatly varies due to many factors involving food matrix structure and composition (Patrick Borel, 2003). For example, the absorption efficiency varies for different species of micronutrients and depends on the oils that contain micronutrient. Due to being insoluble in the aqueous medium of intestinal tract, lipophilic micronutrients are co-digested with lipids and co-transported with lipid digestion products in mixed micelle structures to absorbing sites in the intestine. It is suggested that the digestion of the oil affects the micellar solubilization of micronutrients (bioaccessibility), hence overall absorption efficiency (bioavailability). However, the dynamic coupling between the hydrolysis of triglyceride and the solubilization of lipophilic micronutrients in the gastrointestinal tract remains little known in the literature.

The goal of this PhD study is to gain insights into the interplay between the hydrolysis of triglycerides and the solubilization of lipophilic micronutrients in the gastrointestinal tract. More specifically, in this work, the gastrointestinal digestion of different lipids (tricaprylin, high oleic sunflower seed oil, fish oil) with an added lipophilic micronutrient (beta-carotene or retinyl palmitate) was studied. The digestion of lipids and the solubilization of lipophilic micronutrients were monitored simultaneously in a droplet microfluidic device, and quantitatively analyzed in real time using confocal fluorescence microscopy. Oil droplets containing a lipophilic micronutrient were generated, trapped, and digested using an integrated lab on a chip microfluidic device. This technique enabled the modulation of various structure and composition parameters, namely the oil droplet size, the number of droplets per trap, the types of micronutrient and of triglyceride, the composition of the digestive fluids, the nature of the digestion phases (intestinal and/or gastric)...

In the first stage, a polydimethylsiloxane (PDMS) microfluidic device was designed, built, tested and optimized in order to develop a reliable method for in vitro lipid digestion. As PDMS is natively hydrophobic, enabling only the generation of water-in-oil droplets, various hydrophilic treatments were tested to enable the generation of oil-in-water droplets. The optimization of the microchannel design for droplet generation was achieved with the aid of numerical simulations using a commercial software suite. Monodisperse oil droplets with well-controlled size were generated at a low flow rate ratio of water phase to oil phase. The result of the first stage is presented in the manuscript of the first article.

The main hypothesis of this PhD work is that the kinetics of triglyceride digestion affects the kinetics of lipophilic micronutrient solubilization. Thus, in the second stage, a systematic study with various structure and composition parameters was conducted. Oil droplets made of various edible oils with an added lipophilic micronutrient (beta-carotene or retinyl palmitate) were subjected to intestinal and/or gastric digestion. The data obtained were interpreted in comparison to numerical simulations already developed in the laboratory, and to in vitro digestion of emulsions. All the results of this stage are presented in the manuscript of the second article.

Micellar solubilization is commonly believed to be the key factor affecting the intestinal absorption for both lipids and lipophilic micronutrients. Thus, better understanding about the formation of the mixed micelle structure is required. Thus, small angle X-ray scattering (SAXS) at synchrotron Soleil was performed to characterize the dynamics of creation and transformation of the mixed micelles.

Summarized aims of the study:

- Develop a microfluidic device with an optimization of the design and of the hydrophilic surface treatment to generate and immobilize oil droplets for the digestion.
- Develop an experimental set-up to monitor the digestion and solubilization in real time.
- Study the relation between the micellar solubilization of lipophilic micronutrients (bioaccessibility) and of the triglyceride digestion.
- Study the effect of the gastric phase on the intestinal phase.
- Study the effect of the gastric phase on the degradation of beta-carotene.
- Characterize the dynamics of creation and transformation of the mixed micelles.

The first part of this thesis is dedicated to a literature review which covers all the aspects of the PhD works. These aspects include lipids, lipophilic micronutrients, lipid digestion in the gastrointestinal tract, in vitro digestion models, microfluidic tools, confocal fluorescence analysis, and SAXS. Next, the experimental aspects, results and discussions are presented in the manuscripts of several articles that were submitted to Food Chemistry. Finally, additional preliminary results and discussions, conclusions and perspectives are presented.

2 REVIEW OF LITERATURE

2.1 Lipid and liphophilic micronutrients

2.1.1 Triglycerides

Triglycerides (or triacylglycerols) are biomolecules belonging to the lipid family (triglycerides, phospholipids, steroids, glycolipdis). They account for 90% of dietary lipid we ingest, which could be up to 100 g per day. Triglycerides play crucial role in energy storage. All kinds of triglyceride share the same chemical structure which is made from the esterification of three fatty acid chains on a glycerol head (fig. 1). In the stereochemistry of triglyceride structure, the fatty acids are designated sn1-, sn2-, sn3-. The possible number of different triglycerides can be very large, being n^3 where n is the number of fatty acids (FA) present.

FAs are long hydrocarbon chain with a methyl group (-CH3) at one end (also called the ω/*n* end) and a carboxyl group (COOH) at the other end. The chain length of FAs varies from 3 carbons to 24 carbons (C3 to C24). The FAs can be classified into three groups based on the carbon chain length: short-chain (SC) FA containing 3-6 carbon (3-6C), medium-chain (MC) FA with 7-12C, and long-chain (LC) FA with > 12C. The FAs can also be grouped depending on the number of double bond in the carbon chain. They are called saturated if there is no double bond in the carbon chain. They are classified monounsaturated if there is only one double bond in the carbon chain, and polyunsaturated if more double bonds (≥ 2) are present. The unsaturated FAs contain up to six double bonds (Mu & Høy, 2004). The unsaturated FAs are further differentiated using the n-3, n-6, n-7, n-9 notation referring to the position (counted from the ω end) of the first double bond. The properties of the triglyceride molecule depend on the particular types of fatty acid it carries (for example, chain length of fatty acid, saturated or unsaturated fatty acids, etc..) (Hunter, 2001; McKimmie, Easter, & Weinberg, 2013). Fig. 2 illustrates the notations used to name fatty acids. One of the common shorthand notations is based on the number of carbon in the carbon chain, the number of the double bonds in the chain, and the position of the first double bond (counted from the ω/*n* end). For example, oleic acid (C 18:1 n-9) which is a monounsaturated long-chain FA, contains 18 carbons in the carbon chain, and one double bond between carbons 9 and 10 (fig. 2). For instance, oleic acid (c18:1 n-9) is the major fatty acid in the triglycerides of the high oleic sunflower seed oil (HOSO) that was used in this study (up to 80%). Fig. 2 also shows the chemical structure of docosahexaenoic acid (DHA, c22:6 n-3) which is a polyunsaturated long-chain FA. It contains 22 carbons in the chain, 6 double bonds with the first one between carbons 3 and 4. DHA is the main fatty acid in the triglycerides of the fish oil that was used in this study (up to 60%).

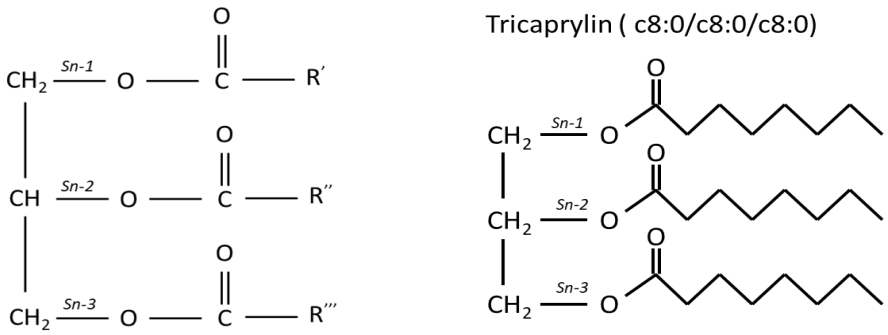

Fig. 1 Chemical structure of triglycerides, with tricaprylin (a saturated medium-chain triglyceride) as an example.

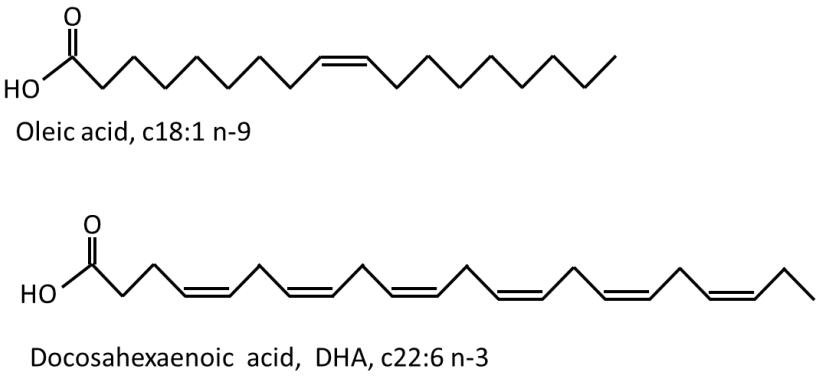

Fig. 2 Examples of the fatty acid notation.

2.1.2 Lipophilic micronutrients

Besides macronutrients, human body also needs many bio active molecules called micronutrients. They only represent a small part of the daily nutrient intake however, they have numerous biochemical functions such as hormone-like activity in bone metabolism (Vitamin D) (Borel, Caillaud, & Cano, 2015; Holick, 2004), antioxidant activity (Vitamin E, C) (Borel, Preveraud, & Desmarchelier, 2013; Doba, Burton, & Ingold, 1985), enzyme cofactor activity (B complex vitamins) (Hoorn, Plikweert, & Westerink, 1975). Thus, sufficient absorption of these micronutrients is a crucial factor in maintaining normal body functions and preventing chronic diseases. The micronutrients may be water soluble (vitamins C, B) or lipid soluble (vitamins A, E, K, D, some carotenoids). The absorption of these lipophilic micronutrients is much less efficient compared to that of macronutrients and greatly varies due to physicochemical and biological factors. These factors affecting the absorption efficiency of micronutrients were listed in a literature review (Borel, 2003). These factors

(named *SLAMENGHI* where each letter stands for one factor) include *S*pecies of micronutrients, molecular *L*inkage, *A*mount of micronutrients in the diet, food *M*atrix that contains micronutrients, *E*ffectors of absorption and bioconversion, *N*utrient status of the host, *G*enetic factors, *H*ost-related factors, and mathematical *I*nteractions. In this study, the factors that are investigated are the *S*pecies of micronutrients and the food *M*atrix composition.

2.1.2.1 Vitamin A

The term vitamin A refers to a group of unsaturated compounds with the biological activity of all-trans retinol (R-OH), that are retinaldehyde (retinal) (R-CHO), retinyl esters (R-OO), retinoic acids (R-OOH). Vitamin A plays important roles for development, proper immune function, and vision health (Gudas, 1994; Haskell, 2012; Ross & Hammerling, 1994; Saari, 1999; WALD, 1968). However, as most micronutrients, it can not be synthesized by the human body, and must be provided by the diet in sufficient amounts to meet physiological requirements. Vitamin A present in the diet is derived from plant sources (provitamin A carotenoids: beta-carotene, alpha-carotene, beta-cryptoxanthin) or from animal sources (pre-formed vitamin A: mostly as retinyl palmitate). The chemical structures of some retinoids and some provitamin A are shown in fig. 3.

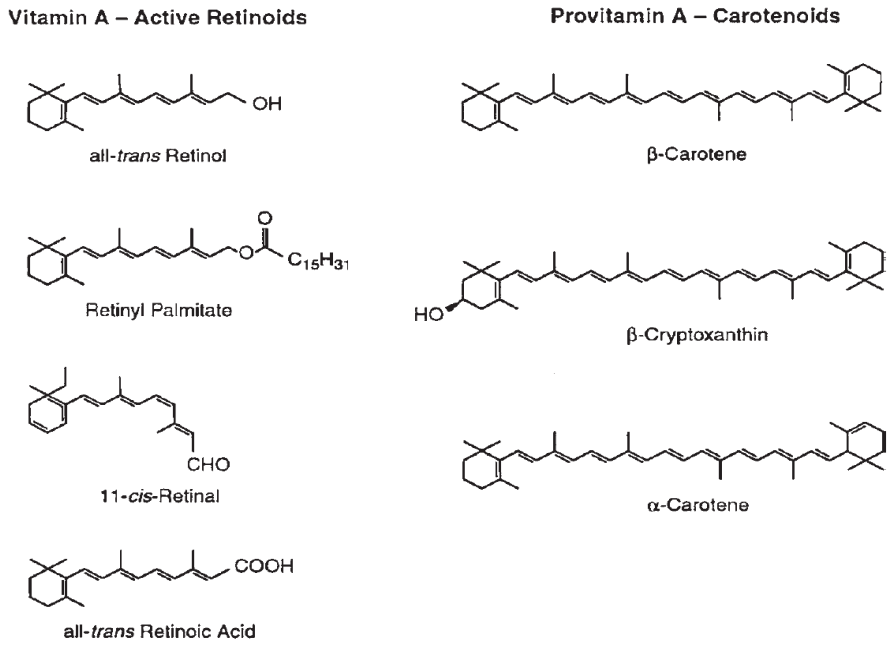

Fig. 3 Chemical structures of vitamin A-active retinoids and some of the most common provitamin A carotenoids (Palmer, Darnton-Hill, & West, 2017).

2.1.2.2 Beta-carotene

Beta-carotene (BC) is one of the most important carotenoids for human health due to its high vitamin A activity (Grune, 2010; Weber & Grune, 2012) and antioxidant activity (Deeming-Adams & Adams, 2002; El-agamey, Cantrell, Land, Mcgarvey, & Truscott, 2004; Sies, Helmut; Stahl, 1995). The absorption of BC was shown to prevent cardiovascular diseases (Omenn et al., 1996) and obesity (Grune, 2010).

Beta-carotene is different from other carotenoids regarding its structure and functions. It consists of 2 beta-ionone rings with unique symmetrical structure, and can in principle be converted into two molecules of vitamin A (Grune, 2010). In reality, the conversion of beta-carotene to vitamin A is done by two pathways (shown in fig. 4). The major conversion pathway, central cleavage, is catalyzed by the enzyme BCO1, cleaving at the central double bond (15,15') to release retinal, a direct precursor of retinol and retinoic acid (Harrison, 2012). Overall, BC metabolism provides a retinol activity equivalent of 1/12 for each BC molecule. Among isomers of beta-carotene, the all-trans (E-isomer) form is predominant in biological systems.

In addition, BC contains 9 fully conjugated double bonds in its structure, resulting into an absorption peak in the visible spectrum (maximum at 450nm) (Britton, 1995). Thus, the compound is normally found in orange to red color. Moreover, BC emits fluorescence when excited by the light with a wavelength of 450 nm, enabling its monitoring by fluorescence microscopy.

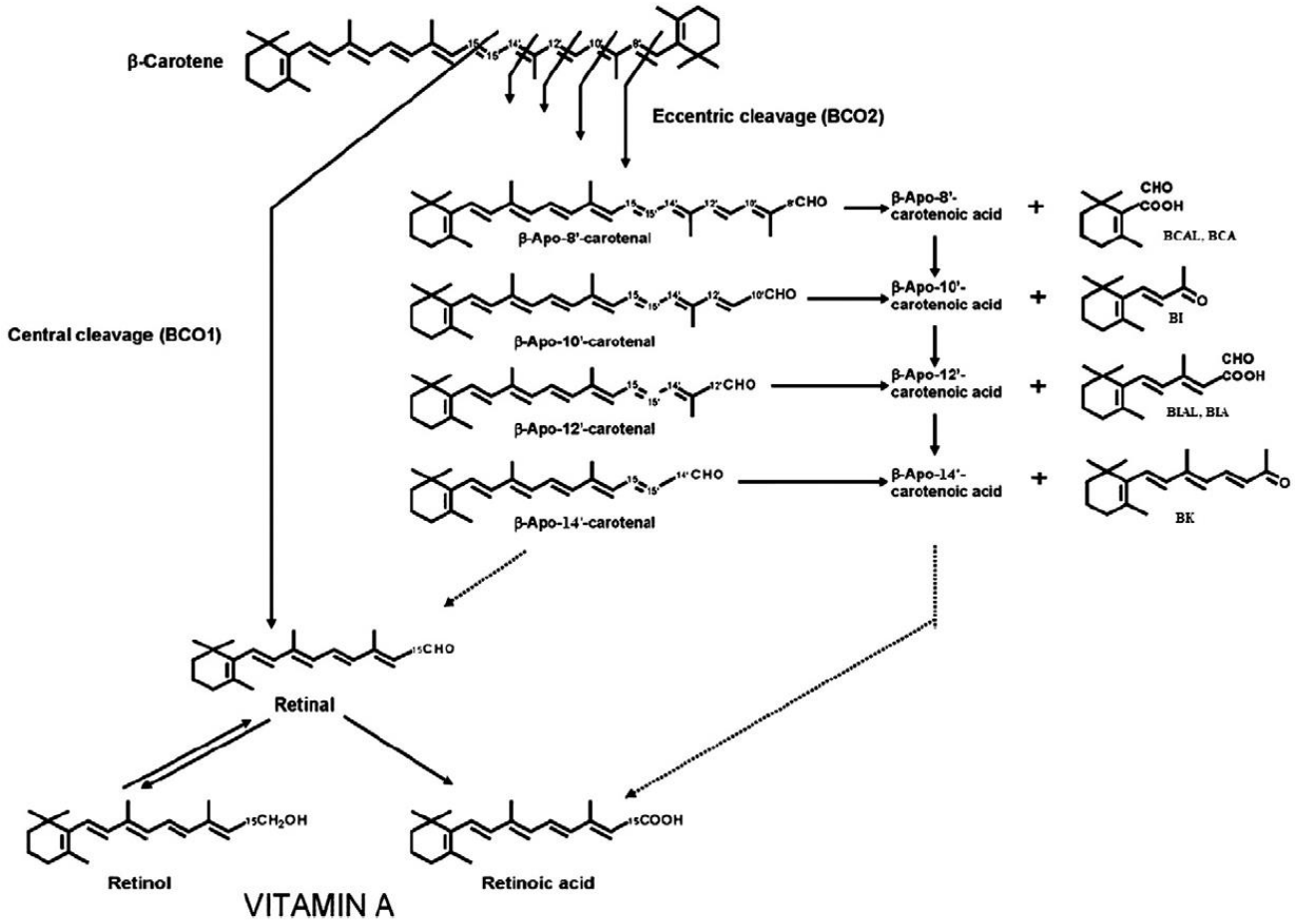

Fig. 4 Two pathways of conversion of beta-carotene to vitamin A (retinol and retinoic acid): central and eccentric. The central cleavage is the major pathway (Harrison, 2012).

2.1.2.3 Retinyl palmitate

Retinyl palmitate (preformed vitamin A) is one of the most abundant retinyl esters present in the body of humans and animals. It is formed by the esterification of retinol (fig. 3) and palmitic acid ($CH_3(CH_2)_{14}COOH$). This retinyl ester serves both as the source of vitamin A in the diet and the retinol storage in the human body (Vogel, Gamble, & Blaner, 1999). The long-term storage of vitamin A in the form of retinyl ester may prevent vitamin A insufficiency. Due to the conjugated double bonds in its structure (fig. 5), retinyl palmitate molecules can emit fluorescence, thus can be monitored by fluorescence microscopy. The maximum excitation and emission wavelengths of retinyl palmitate were found to be of 325 nm and 470 nm, respectively (Antille et al., 2003).

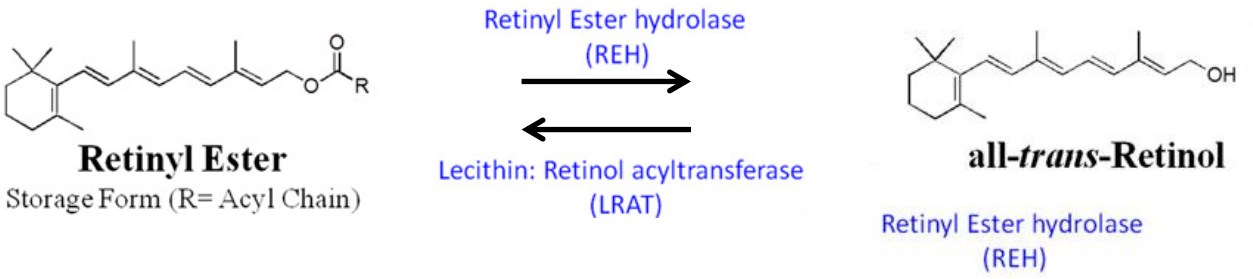

Fig. 5 Metabolic conversion of retinyl ester. Unesterified retinol is liberated by hydrolysis of retinyl ester by the action of a retinyl ester hydrolase (REH). Retinyl rester is synthesized by transferring a fatty acyl moiety from the sn-1 position of membrane phosphatidylcholine to retinol by the action of the acyltransferase LRAT (O'Byrne & Blaner, 2013).

2.2 Digestion of triglycerides and absorption of fats and lipophilic micronutrients

2.2.1 Digestive tract

Human body is an extremely sophisticated system. Its activity is powered by energy provided from food in daily diet. The first step of this conversion is an important process called digestion. Digestion can be simply described as a "breakdown" of the foods containing macronutrients (lipids, proteins, carbohydrates) and micronutrients (vitamins, minerals). The digestion of lipids occurs in 3 main stages, starting in the oral phase followed by the gastric phase and ending in the intestinal phase (fig. 6). In this description, we mainly focus on the two latter regions called the gastrointestinal tract.

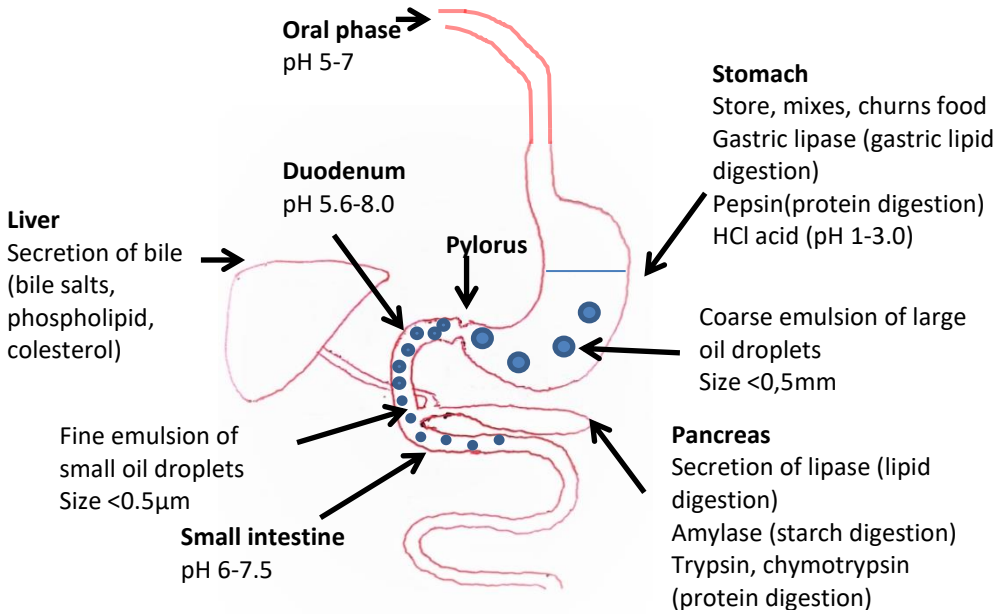

Fig. 6 Schematic diagram of the different regions of the human gastrointestinal tract.

2.2.2 Digestion of lipids in vivo and bioaccessibility of lipophilic micronutrients

In general, lipid digestion is very efficient with approximately 95-98% of the dietary lipids being absorbed in the small intestine (Armand, 2007; Carey, Small, & Bliss, 1983).

First, food is broken down into small pieces by grinding and crushing under the mechanical forces of the chewing action in the oral phase. The saliva (pH ~7) is secreted to form the food bolus. The structure, physical state and interfacial properties of the lipid phase may be altered right from the oral stage. The food bolus is then transferred into the stomach where partial digestion of lipids occurs. Lipids are initially emulsified resulting in the formation of oil droplets in the stomach. Triglycerides (TG) are then partially hydrolyzed by the gastric lipase which is released from the gastric mucosa. This hydrolysis reaction (gastric lipolysis) yields one free fatty acid (FA) and one diglyceride (DG) (Hamosh, 1990). The FA at the sn-3 position is preferentially cleaved by the gastric lipase, with a double activity compared to the sn-1 position (Mu & Høy, 2004). In the stomach, only a small proportion (10-30%) of FAs are released by gastric lipolysis (M Armand et al., 1996; Martine Armand et al., 1994, 1999). The DG and especially the FA molecules being amphiphilic, they cover the lipid droplet surface thus aiding further emulsification and stabilizing droplets (< 0.5 mm) against coalescence.

In contrast to the limited digestion of lipid in the stomach, TGs are mostly hydrolyzed in the small intestine (70-90% FAs released) (Favé, Coste, & Armand, 2004) under the enzymatic activity of pancreatic lipase and co-lipase, with the aid of bile salts and phospholipids. The coarse emulsion (of partially digested lipids) formed in the stomach enters the upper part of the small intestine (the duodenum) via the pyloric valve. Here, it mixes with bile and phospholipids (secreted into the duodenum) and is further emulsified, forming stable oil droplets with the average size less than 0.5 µm (Frazer, 1946; SENIOR, 1964). Bile salts (BS) and phospholipids (PL), both having amphiphilic properties, adsorb to the surface of the oil droplets what stabilizes the emulsion and increases the surface area available for lipase adsorption and activity. Lipase binds to the surface of the oil droplets with the aid of the co-lipase. The co-lipase plays a role of mediator to prevent the expulsion of the lipase from the oil droplet surface caused by the bile salts (Lowe, 1997). In addition, it was shown that BS promotes lipase adsorption (Gómez et al., 2011). So both co-lipase and bile salts are needed to optimize lipase activity. Adsorbed pancreatic lipase and co-lipase catalyze the lipolysis reaction on remaining TG and DG, yielding only FA and MG in the molar proportion of 2:1 (fig. 7). These final products of lipid digestion (FAs, MGs) then incorporate into bile salt/phospholipid mixed micelle which transports them towards the intestinal cells where each species will be absorbed individually. It is shown in literature that, the type of TG affects their digestion kinetics (Li, Hu, & McClements, 2011; Majeed et al., 2016). The widely accepted explanation for this dependence regards to: specific activity of lipase depends on

the type of TG (lower activity of lipase to TG of longer FA) and the solubilization capacity of digestion products in micellar phase (lower micellar solubilization for longer fatty acids). Table 1 presents different lipolysis rate (LR) of various TG (data from the literature and presented by Marze (Marze, 2014)). It is obvious that the LR is inversely dependent on the carbon-chain length of TG (except for the case of oleic glycerides). A similar trend is observed for the micellar solubilization of FA and MG.

Molecules	*n*	LR	SR (FA)	SR (MG)
Caprylic glycerides	8	2.06 ± 0.97		3.5
Capric glycerides	10	1.56 ± 0.62		0.88
Lauric glycerides	12	1.06 ± 0.34	0.78	0.58
Myristic glycerides	14	0.596 ± 0.336		0.16
Palmitic glycerides	16	0.362 ± 0.245	0.086	0.053
Stearic glycerides	18	0.283 ± 0.283	0.042	
Oleic glycerides	18*	1	0.62	0.52
Linoleic glycerides	18*		0.48	
Eicosapentaenoic glycerides	20*	0.162 ± 0.027		
Docosahexaenoic glycerides	22*	0.158 ± 0.071		
Retinol (vitA)				0.0043
α-Tocopherol (vitE)				0.12 ± 0.06

Table 1 Lipolysis rate (LR) of different TG (normalized to triolein), and the mass solubilization ratio (SR) of FA or MG in bile salts (Marze, 2014). The TG type dependence of lipolysis rate and mass micellar solubilization of lipolysis products is the first hypothesis of this thesis.

To be absorbable, lipophilic micronutrients have to be bioaccessible, that is released from food and incorporated into mixed micelles. This consists in four steps: 1) release from the food matrix by a breakdown process, 2) dissolution into lipid droplets, 3) co-digestion with TG and other lipids, 4) co-incorporation into mixed micelles (fig. 8). In the literature, the term bioavailability is defined as the fraction of ingested components (including lipids and lipophilic micronutrients) that reaches the systemic circulation (Holst & Williamson, 2008; Versantvoort, Van de Kamp, & Rompelberg, 2004). The bioaccessibility is the fraction of ingested components released into gastrointestinal juices (in particular in the intestinal mixed micelles for lipids and most lipophilic components). The bioaccessibility of lipophilic micronutrients is improved with the addition of TG, affected by the type of TG (Marze, 2015). In literature, most of the studies reports an increase of MN bioaccessibility with the carbon chain length of TG *in vitro* (Ahmed, Li, McClements, & Xiao, 2012; Huo, Ferruzzi, Schwartz,

& Failla, 2007; Nidhi & Baskaran, 2011; Qian, Decker, Xiao, & McClements, 2012; Salvia-Trujillo, Qian, Martín-Belloso, & McClements, 2013; Von Bonsdorff-Nikander et al., 2005; Yang & McClements, 2013) and *in vivo* (Behrens et al., 1996; Holmberg et al., 1990; Porter, Kaukonen, Boyd, Edwards, & Charman, 2004; Sylven & Borgstrom, 1969). On a contrary, a decrease trend of MN bioaccessibility with the chain length of TG was also reported (Dahan & Hoffman, 2006, 2007; Kaukonen, Boyd, Charman, & Porter, 2004; Yu, Shi, Liu, & Huang, 2012). The simulation work proposed by Marze interpreted this contradiction by taking the bile concentration into account (Marze, 2014). The increase trend of MN bioaccessibility with the chain length of TG was observed with the bile recycled. In the case of saturated bile, the decrease of MN bioaccessibility with the chain length of TG was observed.

	efficiency of micellarization (%)			
	lutein (+zeaxanthin)	α-carotene	β-carotene	lycopene
no oil	45.6 ± 0.6^{c}	2.0 ± 0.3^{a}	2.8 ± 0.2^{a}	1.1 ± 0.1^{a}
c4:0	33.6 ± 1.0^{a}	4.9 ± 0.2^{b}	5.3 ± 0.1^{b}	1.4 ± 0.1^{a}
c8:0	$42.0 \pm 1.5^{b,c}$	8.6 ± 0.7^{c}	10.5 ± 0.9^{c}	2.9 ± 0.2^{b}
c18:1	34.8 ± 1.5^{a}	14.9 ± 1.1^{d}	17.7 ± 1.3^{d}	5.2 ± 0.5^{c}
c18:2	34.9 ± 0.4^{a}	15.3 ± 0.7^{d}	18.5 ± 0.3^{d}	5.6 ± 0.6^{c}
c18:3	$38.2 \pm 1.5^{a,b}$	16.6 ± 1.2^{d}	18.3 ± 0.7^{d}	5.0 ± 0.1^{c}

Table 2 Micellar solubilization of carotenoids during in vitro digestion of salad (Huo et al., 2007).

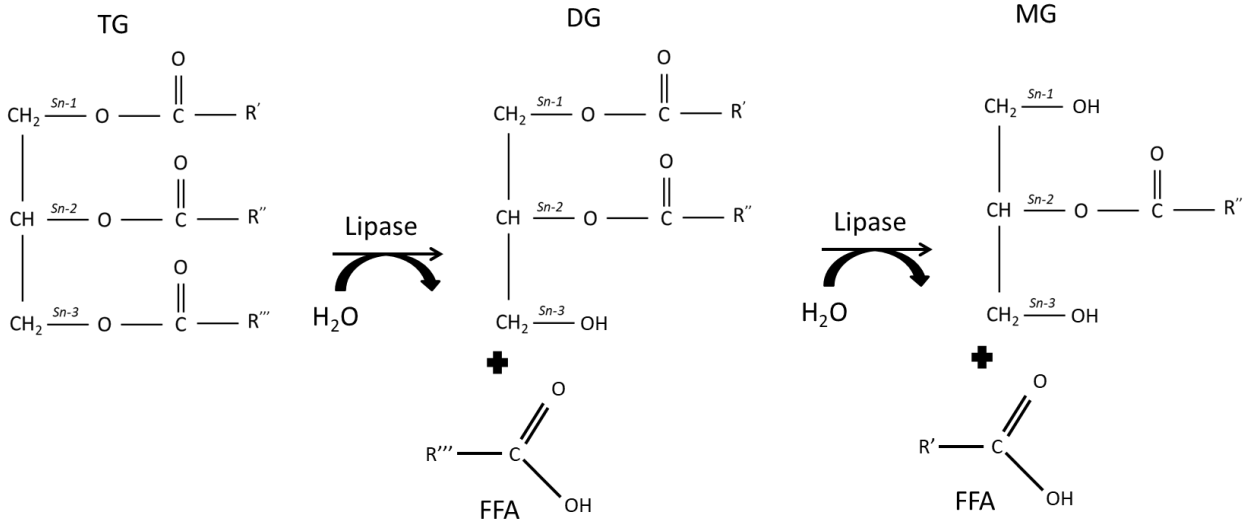

Fig. 7 Lipolysis reaction with catalytic activity of lipases.

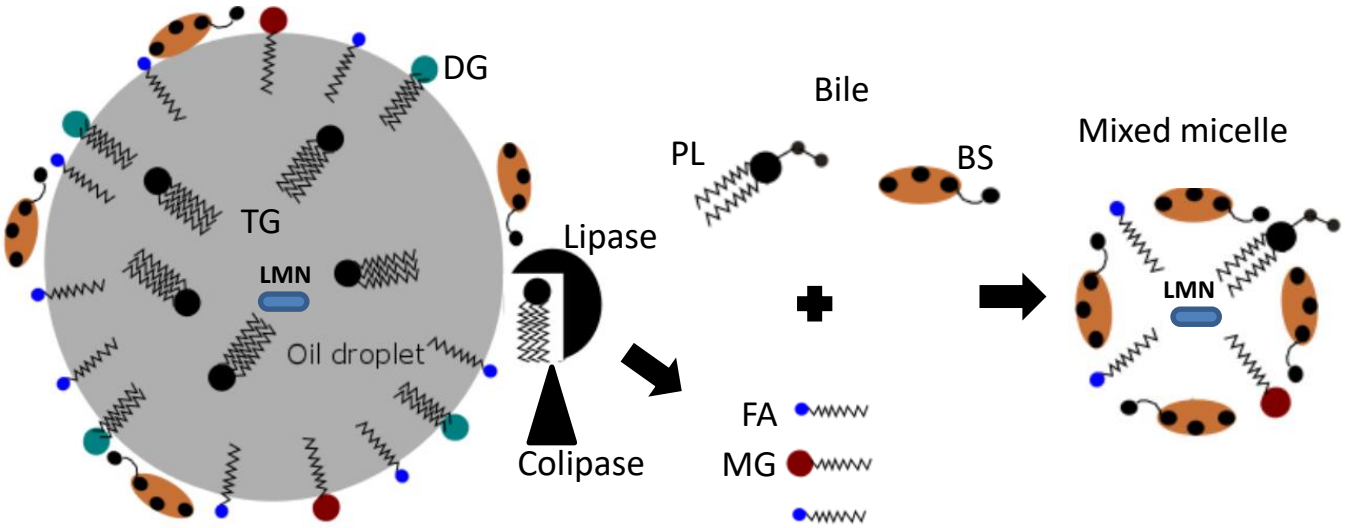

Fig. 8 Summary of intestinal digestion processes of lipids (triglyceride TG) droplet containing lipophilic micronutrients (LMN). Pancreatic lipase and colipase hydrolyze TG at the oil-water interface, releasing a fatty acid (FA) and a diglyceride (DG) which is then hydrolyzed into a monoglyceride (MG) and a FA. The final digestion products (two FAs and one MG) incorporate in the mixed micelle formed by bile salt (BS) and phospholipid (PL). The lipophilic micronutrients are also released from the oil droplet and co-incorporate into the mixed micelle. Adapted from Caballero *et al.*(Caballero, Trugo, & Finglas, 2003).

2.2.3 Bile salts (BS)

BS play various roles in lipid digestion as surfactant, detergent, cofactor and transport vehicle for lipids (Maldonado-Valderrama, Wilde, MacIerzanka, & MacKie, 2011). The presence of bile salt help increasing the surface area available for lipase adsorption, stabilizing intestinal emulsion, and forming mixed micelles to remove the products of lipid digestion from the droplet surface. Thus, BS enhance the hydrolysis of TGs, as the activity of both gastric lipase and pancreatic lipase depends greatly on the available droplet surface area (Armand et al., 1999). TGs with short-chain and medium-chain FAs can be hydrolyzed and their digestion products can be absorbed in the absence of bile salts due to the sufficiently high aqueous solubility of short-chain and medium-chain FAs. However, the presence of bile salt is crucial for the lipolysis of long-chain TGs which are the predominance of dietary lipids in western life.

BS are biosynthesized from cholesterol in the liver, stored in the gall bladder, and secreted into the intestine (Maldonado-Valderrama et al., 2011). BS are soluble amphiphilic molecules. They exhibit planar polarity as they contain a rigid steroid backbone with a hydrophobic face and a hydrophilic face (fig. 9). The hydrophilic face consists of one, two or three hydroxyl groups and an amino group which is conjugated with different amino acids

(taurine, glycine). BS properties depend on the number and position of the hydroxyl groups, and the conjugated amino acid. Above their critical micellar concentrations (CMC) (table 3), BS molecules self-assemble to from micelles via hydrophobic interactions as well as intermolecular hydrogen bonds between hydroxyl and acidic groups (Maldonado-Valderrama et al., 2011). It is known that pure bile salts have a high CMC in the range 2-20 mM (Verde & Frenkel, 2010). BS micelles structure may vary from oblate to spherical and prolate (Warren, Chalmers, Hutchison, Dang, & Pouton, 2006). These dynamic structures facilitate the transport and release of lipophilic nutrients of various molecular lengths and shapes (Verde & Frenkel, 2010). In addition, several studies showed that primary micelles with disk-like structures are formed at low BS concentration while primary micelles aggregates by hydrogen bonds to form rod-like structures at high BS concentration (Calabresi, Andreozzi, & La Mesa, 2007; Mazer, 1990).

In the intestinal phase, bile salts, phospholipids, and cholesterol form dietary mixed micelles. Lipophilic molecules including products of lipid digestion (FAs, MGs), lipophilic micronutrients (vitamins A, K, E, D, carotenoids, sterols…), as well as fat-soluble drugs, are transported in these mixed micelles through the aqueous environment of the lumen to the absorption sites of the small intestine (El-Gorab & Underwood, 1973; Sun, Jaspers, van Hasselt, Hennink, & van Nostrum, 2016). It is known that the stability of the micellar phase depends on the pH. The micellar structure is stable without micelle dissociation at pH 7 in the lumen, whereas low pH (< 6) favor dissociation of the mixed micelles (Thomson, 1989).

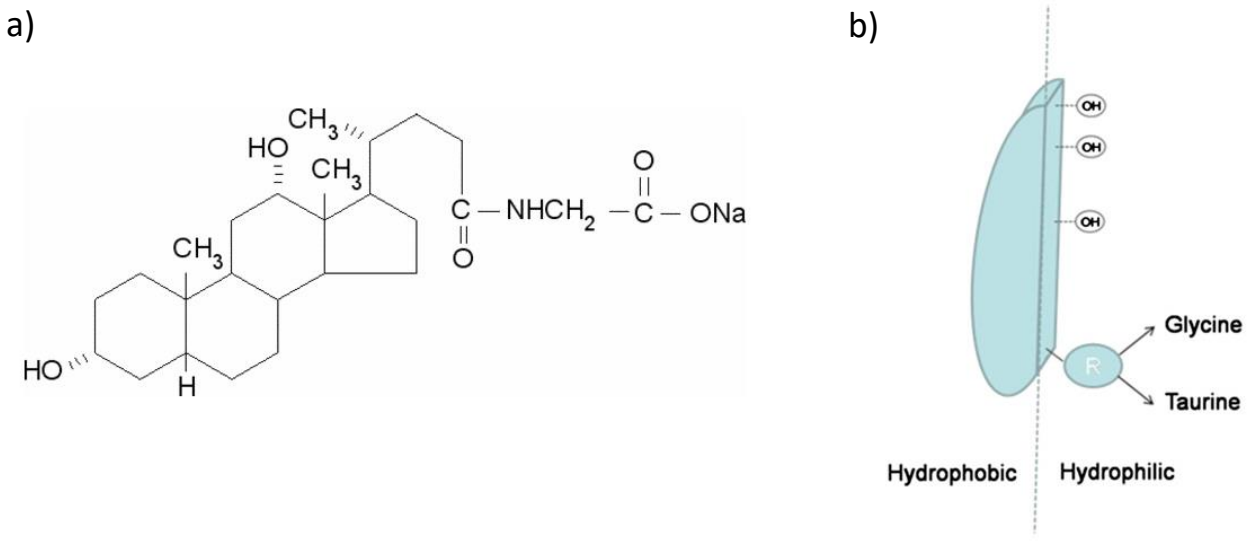

Fig. 9 a) Chemical structure of sodium glycodeoxycholate b) Schematic illustration of the facial amphiphilic structure of bile salts (Maldonado-Valderrama et al., 2011).

Bile salt	CMC (I = 150 mM)
Cholate (NaC)	4–20 mM
Deoxycholate (NaDC)	2–5 mM
Chenodeoxycholate (NaCDC)	6–9 mM
Ursodeoxycholate (NaUDC)	2–19 mM

Table 3 Critical micelle concentration (CMC) of different bile salts (Maldonado-Valderrama et al., 2011).

2.2.4 Lipase-Bile salt interactions

The binding and interaction of bile salt to different lipases and proteins has been observed in the literature. Bile salt can bind to pancreatic lipase and inhibit its activity at concentration above the CMC (Borgström & Erlanson, 1971; Borgström & Erlanson, 1973; Maylie, Charles, Astier, & Desnuelle, 1973). Study of Borgstrom & Donnér showed that taurodeoxycholate does not bind to lipase at concentration below the CMC (Borgström & Donnér, 1976). Other work showed that at concentration below the CMC, conjugated bile salts slightly stimulate the initial hydrolysis rate of tributyrin, but completely inhibit lipase activity above the CMC (Borgström & Erlanson, 1973). Lipase inhibition caused by bile salts can be suppressed by the addition of colipase (Maylie et al., 1973). The binding of bile salts to carboxylester lipases from human pancreatic juice and pig pancreas was characterized by Tsujita et al. (Tsujita, Mizuno, & Brockman, 1987) . The binding of taurocholate to the pig enzyme was mainly due to hydrophobic interactions. Hermoso *et al.* used neutron diffraction to provide the evidence for the activation of lipase by the formation of the lipase-colipase-micelle complex (shown in fig. 10) (Hermoso et al., 1997). In the inactive conformation, the active sites of pancreatic lipase are hidden from the bulk environment by an amphiphilic helix (called as a lid or flap). Thus, the lipase activation involves the conformational changes that expose the active sites of the lipase. Tilbeurgh et al reported interfacial activation of the pancreatic lipase-procolipase complex by the presence of mixed micelles of bile salt (sodium taurodeoxycholate) and phospholipid (glycerophosphorylcholine) (Van Tilbeurgh et al., 1993). Several articles also reported the structural characterization of lipase-bile salt assemblies (Charles, Riva, & Chabre, 1980; Haque & Prakash Prabhu, 2018; Hermoso et al., 1997; Pignol et al., 2000; Rezhdo et al., 2017). In all these studies, an elongated shape for the lipase-colipase-bile salt complex was reported.

Despite the observation and characterization of the lipase-bile salt binding and its effect as presented in the literature, the structural characteristics of assemblies of bile salts and other pancreatic enzymes remain poorly known. Most studies mentioned above only used

pancreatic lipase and colipase. However, pancreatic juice in vivo contains various enzymes other than lipases, with proteases being the most abundant ones (Beaudoin, St-Jean, & Grondin, 1989). Moreover, it was observed that bile salts also bind to proteins (other than lipases) such as apolipoprotein or chymotrypsinogen (Bengt Borgström & Donnér, 1976; Helenius & Simons, 1972). Thus, a part of this thesis is dedicated to the structural characterization of the assemblies of a single bile salt (sodium glycodeoxycholate), or in association with pancreatic enzymes.

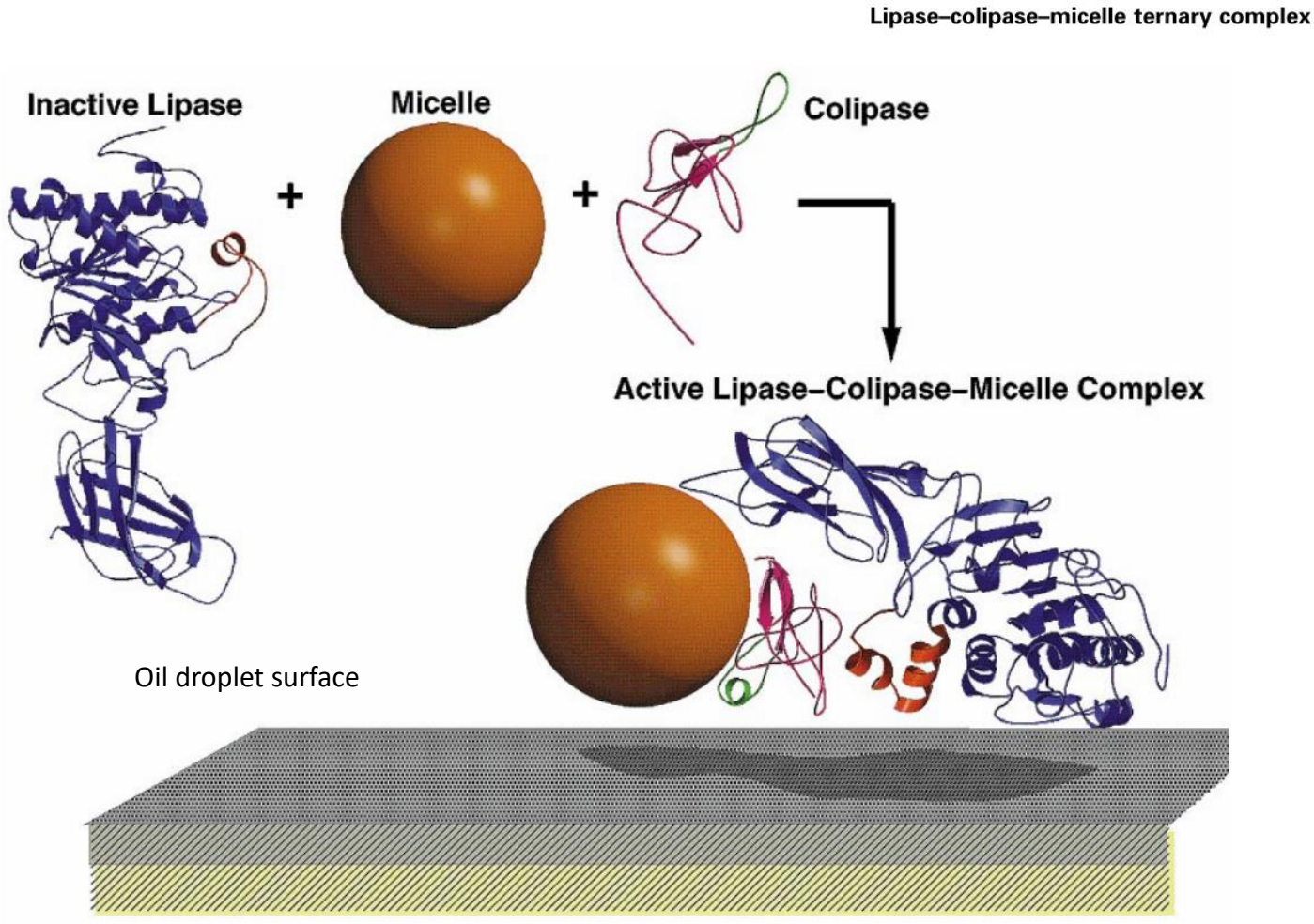

Fig. 10 Schematic summary of pancreatic lipase activation by colipase and bile salts. In the inactive lipase, a large amphiphilic loop (the flap) covers the active site of the lipase. The formation of the ternary complex of lipase-colipase and micelle activates the lipase by making the flap open, thus exposing a large hydrophobic surface, which then facilitate the binding to triglycerides (figure adapted from Hermoso et al., 1997).

2.3 In vitro study of lipid digestion

2.3.1 In vitro models

In vivo studies in humans or animals are normally difficult and costly while *in vitro* studies are much easier and cheaper to carry out. In addition, *in vitro* studies provide more insights into the physicochemical processes occurring during digestion, including structural changes, compositional changes and release mechanisms. They also allow a reduction of the number of experiments carried out in animals or humans, what serves ethical purposes (Li, Kim, Park, & McClements, 2012). Numerous *in vitro* digestion models were used to simulate the gastrointestinal tract (GIT) conditions. Those models usually focus on one particular region of the GIT (mouth, stomach, small intestine, colon) or multiple compartments to mimic the entire digestion (Yoo & Chen, 2006). In a typical *in vitro* experiment, a food sample is prepared and then mixed with a digestive fluid of specific compositions varying in pH, enzymes, buffer, etc... The mixing is carried out at 37 °C to mimic the human body temperature. In practice, it is impossible to simulate all the complex physiological and physicochemical conditions that the lipid droplets encounter in the human GIT. Instead, only the key components (having the most impact on the particular system) are used while other minor components are usually ignored (*e.g*., protease and amylase are not used for systems including only lipids) (McClements & Li, 2010). The conditions in a simplified model could deviate significantly from those lipid droplets undergo in the GIT. However, this approach allows the screening of many samples and reduction of cost and time, while providing mechanistic insights on some of the processes involved. In the conventional in vitro models based on emulsions, the use of fixed amount of digestive components may provoke the issue of stoichiometry, resulting into incomplete digestion of TGs, especially with the long chained TGs (Marze, Meynier, & Anton, 2013).

The key factors considered for the gastric phase are the pH (acid), specific enzymes, and the mechanical/flow profile. The simplest gastric digestion model involves an acid pH and some stirring, while sophisticated models include more components such as salts, organic molecules (glucose, glucuronic acid, urea, glucosamine hydrochloride), phospholipids, biopolymers (polyethylene), proteins (BSA, mucin), gastric lipase (Kalantzi et al., 2006; Lindahl, Ungell, Knutson, & Lennernäs, 1997; Oomen et al., 2003; Versantvoort, Oomen, Van De Kamp, Rompelberg, & Sips, 2005). However, those modes are normally static with pH and enzyme concentrations do not vary over time as *in vivo* conditions. For example, in vivo condition, as the food bolus injected into the stomach, the bulk pH rises from the fasting pH (<2.0) to the pH of the food bolus and eventually revert to the fasting pH (<2.0) at the end of gastric emtying. Thus, some models even include dynamic parameters (gastric emptying, pH profile) to be closer to *in vivo*, in which the changes between fasted phase and fed phase

is taken into account (Wickham, Faulks, Mann, & Mandalari, 2012). The interactions between the lipid droplets and the stomach wall are removed in the in vitro digestion models (McClements & Li, 2010).

The key factors considered for the intestinal phase are the pH (close to neutral), biosurfactants (bile salts, phospholipids), specific enzymes, and salts. The simplest small intestine model contains a mixture of lipase and co-lipase (or pancreatin containing most enzymes from the pancreas), a buffer, and one bile salt at neutral pH (Marze, Algaba, & Marquis, 2014). Sophisticated models can include other enzymes, a mixture of bile salts, various phospholipids, proteins (BSA) (Kalantzi et al., 2006; Lopez-Pena et al., 2016; Oomen et al., 2003). The interactions between the lipid droplets and the intestinal wall are more often considered, using caco-2 cells as an enterocyte model (Versantvoort et al., 2005).

Flow profiles and rheology of digestive fluids in the GI tract can affect the rate and extent of lipid digestion. The role of rheology could be explained by its influence in the flow profile, mechanical forces, as well as mass transport of components in the GI tract. The rheology of digestive juices depends on their composition and the conditions of the environment. Thus, the rheology characteristics and the flow profile of digestive fluids should be taken into account when designing a GI model (Pedersen, Vilmann, Bar-Shalom, Müllertz, & Baldursdottir, 2013).

2.3.2 Emulsion preparation

Conventional in vitro lipid digestion studies are normally based on emulsions (McClements & Li, 2010). An oil phase and an aqueous phase are homogenized together in the presence of a water-soluble emulsifier to form oil-in-water (O/W) emulsions. Various types of homogenizer can be used, including high-shear mixers, high-pressure homogenizers, ultrasonic homogenizers, etc... The emulsion properties (droplet size distribution, droplet concentration) can be controlled by the operation conditions. For example, the droplet size of emulsions prepared by ultrasonic homogenizers is inversely related to the power of the ultrasounds dissipated in the sample (Leong, Wooster, Kentish, & Ashokkumar, 2009).

2.3.3 Quantitative analysis methods

Lipid digestion is quantified by measuring the rate and extent of TG hydrolysis under the activity of the gastric/pancreatic lipase. A common method is based on the measurement of the amount of FFAs (free fatty acids) produced during digestion by titration with an alkali solution (pH-stat method) (Benito-Gallo et al., 2015, Li & Mcclements, 2010). The amount of

FFA released (mol) is calculated from the amount of NaOH (mol) required to neutralize the FAs:

$FA(mol)=V_{NaOH}\times M_{NaOH}$

where V_{NaOH} is the volume of the sodium hydroxide (NaOH) solution required to neutralize the FAs produced during digestion, and M_{NaOH} is the molar concentration of the NaOH solution used for the titration.

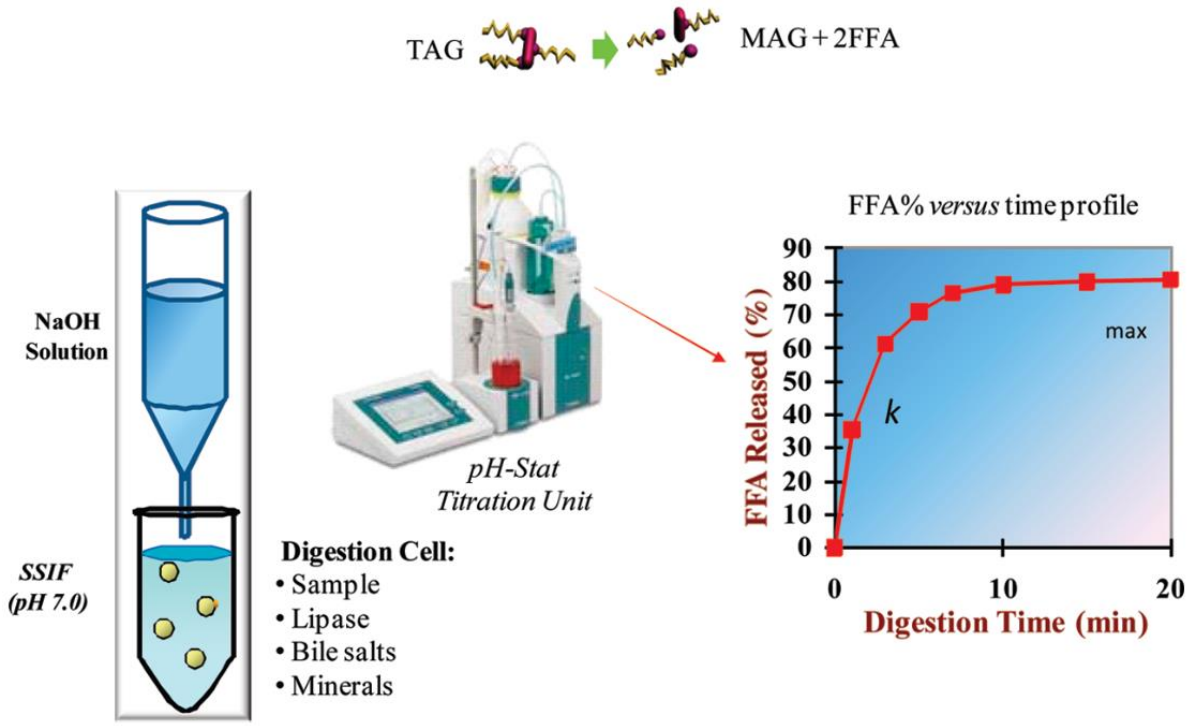

Fig. 11 Schematic representation of the pH-stat in vitro digestion method. The amount of alkali required to maintain the pH at a constant value is measured and then used to calculate the amount of FFAs released (Y. Li & Mcclements, 2010).

The advantage of the method is to provide lipid digestion kinetics in real time. Kinetics of lipid digestion is always of interest as it can provide more insights into the key parameters that involve into the digestion process. Thus, several mathematical models have been presented to analyze the kinetics profiles. Li and McClements proposed a mathematical model to interpret digestion profiles measured by pH-stat method (Li & McClements, 2010). The model was developed basing on assumptions that the release rate of FFA is proportional to the surface area per unit volume of the oil droplets and at any time during the digestion, emulsion always contains identical droplets in size. The expression of the model is presented by the equation:

$$\Phi = \phi_{max}\left(1 - \left(1 + \frac{3k_S M_W t}{2d_{0\rho_0}}\right)^{-2}\right)$$

Here, k_S is a rate constant which is the number of moles of FFA release per unit time per unit surface area (mol s^{-1} m^{-2}), Φ is the ratio of released FFA to the total initial amount of FFA before digestion. ϕ_{max} is the final fraction of the released FFA, ϕ_{max} <1 as not all of the FFA will be released due to the inhibition of the lipolysis reaction at the end of the digestion, M_W is the molecular weight of the TG, ρ_0 is the density of the oil, d_0 is the initial droplet diameter, and *t* is the time.

In this model, the kinetics is independent of the initial lipid concentration in the emulsion. Instead, it depends on the initial droplet size. The smaller the initial oil droplet size is, the smaller time required to reach the same degree of FFA release (with the same rate constant *k*).

The rate constant *k* is proportional to the first order time derivative of the droplet radius (Marze & Choimet, 2012):

$$\frac{dr}{dt} = -k_S \frac{M_W}{\rho_0}$$

This model is also called as zeroth order kinetics (Marze & Choimet, 2012).

A work of McClements and Dungan first proposed another model based on an assumption that the release rate of FFA depends on the surface area per unit volume of the oil droplets, the total volume of the emulsion and the FFA release, thus the so-called first order kinetics,

$$\frac{dw_t}{dt} = \frac{kS}{V}\frac{(m_\infty - m_t)}{m_0}$$

$$\frac{dr}{dt} = -k\emptyset_0\left(\frac{r}{r_0}\right)^3$$

Other methods based on chromatography are used to determine the amount of TG, DG, MG, FA at specific digestion times (Amara et al., 2010; Sek, Porter, & Charman, 2001). These methods allow better insight into the TG hydrolysis (e.g., which chain lengths, degrees of unsaturation, sn-positions of FAs are preferentially cleaved by the lipases). However, this method is not convenient for kinetic studies, as a long and destructive extraction work needs to be carried out before the analysis.

Lipid digestion is a surface-dependent process, thus the surface area (or surface to volume ratio) as well as the nature of the water-lipid interface are crucial factors affecting the rate

and extent of digestion. The surface area in an emulsion is inversely related to the size of the droplets (McClements, 2010). Consequently, the kinetics of lipid digestion depends on the droplet size distribution of the emulsion, which is susceptible to change due to flocculation or coalescence occurring in the GIT. Several methods are used to characterize the droplet size distribution of the emulsion. Dynamic light scattering (DLS) can be used to detect particles in the range 1 nm to 5 µm, while static light scattering (SLS) typically detects particles from 0.1 to 1000 µm (McClements & Li, 2010).

Surface electrical charge is one of the key factors (besides interfacial tension and interfacial rheology) defining the properties of the droplet surface and related to the functional performance and stability of the droplets. The charge of a droplet surface is normally determined by the zeta (ζ)-potiential. The ζ-potiential is the electrical potential at the distance (counted from the droplet surface) where counter-ions remain strongly attached to the droplet. ζ-potiential can provide information about changes in the interfacial composition (e.g., displacement of surface-active molecules) (Mun, Decker, & McClements, 2007) and how the oil droplets interact with each other as well as with other components. The electrical characteristics of oil droplets depend on the emulsifier type. Nonionic surfactants (e.g., Tweens, Spans) normally give a low droplet charge. Anionic surfactants (e.g., fatty acids, lecithin) give a negative charge to the droplet while cationic surfactants give a positive charge to the droplet. Oil droplets stabilized by proteins (whey protein, casein, egg proteins) have a negative charge above the protein isoelectric point (pI) (McClements, 2010).

Emulsion has become a standard system in lipid digestion studies. However, this approach presents several drawbacks. First, even in a simple system such as an emulsion, it is still difficult to control the many physicochemical characteristics that affect lipid digestion. Second, there is an issue of lipid/digestive molecules stoichiometry caused by the use of fixed amounts. Moreover, the real-time kinetics study of lipophilic molecules digestion using the emulsion approach is time-consuming, so rarely found in the literature. Recently, a new approach based on microfluidics has been developed (Marze et al., 2014). This work showed that microfluidics could be used to miniaturize an in vitro digestion system, providing equivalent results and several advantages compared to the emulsion-based method. Then, a similar approach based on lipid droplet digestion with multiple oil droplets trapping to study the coalescence effect was proposed by Scheuble et al. (Scheuble et al., 2017). However, those studies were limited to the lipid digestion, with no lipophilic micronutrient, and no bile salt was used in the work of Scheuble et al.

The advantages of using microfluidics include avoiding the issue of stoichiometry as digestive fluid continuously flows, reducing the volumes of materials used, enabling real-time

kinetic studies of lipophilic micronutrients or drugs during GI digestion. Thus, droplet based microfluidics was seen as a new approach to screen lipid digestion and potentially to screen the bioaccessibility of lipophilic micronutrients.

2.4 Droplet based-microfluidics

Microfluidics is the general term for a multidisciplinary field of science and technology involving generation, manipulation and study of small volumes of fluids in µm-scale channels (few µm to hundreds of µm) (Whitesides, 2006). Among the various domains of microfluidics, droplet microfluidics involves manipulating discrete volumes of immiscible fluids in laminar flow regimes (small Reynolds number) (Mashaghi, Abbaspourrad, Weitz, & van Oijen, 2016). Interest and attention raised for droplet microfluidics in the past decades, mostly regarding droplet generation and manipulation (droplet merging, droplet breakup, droplet trapping). This technology is considered a powerful tool for chemistry, physics, biology, and nanotechnology (Chou, Lee, Yang, Huang, & Lin, 2015). In particular, many applications emerged in chemical and biological analysis, in which each droplet can be used as a micro-reactor (Bai et al., 2010; Windbergs & Weitz, 2011). It comes with many advantages for analysis such as small volumes reducing cost, high surface to volume ratio that allows rapid kinetic studies, monodispersity of droplets to control reaction repeatability, and easy incorporation of external light-based analysis technique.

2.4.1 Polydimethylsiloxane (PDMS)

Microfluidic devices are usually fabricated from solid polydimethylsiloxane (PDMS). The popular use of PDMS over other common microfluidic materials (PMMA, glass) results from several advantages. First, PDMS offers low cost, robustness and straightforward fabrication allowing rapid prototyping for the experiments (Bourbaba, Ben Achaiba, & Mohamed, 2013). Secondly, PDMS is a hyperelastic polymer that can handle large distortions without deteriorating, making it an ideal material to incorporate microfluidic components (valves, pumps) (Unger, Chou, Thorsen, Scherer, & Quake, 2000). Moreover, it is biocompatible, non-porous for lipids, and « air breathing » for living cells. Finally, it offers a slightly broader transmission range than glass and PMMA, being an advantage for the fluorescence analysis (shown in the fig. 12) (Žukauskas et al., 2014).

However, unmodified PDMS surface is natively hydrophobic, hardly wet by aqueous solutions, prone to interactions with other hydrophobic species (e.g., oil droplets) and air bubble formation (McDonald et al., 2000).

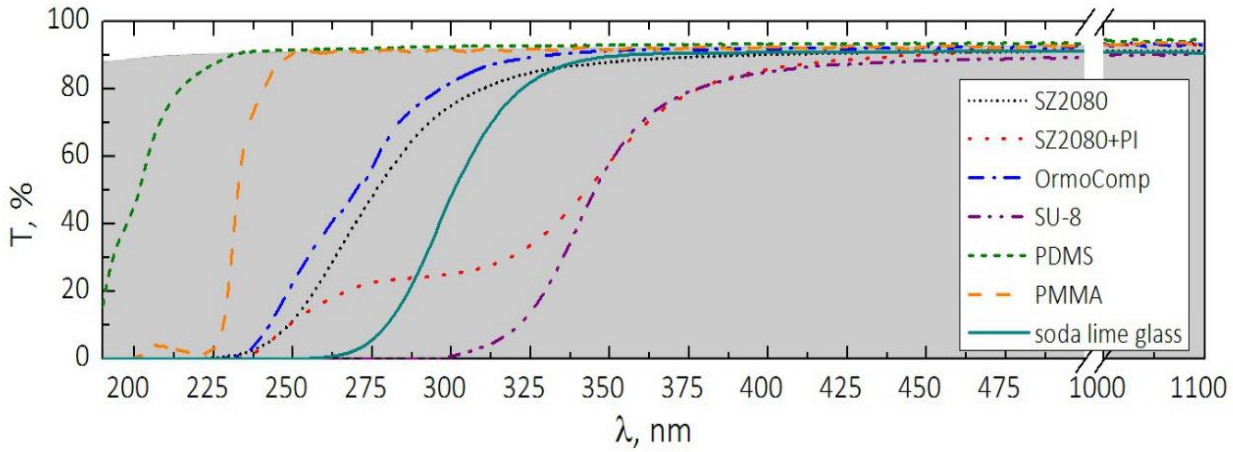

Fig. 12 Transmittance spectrum of PDMS (green dash line) compared to PMMA (orange dash line) and other materials. The thickness of the PDMS and PMMA thin film (used for the measurement) is 12.2 and 1.97 µm, respectively (Žukauskas et al., 2014).

2.4.2 PDMS microfluidic device fabrication

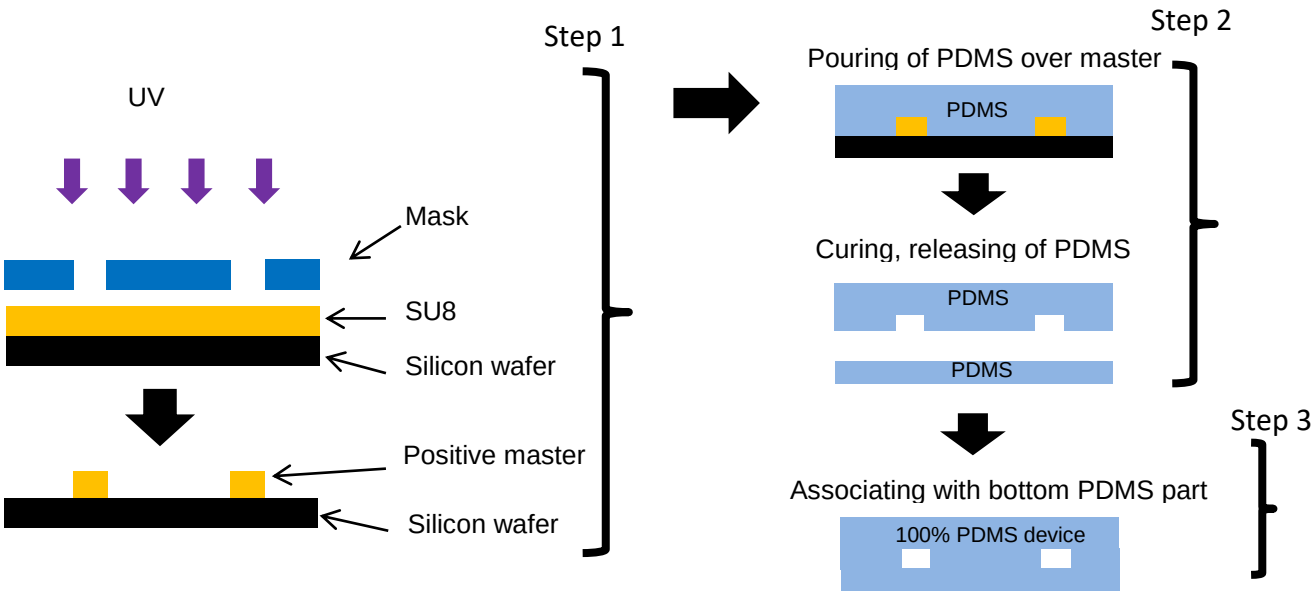

Fig. 13 Fabrication of a PDMS microfluidic device: mold making by photolithography (step 1), fabrication of PDMS parts by soft-lithography (step 2), association of PDMS parts to obtain a single device (step 3).

The fabrication of a microfluidic device consists of three main steps (shown in fig. 13). The first step is to prepare a mold (or master) by using photolithography technique (Pimpin &

Srituravanich, 2012). A thin layer of negative photoresist (SU8) is deposited on a silicon wafer by the spin coating technique. The thickness of the photoresist layer is defined by the height of the microfluidic device micro-channel. After UV exposure (patterned by a UV mask), the unexposed parts are dissolved by a development solution, leaving the pattern (defined by the mask) of the micro-channel.

After the fabrication of the mold, the second step is to fabricate the PDMS parts of the microfluidic device using soft lithography techniques (Xia & Whitesides, 1998). A mixture of liquid siloxane oligomers (base agent) and cross-linkers (curing agent) at a specific ratio (usually 10:1) is poured on the mold. Then the mold containing the mixture is baked at high temperature (70-80 °C) to cross-link the liquid mixture into solid PDMS. The chemistry resulting in the cross-linked polymer is presented in fig. 14. Both the base agent and the curing agent contain siloxane oligomers terminated with vinyl groups (-CH=CH_2). The curing agent includes cross-linking siloxane oligomers and also contains silicon-hydride bonds (Si-H) which is then crossed with the double bond of vinyl groups of the base agent, resulting in Si-CH_2-CH_2-Si linkages. This cross-linking network is three dimensional, forming a solid elastomer. After thermal curing, the solid PDMS can be peeled off the mold, with the pattern of the master mold embedded into the PDMS.

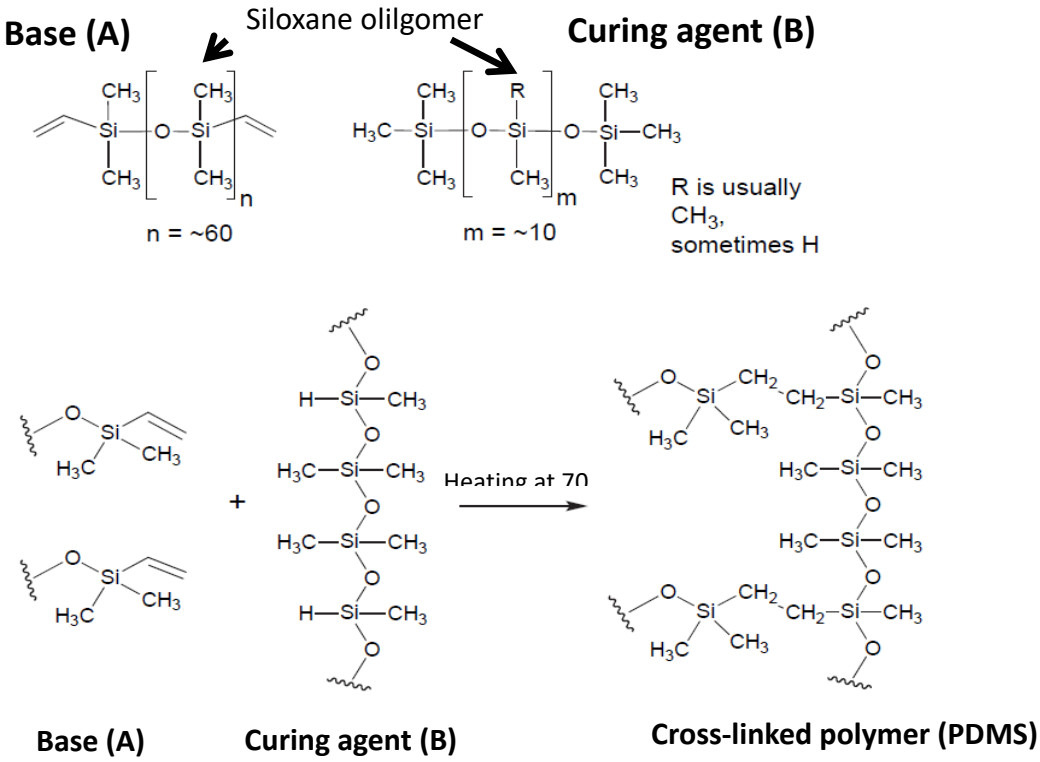

Fig. 14 Chemical scheme PDMS thermal curing process (figure adapted from Lisensky et al., 1999).

The third step consists of the association of two (or more) PDMS layers (or with a glass slide) to obtain a complete device. The association of the PDMS layers can be done by several PDMS-PDMS bonding techniques. Comparison of the bonding strength obtained by different techniques is shown in fig. 15. The first technique is based on hydrophobic bonding of two fully cured PDMS layers. Another bonding strategy uses surface plasma oxidation to activate layers of cross-linked PDMS. The plasma oxidation removes the methyl groups and introduces silanol groups at the surface of the PDMS layers. These silanol groups form covalent siloxane bonds (Si-O-Si) when two plasma-oxidized PDMS layers are brought together. This technique allows a strong association of PDMS-PDMS or PDMS-glass layers and a hydrophilic treatment of the micro-channel simultaneously. However, the surface can quickly recover hydrophobicity, and the oxygen plasma adds cost and time the fabrication. (Marze et al., 2014).

Another bonding technique is based on varying curing ratio (gradient cross-linker) (Marquis, Renard, & Cathala, 2012; Unger et al., 2000). One layer containing base agent in excess is combined with a layer containing the crosslinker in excess. This results in the migration of reactive molecules to the layers interface. Those reactive molecules then form an irreversible bonding after curing.

Adding an intermediate adhesive layer of curing agent, uncured PDMS or UV-curable glue can be used to bond PDMS layers (Samel, Chowdhury, & Stemme, 2007; Satyanarayana, Karnik, & Majumdar, 2005). This technique allows the bonding with other materials (not restricted to PDMS or glass), however it requires a significant care to prevent the adhesive layer from spreading into the channels of the device.

Partial curing of PDMS has also been used to bond the layers. Mixture of base and cross-linking agent (10:1) is partly cured for a short period of time or at low temperature (<60 °C). The partial curing of PDMS allows the remaining cross-linker to migrate to the interface of the layers and form a bonding (Eddings & Gale, 2006; Go & Shoji, 2004).

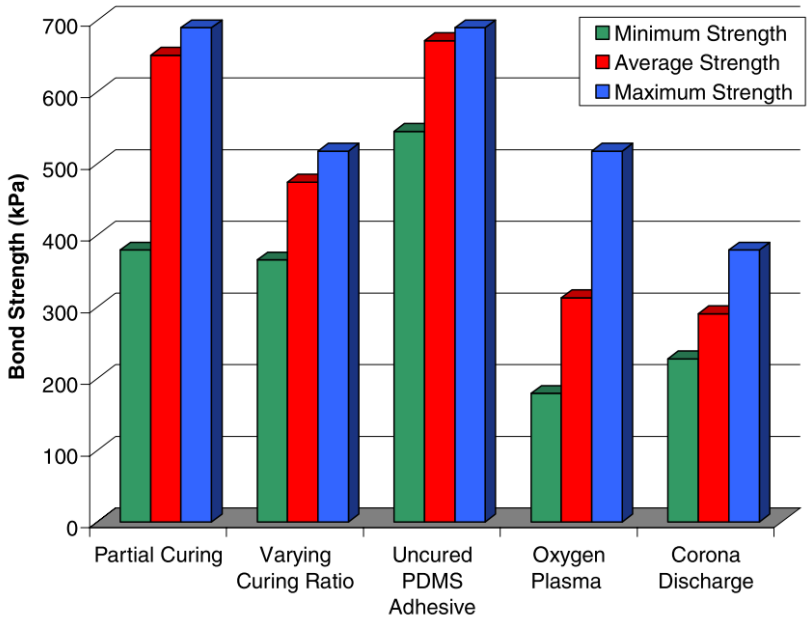

Fig. 15 Bonding strength of different bonding techniques (Eddings, Johnson, & Gale, 2008).

2.4.3 Droplet generation

In droplet microfluidics, there are many ways to produce droplets including flow-based methods, electrowetting-based techniques, and emulsification-based ones (step emulsification, centrifugal microfluidic step emulsification) (Dangla, Fradet, Lopez, & Baroud, 2013; Liu, Sun, Yang, & Xu, 2016; Teh, Lin, Hung, & Lee, 2008). Well-controlled droplets are commonly produced using flow-based methods (mainly flow-focusing device FFD or T-junction) (Garstecki, Fuerstman, Stone, & Whitesides, 2006; Ward, Faivre, Abkarian, & Stone, 2005). The advantages of flow-based methods include high throughput droplet generation, high monodispersity of droplets, control over the droplet size. Interfacial properties, viscosity of the two phases, and channel geometry play important roles in droplet generation (Dangla et al., 2013; Gupta & Kumar, 2010; Jamalabadi, DaqiqShirazi, Kosar, & Shadloo, 2017; H. Liu & Zhang, 2009, 2011; Ngo, Woo Joo, & Byon, 2016; Schuler, Schwemmer, Trotter, & Wadle, 2015; Schulze & Belder, 2012; Song, Zhang, & Gupta, 2009; Trantidou, Elani, Parsons, & Ces, 2017). The scheme of the most popular junctions for droplet generation: flow focusing junction (FFJ) and T-junction is shown in fig. 16. The shear force of continuous phase at the junction splits the disperse phase to form droplets. Oil droplet or water droplet can be generated depending on the choice of the continuous and disperse phase and the hydrophilicity of the channel. Oil and water droplets are generated in the hydrophilic and hydrophobic channel, respectively. The droplet size decreases with the increase of the flow rate ratio and the viscosity ratio of the continuous phase to the disperse phase. The droplet formation is regulated by two main forces: the viscous shear force to deform and disrupt the liquid interface for droplet formation and the surface tension to resis

the deformation. Thus, in the literature, the droplet formation and also its subsequent stability is normally described by an dimensionless capillary number *Ca* which represents the relative strength of the viscous force and the interfacial surface tension.

$$Ca = \frac{\mu_c u_c}{\gamma}$$

With μ_c and u_c are the viscosity and the velocity of the continuous phase, respectively, γ is the oil/water interfacial tension. For most microfluidic device for droplet generation, the capillary number Ca varies between 10^{-3} to 10.

Xu et al proposed a physical model to predict the droplet size, in which the droplet size d_{av} is related to the capillary number *Ca*) (Xu et al., 2006).

$$d_{av} \infty \frac{1}{Ca}$$

Thus, the droplet size decreases with the increase of the continuous phase velocity μ_c and continuous phase viscosity u_c, and with the decrease of the oil/water interfacial tension γ.

The droplet size also depends on the geometry of junction. For the case of the FFJ, the channel size of the disperse phase, continuous phase, throat region and junction angle are of the geometrical factors. For example, the droplet size decreased with the reduced size of the throat region(Li et al., 2008). For the case of T-junction, size of main channel and side channel are of the geometrical factors. Garstecki *et al* reported the crucial role of the main channel size in limiting the minimum size of the droplet formed in *squeezing* regime at small capillary number Ca (Garstecki et al., 2006).

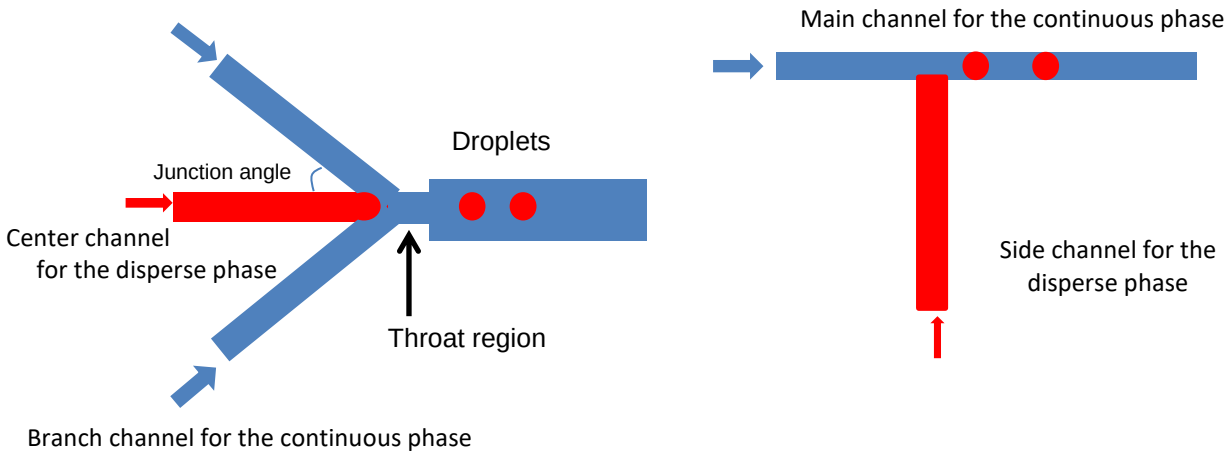

a) flow focusing junction (FFJ) b) T-junction

Fig. 16 Schematic illustration of a) flow focusing junction (FFJ) and b) T-junction.

Oil droplets in a continuous water phase can only be generated in hydrophilic micro-channels. As PDMS surface is natively hydrophobic, a surface chemistry treatment is needed. Various methods can be used to obtain hydrophilic PDMS surfaces, such as plasma treatment, active hydrophilic polymers, or layer coating (Abate, Lee, Do, Holtze, & Weitz, 2008; Marze et al., 2014; M H Schneider et al., 2010; Schulze & Belder, 2012). However, the hydrophilicity of PDMS surfaces obtained by the plasma treatment does not last long (typically 24h), while the layer coating technique causes some changes in the PDMS device geometry (Abate et al., 2008). An effective hydrophilic treatment is achieved by UV-initiated graft polymerization of polyacrylic acid as proposed by Schneider et al. (M H Schneider et al., 2010). In this method, the PDMS channel is first flowed with a solution of acetone containing benzophenone (BP), causing the diffusion of BP molecules into the PDMS matrix. Then, a solution of acrylic acid (AA) monomers is injected into the channel, before an exposure of the device to UV light. The BP molecules generate free radicals which turn the AA monomers into an embedded layer of poly-acrylic acid (PAA). This PAA layer gives the hydrophilicity to the PDMS surface. Fig. 17 shows the schematic of the method. The hydrophilicity can last for months under proper storage conditions.

Another difficulty for oil droplet generation is due to the much higher viscosity of most oils compared to water. This condition is not favorable for droplet formation as a higher energy is needed to break up the oil droplet. High flow rate of aqueous continuous phase is normally required to generate oil droplet (Marze et al., 2014). The geometry of the channel where the oil droplets are formed must be optimized. Some studies increased the water phase viscosity by adding viscous water-miscible fluids to facilitate the oil droplet formation (Xu et al., 2006).

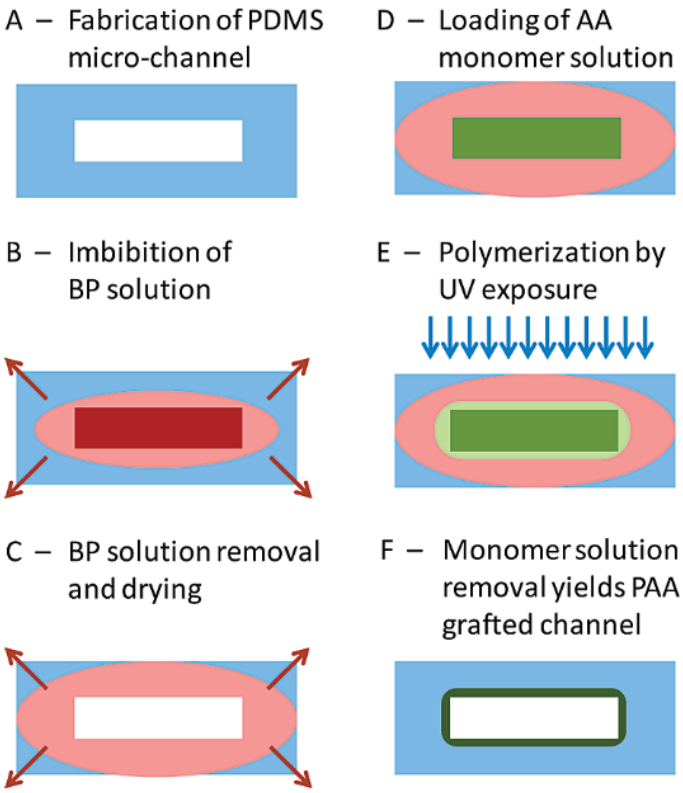

Fig. 17 Schematic of UV-induced graft polymerization treatment. A- Cross-sectional view of a PDMS microfluidic channel (white area enclosed in blue region of PDMS); B- Solution of acetone containing photoinitiator BP is flowed through the channel (dark red), diffusion of BP molecules into PDMS matrix (light red); C- Removal of the BP solution and drying in vacuum for further diffusion of BP molecules in the PDMS matrix; D- Injection of AA monomer solution (green) into the channel ; E- BP molecules generate free radicals under UV light exposure, those free radicals initiate the AA polymerization of the diffused monomers in the PDMS matrix (light green). F- Removal of the monomer solution leaving a covalently bound PAA grafted layer embedded on the inner surface of the channel (dark green) (M H Schneider et al., 2010).

2.4.4 Droplet manipulation and trapping

Droplet manipulation is another main concern of droplet-based microfluidics. Droplet control strategies are needed to lead droplets for particular purposes. For example, droplet processes could be splitting, sorting, guiding, or immobilization for fabrication, analysis or detection. In general, droplets can be manipulated by passive or active techniques. Passive techniques use dedicated microfluidic geometry structures to control droplet without any interference. The principle of the control can be based on drag force of the flow medium, geometric structure, or surface energy wells. For example, dividing junctions (Y or T shaped) or obstacles can be used to split droplets (Link, Anna, Weitz, & Stone, 2004). Huebner *et al*. proposed a chamber with an elegant passive trapping array (A. Huebner et al., 2009). It consists of a pattern of independent traps, each equipped with a central exhaust channel to

enable single droplet trapping. Dangla *et al*. used the local expansion of the channel to create a surface energy wells to immobilize a squeezed droplet against a flow (Dangla, Lee, & Baroud, 2011). When a squeezed droplet passes a channel with a small hole on the top of the channel, the droplet expands in the hole reducing the surface interfacial energy. Thus, the droplet is immobilized in the energy trap. The mechanism of surface energy wells is also applied to drive droplets with gradient confinement caused by a rail system (Dangla, Kayi, & Baroud, 2013). The passive droplet methods are applicable for all types of liquid including oils and suitable for high throughout applications.

In contrary to a passive technique, active manipulation involves external mechanism that can be actively controlled. One of the most common active technique is to control the flow by the incorporation of pneumatic valves (Unger et al., 2000), torque-actuated valves (Weibel et al., 2005) or a system of pushing-withdrawing pumps (A. Huebner et al., 2009).

Other active control strategies are based on external forces that are directly applied on the droplet. The external forces are normally optically driven forces (Park & Chiou, 2011), dielectrophoresis or electrowetting (Hunt, Issadore, & Westervelt, 2007; Pit, Bonestroo, Wijnperlé, Duits, & Mugele, 2016). Those methods allow precise single droplet manipulation, however, they are not suitable for multiple droplets manipulation, and electrostatic force methods using dielectrophoresis or electroweting can not be applied directly to non-polarizable liquids such as oils. Fig. 18 shows the overview of different droplet manipulation techniques.

A part of this thesis focuses on the manipulation the oil droplet size. In which the key factors involved in the droplet generation (channel geometry, viscous ratio) were studied by comparing both experimental results done in the lab and simulation data achieved by commercial software. The details of the device optimization process with the aid of simulation data for the droplet size control are presented in the part 4.1 of this thesis.

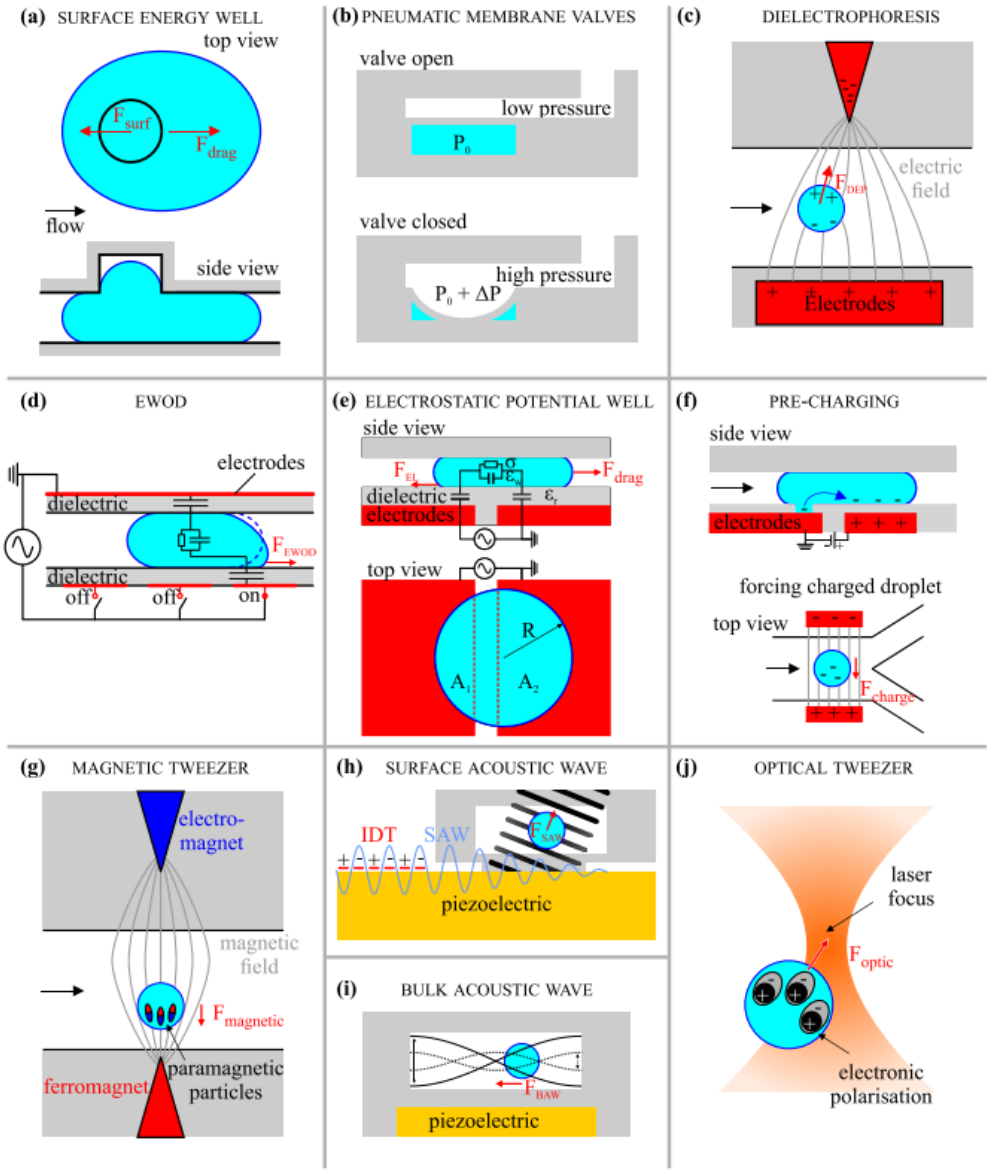

Fig. 18 Overview of different droplet manipulation techniques. (a) Droplet immobilization by interfacial energy gradient caused by local expansion of the channel; (b) Pneumatic valves to control the droplet flow by blocking or opening the channel; (c) Droplet drag by dielectrophoresis forces; (d) Droplet drag by electrowetting; (e) Droplet trapping by electrostatic potential well; (f) Pre-charged droplet by an open electrode; (g) Magnetic tweezer applied for paramagnetic particles; (h) Surface acoustic wave causes upward pressure that move droplets; (i) Droplet trapped at the antinodes of resonating pressure waves caused by a piezoelectric at specific frequencies; (j) Droplet trapping by optical tweezer (Pit, Duits, & Mugele, 2015).

2.4.5 Real-time monitoring of the release of lipophilic molecules by fluorescence

The use of microfluidic system integrated with light-based analysis techniques has been widely used for various purposes in biology, from the simple detection to the quantitative analysis (Desai & Zaman, 2015; A. Huebner et al., 2009; Mongersun, Smeenk, Pratx, Asuri,

& Abbyad, 2016; Proctor, Vine, & Mamo, 2004). In most of these studies, target biomolecules need to be marked or stained to detect fluorescence. In the case of micronutrients that are auto-fluorescent (retinyl palmitate, beta-carotene, vitamin D, vitamin E, vitamin K, etc…), no fluorescence probe is needed. A variety of fluorescence-based set-up can be used from the simplest one containing only a photodetector to the sophisticated confocal microscopy. The choice of the setup depends on various factors including the sample nature, the accuracy requirement, etc…

2.4.6 Confocal microscopy

Besides major applications in imaging, laser scanning confocal microscopy (LSCM) can also be used for quantitative analysis (Fagotto & Maxfield, 1994; Phee, Rodgers, & Coggeshall, 2001; Proctor et al., 2004).

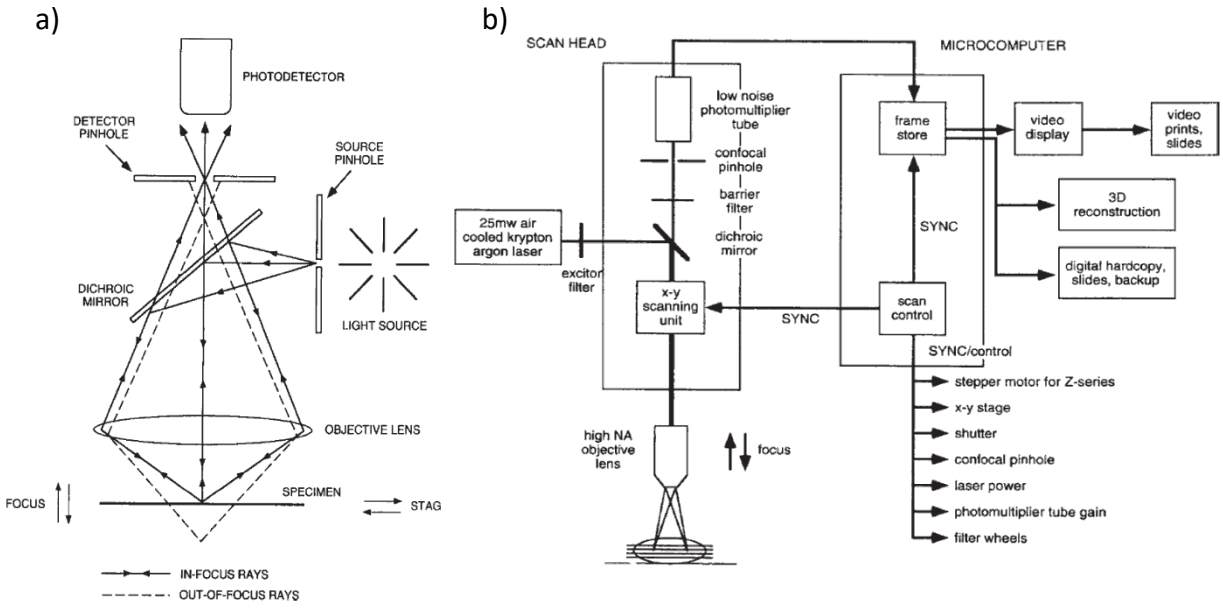

Fig. 19 a) The light path in a typical laser scanning confocal microscope. A pinhole is placed in front of the light source (laser) and another pinhole is placed in front of the photodetector, b) Information flow in the LSCM technique (Paddock, 2000).

In the confocal fluorescence microscopy technique, both excitation and fluorescence detections are confined to a single point in the specimen by the focus of the objective lens. The focus point is scanned across the specimen by a scanning device. The emission light

from the detected point crosses the detector pinhole (confocal pinhole), collected by a photomultiplier tube (PMT). The output signal of the PMT is processed by the computer to build fluorescence light images (Paddock, 2000). The thickness of the optical sections is controlled by varying the diameter of the detector pinhole. A transmitted light detector collects the light passing the specimen and then transfers its signal to one of the PMTs in the scan head. Fluorescence image is normally merged with transmitted light image in order to provide a combined informative image containing both the information of fluorescent species as well as the precise localization of the species in the specimen.

2.4.7 Small-angle X-ray scattering (SAXS)

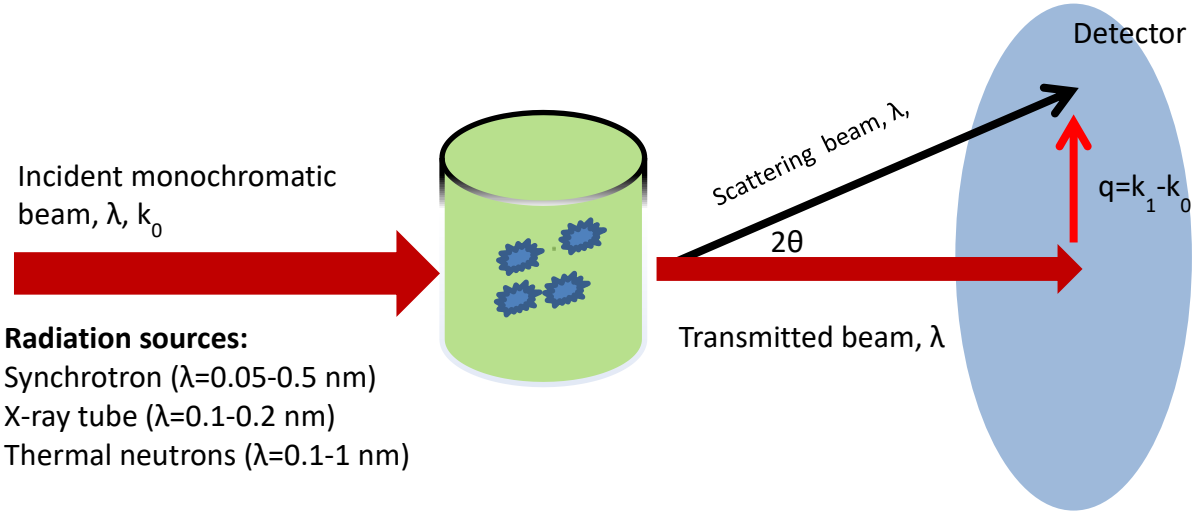

Fig. 20 Schematic illustration of a SAXS experiment with solution sample.

Small angle X-ray scattering is a powerful technique for characterization of nano-scale structures. The X-ray scattering pattern is measured at small angles of typically 0.1-10°. X-ray with a wavelength of (0.07-0.2 nm) is normally used. This technique is used to characterize the size and shape of nanoparticles (1-100nm). In the SAXS measurement, an incident monochromatic X-ray beam with wave vector k_0 is shot through the sample. The intensity of elastically scattered X-ray beam (wave vector k_1) is collected at the scattering angle 2θ (shown in fig. 20).

A scattering pattern shows the evolution of the scattering intensity I(q) as a function of the scattering variable, in which the scattering variable is the momentum transfer or scattering wave vector $q = k_1 - k_0$ (in nm^{-1} or $Å^{-1}$).

The scattering intensity I(q) is the Fourier Transform of the correlation function of the electronic density, thus revealing the spatial correlations in the sample. The absolute scattered intensity must be normalized with the transmitted intensity through the sample (a part of the incident beam is absorbed as passing through the sample) (Fan, Degen, Bendle, Grupido, & Ilavsky, 2010). This involves the sample thickness (cm) and transmission T, hence the absolute scattering intensity is measured in cm^{-1} unit.

In the scattering pattern, the region of high q (high q domain) is called the Porod's region, giving information about the surfaces, while the low q region provides the structure factor S(q), which is used to calculate the interactions in the system. The domain between the low q and high q is called intermediary zone, in which the size, shape and structure of one particle can be determined via the so-called form factor P(q).

The SAXS data for colloidal and polymer systems consisting of particles in a solvent can be analyzed by model-independent approaches or by direct modeling approaches. The model-independent approaches require a Fourier transformation (Indirect Fourier Transformation) of the measured scattering curve to provide the pair distance distribution function p(r) which yields real-space information of the analyzed system. This approach could be applied for all system. For particular systems of monodisperse particles, data analysis can be simplified by applying a direct fitting to the scattering data. There are many fitting models proposed in the literature. A few of them are detailed hereafter.

2.4.7.1 The Guinier-Porod model

In order to characterize various structures (spheres, rods or lamellae), a generalized Guinier-Porod model was introduced by Hammouda (Hammouda, 2010):

$$I(q) = \frac{G}{q^s} exp\left(\frac{-q^2 R_g^2}{3-s}\right) \quad \text{for } q \leq q_1,$$

And $$I(q) = \frac{D}{q^d} \quad \text{for } q \geq q_1$$

in which R_g is radius of gyration which represents the particle size,

d is the Porod exponent which gives the nature of scattering inhomogeneities: smooth surface (*d*=4), rough surfaces (*d*=3), two-dimensional structure (*d*=2), rod structure (*d*=1),

s is related to the shape of the objects: spheres (s=0), rods (s=1); lamellae or platelets (s=2),

G and D are the Guinier and Porod scale factors, respectively

q_1 is the transition point which is defined by:

$$q_1 = \frac{1}{R_g}\left(\frac{3d}{2}\right)^{1/2}$$

Thus, the size (R_g) and shape (s, d) can be determined by fitting the measured scattering curve with this model.

2.4.7.2 Shape-dependent models

Shape-dependent models are presented in the form (Pedersen, 1997):

$$I(q) = N_p \Delta\rho^2 V_p^2 P(q) S(q) = \emptyset_p \Delta\rho^2 V_p P(q) S(q)$$

in which, N_p and ϕ_p are the number density (cm^{-3}) and the volume fraction of the dispersed particles, respectively, $\Delta\rho$ is the scattering length density contrast (cm^{-2}), V_p is the volume of one particle (cm^3), $P(q)$ is the form factor (discribes the particle structure), and $S(q)$ is the structure factor (describes interaction between the particles).

Below are examples of the form factor $P(q)$.

For a homogeneous sphere of radius R, $P(q)=F^2(q)$, with:

$$F_1(q,R) = \frac{3[\sin(qR) - qR\cos(qR)]}{(qR)^3}$$

For a cylinder of radius R and length L:

$$P(q) = \int_0^{\pi/2} \left[\frac{2B_1(qR\sin\alpha)}{qR\sin\alpha}\frac{\sin(qL\cos\alpha)/2}{(qL\cos\alpha)/2}\right]^2 \sin\alpha \, d\alpha$$

Here, $B_1(x)$ is the first order Bessel function.

References

Abate, A. R., Lee, D., Do, T., Holtze, C., & Weitz, D. A. (2008). Glass coating for PDMS microfluidic channels by sol-gel methods. Lab on a Chip, 8(4), 516–518.

Ahmed, K., Li, Y., McClements, D. J., & Xiao, H. (2012). Nanoemulsion- and emulsion-based delivery systems for curcumin: Encapsulation and release properties. Food Chemistry, 132(2), 799–807.

Amara, S., Barouh, N., Lecomte, J., Lafont, D., Robert, S., Villeneuve, P., … Carrière, F. (2010). Lipolysis of natural long chain and synthetic medium chain galactolipids by pancreatic lipase-related protein 2. Biochimica et Biophysica Acta - Molecular and Cell Biology of Lipids, 1801(4), 508–516.

Antille, C., Tran, C., Sorg, O., Carraux, P., Didierjean, L., & Saurat, J. H. (2003). Vitamin A Exerts a Photoprotective Action in Skin by Absorbing Ultraviolet B Radiation. Journal of Investigative Dermatology, 121(5), 1163–1167.

Armand, M. (2007). Lipases and lipolysis in the human digestive tract: where do we stand? Current Opinion in Clinical Nutrition & Metabolic Care, 10(2), 156–164.

Armand, M., Borel, P., Dubois, C., Senft, M., Peyrot, J., Salducci, J., … Lairon, D. (1994). Characterization of emulsions and lipolysis of dietary lipids in the human stomach. The American Journal of Physiology, 266, G372–G381.

Armand, M., Borel, P., Pasquier, B., Dubois, C., Senft, M., Andre, M., … Andre, M. (1996). Physicochemical characteristics of emulsions during fat digestion in human stomach and duodenum Physicochemical characteristics of emulsions during fat digestion in human stomach and duodenum. The American Physiological Society, (271), 172–183.

Armand, M., Pasquier, B., André, M., Borel, P., Senft, M., Peyrot, J., … Lairon, D. (1999). Digestion and absorption of 2 fat emulsions with different droplet sizes in the human digestive tract. American Journal of Clinical Nutrition, 70(6), 1096–1106.

Bai, Y., He, X., Liu, D., Patil, S. N., Bratton, D., Huebner, A., … Huck, W. T. S. (2010). A double droplet trap system for studying mass transport across a droplet-droplet interface. Lab on a Chip, 10(10), 1281–1285.

Beaudoin, A. R., St-Jean, P., & Grondin, G. (1989). Pancreatic juice composition: new views about the cellular mechanisms that control the concentration of digestive and nondigestive proteins. Digestive Diseases, 7(4), 210–220.

Behrens, D., Fricker, R., Bodoky, A., Drewe, J., Harder, F., & Heberer, M. (1996). Comparison of cyclosporin A absorption from LCT and MCT solutions following intrajejunal administration in conscious dogs. Journal of Pharmaceutical Sciences, 85(6), 666–668.

Benito-gallo, P., Franceschetto, A., Wong, J. C. M., Marlow, M., Zann, V., Scholes, P., & Gershkovich, P. (2015). European Journal of Pharmaceutics and Biopharmaceutics Chain length affects pancreatic lipase activity and the extent and pH – time profile of triglyceride lipolysis. European Journal of Pharmaceutics and Biopharmaceutics, 93, 353–362.

Borel, P. (2003). Factors affecting intestinal absorption of highly lipophilic food microconstituents (fat-soluble vitamins, carotenoids and phytosterols). Clinical Chemistry and Laboratory Medicine, 41(8), 979–994.

Borel, P., Caillaud, D., & Cano, N. J. (2015). Vitamin D Bioavailability: State of the Art. Critical Reviews in Food Science and Nutrition, 55(9), 1193–1205.

Borel, P., Preveraud, D., & Desmarchelier, C. (2013). Bioavailability of vitamin E in humans: An update. Nutrition Reviews, 71(6), 319–331.

Borgström, B., & Donnér, J. (1976). On the binding of bile salt to pancreatic lipase. Biochimica et Biophysica Acta (BBA)/Lipids and Lipid Metabolism, 450(3), 352–357.

Borgström, B., & Erlanson, C. (1971). Pancreatic juice co-lipase: physiological importance. Biochimica et Biophysica Acta, 242(2), 509.

Borgström, B., & Erlanson, C. (1973). Pancreatic lipase and co-lipase: interactions and effects of bile salts and other detergents. European Journal of Biochemistry, 37(1), 60–68.

Bourbaba, H., Ben Achaiba, C., & Mohamed, B. (2013). Mechanical behavior of polymeric membrane: Comparison between PDMS and PMMA for micro fluidic application. Energy Procedia, 36, 231–237.

Britton, G. (1995). UV/visible spectroscopy. Carotenoids: Spectroscopy, 13–63.

Caballero, B., Trugo, L., & Finglas, P. (2003). Encyclopedia of food sciences and nutrition: Volumes 1-10. Elsevier Science BV.

Calabresi, M., Andreozzi, P., & La Mesa, C. (2007). Supra-molecular association and polymorphic behaviour in systems containing bile acid salts. Molecules, 12(8), 1731–

1754.

Carey, M. C., Small, D. M., & Bliss, C. M. (1983). Lipid Digestion and Absorption. Annual Review of Physiology, 45(1), 651–677.

Charles, M., Riva, M. G. M., & Chabre, M. (1980). Small-angle Neutron Scattering Study of the Association between Porcine Pancreatic Colipase and Taurodeoxycholate Micelles, 297–317.

Chou, W. L., Lee, P. Y., Yang, C. L., Huang, W. Y., & Lin, Y. S. (2015). Recent advances in applications of droplet microfluidics. Micromachines, 6(9), 1249–1271.

Dahan, A., & Hoffman, A. (2006). Use of a dynamic in vitro lipolysis model to rationalize oral formulation development for poor water soluble drugs: Correlation with in vivo data and the relationship to intra-enterocyte processes in rats. Pharmaceutical Research, 23(9), 2165–2174.

Dahan, A., & Hoffman, A. (2007). The effect of different lipid based formulations on the oral absorption of lipophilic drugs: The ability of in vitro lipolysis and consecutive ex vivo intestinal permeability data to predict in vivo bioavailability in rats. European Journal of Pharmaceutics and Biopharmaceutics, 67(1), 96–105.

Dangla, R., Fradet, E., Lopez, Y., & Baroud, C. N. (2013). The physical mechanisms of step emulsification. Journal of Physics D: Applied Physics, 46(11).

Dangla, R., Kayi, S. C., & Baroud, C. N. (2013). Droplet microfluidics driven by gradients of confinement. Proceedings of the National Academy of Sciences, 110(3), 853–858.

Dangla, R., Lee, S., & Baroud, C. N. (2011). Trapping microfluidic drops in wells of surface energy. Physical Review Letters, 107(12).

Deeming-Adams, B., & Adams, W. (2002). Antioxidants in phothosynthesis and human nutrition. Science, 298(December), 2149–2153.

Desai, D., & Zaman, M. H. (2015). Continuous flow microfluidic solution for quantitative analysis of active pharmaceutical ingredient content and kinetic release. Analytical Methods, 7(5), 1914–1923.

Doba, T., Burton, G. W., & Ingold, K. U. (1985). Antioxidant and co-antioxidant activity of vitamin C. The effect of vitamin C, either alone or in the presence of vitamin E or a water-soluble vitamin E analogue, upon the peroxidation of aqueous multilamellar phospholipid liposomes. Biochimica et Biophysica Acta (BBA)/Lipids and Lipid

Metabolism, 835(2), 298–303.

Eddings, M. A., & Gale, B. K. (2006). A PDMS-based gas permeation pump for on-chip fluid handling in microfluidic devices. Journal of Micromechanics and Microengineering, 16(11), 2396–2402.

Eddings, M. A., Johnson, M. A., & Gale, B. K. (2008). Determining the optimal PDMS-PDMS bonding technique for microfluidic devices. Journal of Micromechanics and Microengineering, 18(6).

El-agamey, A., Cantrell, A., Land, E. J., Mcgarvey, D. J., & Truscott, T. G. (2004). Are dietary carotenoids bene fi cial? Reactions of carotenoids with oxy-radicals and singlet oxygen. Photochemical & Photobiological Sciences, 3, 802–811.

El-Gorab, M., & Underwood, B. A. (1973). SOLUBILIZATION OF Beta-CAROTENE AND RETINOL INTO AQUEOUS SOLUTIONS OF MIXED MICELLES, 306, 58–66.

Fagotto, F., & Maxfield, F. R. (1994). Changes in yolk platelet pH during Xenopus laevis development correlate with yolk utilization. A quantitative confocal microscopy study. Journal of Cell Science, 107 (Pt 1, 3325–3337.

Fan, L., Degen, M., Bendle, S., Grupido, N., & Ilavsky, J. (2010). The absolute calibration of a small-angle scattering instrument with a laboratory X-ray source. Journal of Physics: Conference Series, 247.

Favé, G., Coste, T. C., & Armand, M. (2004). Physicochemical properties of lipids: new strategies to manage fatty acid bioavailability. Cellular and Molecular Biology (Noisy-Le-Grand, France), 50(7), 815–831.

Frazer, A. C. (1946). The absorption of triglyceride fat from the intestine. Physiol. Rev, 26, 103.

Garstecki, P., Fuerstman, M. J., Stone, H. A., & Whitesides, G. M. (2006). Formation of droplets and bubbles in a microfluidic T-junction - Scaling and mechanism of break-up. Lab on a Chip, 6(3), 437–446.

Go, J. S., & Shoji, S. (2004). A disposable, dead volume-free and leak-free in-plane PDMS microvalve. Sensors and Actuators, A: Physical, 114(2–3), 438–444.

Grune, T. et al. (2010). b -Carotene Is an Important Vitamin A Source. The Journal of Nutrition, 140(12), 2268S–2285S.

Gudas, L. J. (1994). Cellular biology and biochemistry of the retinoids. The Retinoids, 443–520.

Gupta, A., & Kumar, R. (2010). Effect of geometry on droplet formation in the squeezing regime in a microfluidic T-junction. Microfluidics and Nanofluidics, 8(6), 799–812.

Hammouda, B. (2010). A new Guinier – Porod model A new Guinier – Porod model, 716–719.

Hamosh, M. (1990). Lingual and gastric lipases: their role in fat digestion. CRC Press, Inc.

Haque, N., & Prakash Prabhu, N. (2018). Binding orientation and interaction of bile salt in its ternary complex with pancreatic lipase-colipase system. Biochemical and Biophysical Research Communications, 499(4), 907–912.

Harrison, E. H. (2012). Mechanisms involved in the intestinal absorption of dietary vitamin A and provitamin A carotenoids. Biochimica et Biophysica Acta - Molecular and Cell Biology of Lipids, 1821(1), 70–77.

Haskell, M. J. (2012). The challenge to reach nutritional adequacy for vitamin A: β-carotene bioavailability and conversion - Evidence in humans. American Journal of Clinical Nutrition.

Helenius, A., & Simons, K. (1972). The binding of detergents to lipophilic and hydrophilic proteins. Journal of Biological Chemistry, 247(11), 3656–3661.

Hermoso, J., Pignol, D., Penel, S., Roth, M., Chapus, C., & Fontecilla-Camps, J. C. (1997). Neutron crystallographic evidence of lipase-colipase complex activation by a micelle. EMBO Journal, 16(18), 5531–5536.

Holick, M. F. (2004). Sunlight and vitamin D for bone health and prevention of autoimmune diseases , cancers , and cardiovascular disease 1 – 4, 80(June), 1678–1688.

Holmberg, I., Aksnes, L., Berlin, T., Lindbäck, B., Zemgals, J., & Lindeke, B. (1990). Absorption of a pharmacological dose of vitamin D3from two different lipid vehicles in man: Comparison of peanut oil and a medium chain triglyceride. Biopharmaceutics & Drug Disposition, 11(9), 807–815.

Holst, B., & Williamson, G. (2008). Nutrients and phytochemicals: from bioavailability to bioefficacy beyond antioxidants. Current Opinion in Biotechnology, 19(2), 73–82.

Hoorn, R. K. J., Plikweert, J. P., & Westerink, D. (1975). Vitamin B-1, B-2 and B-6

deficiencies in geriatric patients, measured by coenzyme stimulation of enzyme activities. Clinica Chimica Acta, 61(2), 151–162.

Huebner, A., Bratton, D., Whyte, G., Yang, M., Demello, A. J., Abell, C., & Hollfelder, F. (2009). Static microdroplet arrays: A microfluidic device for droplet trapping, incubation and release for enzymatic and cell-based assays. Lab on a Chip, 9(5), 692–698.

Hunt, T. P., Issadore, D., & Westervelt, R. M. (2007). Integrated circuit/microfluidic chip to programmably trap and move cells and droplets with dielectrophoresis. Lab on a Chip, 8(1), 81–87.

Hunter, E. J. (2001). Studies on effects of dietary fatty acids as related to their position on triglycerides. Lipids, 36(7), 655–668.

Huo, T., Ferruzzi, M. G., Schwartz, S. J., & Failla, M. L. (2007). Impact of fatty acyl composition and quantity of triglycerides on bioaccessibility of dietary carotenoids. Journal of Agricultural and Food Chemistry, 55(22), 8950–8957.

Jamalabadi, M. Y. A., DaqiqShirazi, M., Kosar, A., & Shadloo, M. S. (2017). Effect of injection angle, density ratio, and viscosity on droplet formation in a microfluidic T-junction. Theoretical and Applied Mechanics Letters, 7(4), 243–251.

Kalantzi, L., Goumas, K., Kalioras, V., Abrahamsson, B., Dressman, J. B., & Reppas, C. (2006). Characterization of the human upper gastrointestinal contents under conditions simulating bioavailability/bioequivalence studies. Pharmaceutical Research, 23(1), 165–176.

Kaukonen, A. M., Boyd, B. J., Charman, W. N., & Porter, C. J. H. (2004). Drug Solubilization Behavior during in Vitro Digestion of Suspension Formulations of Poorly Water-Soluble Drugs in Triglyceride Lipids. Pharmaceutical Research, 21(2), 254–260.

Leong, T. S. H., Wooster, T. J., Kentish, S. E., & Ashokkumar, M. (2009). Minimising oil droplet size using ultrasonic emulsification. Ultrasonics Sonochemistry, 16(6), 721–727.

Li, W., Young, E. W. K., Seo, M., Nie, Z., Garstecki, P., Simmons, C. A., & Kumacheva, E. (2008). Simultaneous generation of droplets with different dimensions in parallel integrated microfluidic droplet generators. Soft Matter, 4(2), 258.

Li, Y., Hu, M., & McClements, D. J. (2011). Factors affecting lipase digestibility of emulsified lipids using an in vitro digestion model: Proposal for a standardised pH-stat method. Food Chemistry, 126(2), 498–505.

Li, Y., Kim, J., Park, Y., & McClements, D. J. (2012). Modulation of lipid digestibility using structured emulsion-based delivery systems: Comparison of in vivo and in vitro measurements. Food and Function, 3(5), 528–536.

Li, Y., & Mcclements, D. J. (2010). New mathematical model for interpreting ph-stat digestion profiles: Impact of lipid droplet characteristics on in vitro digestibility. Journal of Agricultural and Food Chemistry, 58(13), 8085–8092.

Lindahl, A., Ungell, A. L., Knutson, L., & Lennernäs, H. (1997). Characterization of fluids from the stomach and proximal jejunum in men and women. Pharmaceutical Research.

Link, D. R., Anna, S. L., Weitz, D. A., & Stone, H. A. (2004). Geometrically Mediated Breakup of Drops in Microfluidic Devices. Physical Review Letters, 92(5), 4.

Lisensky, G. C., Campbell, D. J., Beckman, K. J., Calderon, C. E., Doolan, P. W., Ottosen, R. M., & Ellis, A. B. (1999). Replication and Compression of Surface Structures with Polydimethylsiloxane Elastomer. Journal of Chemical Education, 76(4), 537.

Liu, H., & Zhang, Y. (2009). Droplet formation in a T-shaped microfluidic junction. Journal of Applied Physics, 106(3), 34906.

Liu, H., & Zhang, Y. (2011). Droplet formation in microfluidic cross-junctions. Physics of Fluids, 23(8), 1–12.

Liu, M., Sun, X. T., Yang, C. G., & Xu, Z. R. (2016). On-chip preparation of calcium alginate particles based on droplet templates formed by using a centrifugal microfluidic technique. Journal of Colloid and Interface Science, 466(3), 20–27.

Lopez-Pena, C. L., Zheng, B., Sela, D. A., Decker, E. A., Xiao, H., & McClements, D. J. (2016). Impact of ε-polylysine and pectin on the potential gastrointestinal fate of emulsified lipids: In vitro mouth, stomach and small intestine model. Food Chemistry, 192, 857–864.

Lowe, M. E. (1997). Structure and function of pancreatic lipase and colipase. Annual Review of Nutrition, 17, 141–158.

Majeed, H., Antoniou, J., Hategekimana, J., Sharif, H. R., Haider, J., Liu, F., … Zhong, F. (2016). Influence of carrier oil type, particle size on invitro lipid digestion and eugenol release in emulsion and nanoemulsions. Food Hydrocolloids.

Maldonado-Valderrama, J., Wilde, P., MacIerzanka, A., & MacKie, A. (2011). The role of bile salts in digestion. Advances in Colloid and Interface Science, 165(1), 36–46.

Marquis, M., Renard, D., & Cathala, B. (2012). Microfluidic generation and selective degradation of biopolymer-based Janus microbeads. Biomacromolecules, 13(4), 1197–1203.

Marze, S. (2014). A coarse-grained simulation to study the digestion and bioaccessibility of lipophilic nutrients and micronutrients in emulsion. Food Funct., 5(1), 129–139.

Marze, S. (2015). Bioaccessibility of lipophilic micro-constituents from a lipid emulsion. Food and Function, 6(10), 3218–3227.

Marze, S., Algaba, H., & Marquis, M. (2014). A microfluidic device to study the digestion of trapped lipid droplets. Food Funct., 5(7), 1481–1488.

Marze, S., & Choimet, M. (2012). In vitro digestion of emulsions: Mechanistic and experimental models. Soft Matter, 8(42), 10982–10993.

Marze, S., Meynier, A., & Anton, M. (2013). In vitro digestion of fish oils rich in n-3 polyunsaturated fatty acids studied in emulsion and at the oil-water interface. Food and Function, 4(2), 231–239.

Mashaghi, S., Abbaspourrad, A., Weitz, D. A., & van Oijen, A. M. (2016). Droplet microfluidics: A tool for biology, chemistry and nanotechnology. TrAC - Trends in Analytical Chemistry, 82, 118–125.

Maylie, M. F., Charles, M., Astier, M., & Desnuelle, P. (1973). On porcine pancreatic colipase: large scale purification and some properties. Biochemical and Biophysical Research Communications, 52(1), 291–297.

Mazer, N. A. (1990). Quasielastic light scattering studies of aqueous biliary lipid systems and native bile. Hepatology (Baltimore, Md.), 12(3 Pt 2), 39S–44S.

McClements, D. J. (2010). Emulsion Design to Improve the Delivery of Functional Lipophilic Components. Annual Review of Food Science and Technology, 1(1), 241–269.

McClements, D. J., & Li, Y. (2010). Review of in vitro digestion models for rapid screening of emulsion-based systems. Food and Function, 1(1), 32–59.

McDonald, J. C., Duffy, D. C., Anderson, J. R., Chiu, D. T., Wu, H., Schueller, O. J. A., & Whitesides, G. M. (2000). Fabrication of microfluidic systems in poly (dimethylsiloxane). ELECTROPHORESIS: An International Journal, 21(1), 27–40.

McKimmie, R. L., Easter, L., & Weinberg, R. B. (2013). Acyl chain length, saturation, and

hydrophobicity modulate the efficiency of dietary fatty acid absorption in adult humans. AJP: Gastrointestinal and Liver Physiology, 305(9), G620–G627.

Mongersun, A., Smeenk, I., Pratx, G., Asuri, P., & Abbyad, P. (2016). Droplet Microfluidic Platform for the Determination of Single-Cell Lactate Release. Analytical Chemistry, 88(6), 3257–3263.

Mu, H., & Høy, C. E. (2004). The digestion of dietary triacylglycerols. Progress in Lipid Research, 43(2), 105–133.

Mun, S., Decker, E. A., & McClements, D. J. (2007). Influence of emulsifier type on in vitro digestibility of lipid droplets by pancreatic lipase. Food Research International, 40(6), 770–781.

Ngo, I.-L., Woo Joo, S., & Byon, C. (2016). Effects of Junction Angle and Viscosity Ratio on Droplet Formation in Microfluidic Cross-Junction. Journal of Fluids Engineering, 138(5), 051202.

Nidhi, B., & Baskaran, V. (2011). Influence of vegetable oils on micellization of lutein in a simulated digestion model. JAOCS, Journal of the American Oil Chemists' Society, 88(3), 367–372.

O'Byrne, S. M., & Blaner, W. S. (2013). Retinol and retinyl esters: biochemistry and physiology. Journal of Lipid Research, 54(7), 1731–1743.

Omenn, G. S., Goodman, G. E., Thornquist, M. D., Balmes, J., Cullen, M. R., Glass, A., … Hammar, S. (1996). Effects of a combination of beta carotene and vitamin A on lung cancer and cardiovascular disease. N Engl J Med, 334(18), 1150–1155.

Oomen, A. G., Rompelberg, C. J. M., Bruil, M. A., Dobbe, C. J. G., Pereboom, D. P. K. H., & Sips, A. J. A. M. (2003). Development of an in vitro digestion model for estimating the bioaccessibility of soil contaminants. Archives of Environmental Contamination and Toxicology, 44(3), 281–287.

Paddock, S. W. (2000). Principles and Practices of Laser Scanning Confocal Microscopy. Molecular Biotechnology, 16(2), 127–150.

Palmer, A. C., Darnton-Hill, I., & West, K. P. (2017). Vitamin A Deficiency. In S. de Pee, D. Taren, & M. W. Bloem (Eds.), Nutrition and Health in a Developing World (pp. 181–234). Cham: Springer International Publishing.

Park, S. Y., & Chiou, P. Y. (2011). Light-driven droplet manipulation technologies for lab-on-

a-chip applications. Advances in OptoElectronics, 2011(1).

Pedersen, J. S. (1997). Analysis of small-angle scattering data from colloids and polymer solutions: modeling and least square fitting. Advances in Colloid and Interface Science, 70, 171–210.

Pedersen, P. B., Vilmann, P., Bar-Shalom, D., Müllertz, A., & Baldursdottir, S. (2013). Characterization of fasted human gastric fluid for relevant rheological parameters and gastric lipase activities. European Journal of Pharmaceutics and Biopharmaceutics, 85(3 PART B), 958–965.

Phee, H., Rodgers, W., & Coggeshall, K. M. (2001). Visualization of negative signaling in B cells by quantitative confocal microscopy. Mol.Cell Biol., 21(0270–7306 (Print)), 8615–8625.

Pignol, D., Ayvazian, L., Kerfelec, B., Timmins, P., Crenon, I., Hermoso, J., … Chapus, C. (2000). Critical Role of Micelles in Pancreatic Lipase Activation Revealed by Small Angle Neutron Scattering. J. Biol. Chem., 275(6), 4220–4224.

Pimpin, A., & Srituravanich, W. (2012). Reviews on micro- and nanolithography techniques and their applications. Engineering Journal, 16(1), 37–55.

Pit, A. M., Bonestroo, S., Wijnperlé, D., Duits, M. H. G., & Mugele, F. (2016). Electrode-assisted trapping and release of droplets on hydrophilic patches in a hydrophobic microchannel. Microfluidics and Nanofluidics, 20(9), 1–12.

Pit, A. M., Duits, M. H. G., & Mugele, F. (2015). Droplet manipulations in two phase flow microfluidics. Micromachines, 6(11), 1768–1793.

Porter, C. J. H., Kaukonen, A. M., Boyd, B. J., Edwards, G. A., & Charman, W. N. (2004). Susceptibility to lipase-mediated digestion reduces the oral bioavailability of danazol after administration as a medium-chain lipid-based microemulsion formulation. Pharmaceutical Research, 21(8), 1405–1412.

Proctor, S. D., Vine, D. F., & Mamo, J. C. L. (2004). Arterial permeability and efflux of apolipoprotein B-containing lipoproteins assessed by in situ perfusion and three-dimensional quantitative confocal microscopy. Arteriosclerosis, Thrombosis, and Vascular Biology, 24(11), 2162–2167.

Qian, C., Decker, E. A., Xiao, H., & McClements, D. J. (2012). Nanoemulsion delivery systems: Influence of carrier oil on β-carotene bioaccessibility. Food Chemistry, 135(3),

1440–1447.

Rezhdo, O., Di Maio, S., Le, P., Littrell, K. C., Carrier, R. L., & Chen, S. H. (2017). Characterization of colloidal structures during intestinal lipolysis using small-angle neutron scattering. Journal of Colloid and Interface Science, 499, 189–201.

Ross, A. C., & Hammerling, U. G. (1994). Retinoids and the immune system. The Retinoids: Biology, Chemistry and Medicine, 2, 597–630.

Saari, J. C. (1999). Retinoids in Mammalian Vision. In H. Nau & W. S. Blaner (Eds.), Retinoids: The Biochemical and Molecular Basis of Vitamin A and Retinoid Action, 563–588.

Salvia-Trujillo, L., Qian, C., Martín-Belloso, O., & McClements, D. J. (2013). Modulating β-carotene bioaccessibility by controlling oil composition and concentration in edible nanoemulsions. Food Chemistry, 139(1–4), 878–884.

Samel, B., Chowdhury, M. K., & Stemme, G. (2007). The fabrication of microfluidic structures by means of full-wafer adhesive bonding using a poly(dimethylsiloxane) catalyst. Journal of Micromechanics and Microengineering, 17(8), 1710–1714.

Satyanarayana, S., Karnik, R. N., & Majumdar, A. (2005). Stamp-and-stick room-temperature bonding technique for microdevices. Journal of Microelectromechanical Systems, 14(2), 392–399.

Scheuble, N., Iles, A., Wootton, R. C. R., Windhab, E. J., Fischer, P., & Elvira, K. S. (2017). Microfluidic Technique for the Simultaneous Quantification of Emulsion Instabilities and Lipid Digestion Kinetics. Analytical Chemistry, 89(17), 9116–9123.

Schneider, M. H., Kozlov, B., Willaime, H., Tran, Y., Rezgui, F., & Tabeling, P. (2010). Wettability Patterning in Microfluidic Systems By Poly (Acrylic Acid) Graft Polymerization. 14th International Conference on Miniaturized Systems for Chemistry and Life Sciences, 82(October), 1949–1951.

Schuler, F., Schwemmer, F., Trotter, M., & Wadle, S. (2015). Centrifugal Microfluidic Step Emulsification for Digital Droplet Recombinase Polymerase Amplification, 188–190.

Schulze, M., & Belder, D. (2012). Poly(ethylene glycol)-coated microfluidic devices for chip electrophoresis. Electrophoresis, 33(2), 370–378.

Sek, L., Porter, C. J. H., & Charman, W. N. (2001). Sek 2001_Characterisation and quantification of medium chain and long chain triglycerides and their in vitro digestion

products, by HPTLC coupled with in situ densitometric analysis.pdf, 25, 651–661.

SENIOR, J. R. (1964). Intestinal Absorption of Fats. Journal of Lipid Research, 5(4), 495–521.

Sies, Helmut; Stahl, W. (1995). Vitamins E and C , a-carotene , and other carotenoids as. The American Journal of Clinical Nutrition, 62, 1315S–1321S.

Song, K., Zhang, W. J., & Gupta, M. M. (2009). Uniform Microdroplet Formation By Enhanced Instability Utilizing a Pzt Actuator : a Theoretical and Simulation Study. 3rd International Conference on Bioinformatics and Biomedical Engineering, (Isbme), 1–4.

Sun, F., Jaspers, T. C. C., van Hasselt, P. M., Hennink, W. E., & van Nostrum, C. F. (2016). A Mixed Micelle Formulation for Oral Delivery of Vitamin K. Pharmaceutical Research, 33(9), 2168–2179.

Sylven, C., & Borgstrom, B. (1969). Intestinal absorption and lymphatic transport of cholesterol in the rat: influence of the fatty acid chain length of the carrier triglyceride. Journal of Lipid Research, 10(4), 351–355.

Teh, S. Y., Lin, R., Hung, L. H., & Lee, A. P. (2008). Droplet microfluidics. Lab on a Chip, 8(2), 198–220.

Thomson, A. B. R. (1989). Intestinal aspects of lipid absorption: In review. Nutrition Today, 24(4), 16–20.

Torcello-Gómez, A., Maldonado-Valderrama, J., de Vicente, J., Cabrerizo-Vílchez, M. A., Gálvez-Ruiz, M. J., & Martín-Rodríguez, A. (2011). Investigating the effect of surfactants on lipase interfacial behaviour in the presence of bile salts. Food Hydrocolloids, 25(4), 809–816.

Trantidou, T., Elani, Y., Parsons, E., & Ces, O. (2017). Hydrophilic surface modification of PDMS for droplet microfluidics using a simple, quick, and robust method via PVA deposition. Microsystems & Nanoengineering, 3(April 2016), 16091.

Tsujita, T., Mizuno, N. K., & Brockman, H. L. (1987). Nonspecific high affinity binding of bile salts to carboxylester lipases. Journal of Lipid Research, 28, 1434–1443.

Unger, M. A., Chou, H. P., Thorsen, T., Scherer, A., & Quake, S. R. (2000). Monolithic microfabricated valves and pumps by multilayer soft lithography. Science, 288(5463), 113–116.

Van Tilbeurgh, H., Egloff, M. P., Martinez, C., Rugani, N., Verger, R., & Cambillau, C. (1993). Interfacial activation of the lipase-procolipase complex by mixed micelles revealed by X-ray crystallography. Nature, 362(6423), 814–820.

Verde, A. V., & Frenkel, D. (2010). Simulation study of micelle formation by bile salts. Soft Matter, 6(16), 3815–3825.

Versantvoort, C. H. M., Oomen, A. G., Van De Kamp, E., Rompelberg, C. J. M., & Sips, A. J. A. M. (2005). Applicability of an in vitro digestion model in assessing the bioaccessibility of mycotoxins from food. Food and Chemical Toxicology, 43(1), 31–40.

Versantvoort, C. H. M., Van de Kamp, E., & Rompelberg, C. J. M. (2004). Development and applicability of an in vitro digestion model in assessing the bioaccessibility of contaminants from food. RIVM Rapport 320102002.

Vogel, S., Gamble, M. V, & Blaner, W. S. (1999). Biosynthesis, Absorption, Metabolism and Transport of Retinoids. In H. Nau & W. S. Blaner (Eds.), Retinoids: The Biochemical and Molecular Basis of Vitamin A and Retinoid Action (pp. 31–95). Berlin, Heidelberg: Springer Berlin Heidelberg.

Von Bonsdorff-Nikander, A., Christiansen, L., Huikko, L., Lampi, A. M., Piironen, V., Yliruusi, J., & Kaukonen, A. M. (2005). A comparison of the effect of medium- vs. long-chain triglycerides on the in vitro solubilization of cholesterol and/or phytosterol into mixed micelles. Lipids, 40(2), 181–190.

WALD, G. (1968). The Molecular Basis of Visual Excitation. Nature, 219, 800.

Ward, T., Faivre, M., Abkarian, M., & Stone, H. A. (2005). Microfluidic flow focusing: Drop size and scaling in pressure versus flow-rate-driven pumping. Electrophoresis, 26(19), 3716–3724.

Warren, D. B., Chalmers, D. K., Hutchison, K., Dang, W., & Pouton, C. W. (2006). Molecular dynamics simulations of spontaneous bile salt aggregation. Colloids and Surfaces A: Physicochemical and Engineering Aspects, 280(1–3), 182–193.

Weber, D., & Grune, T. (2012). The contribution of β-carotene to vitamin A supply of humans. Molecular Nutrition and Food Research, 56(2), 251–258.

Weibel, D. B., Kruithof, M., Potenta, S., Sia, S. K., Lee, A., & Whitesides, G. M. (2005). Torque-actuated valves for microfluidics. Analytical Chemistry, 77(15), 4726–4733.

Whitesides, G. M. (2006). The origins and the future of microfluidics. Nature, 442(7101), 368.

Wickham, M. J. S., Faulks, R. M., Mann, J., & Mandalari, G. (2012). The design, operation, and application of a dynamic gastric model. Dissolution Technologies, 19(3), 15–22.

Windbergs, M., & Weitz, D. A. (2011). Drug Dissolution Chip (DDC): A microfluidic approach for drug release. Small, 7(21), 3011–3015.

Xia, Y., & Whitesides, G. M. (1998). Soft lithography. Angew. Chem. Int. Ed.

Xu, J. H., Li, S. W., Tan, J., Wang, Y. J., & Luo, G. S. (2006). Preparation of highly monodisperse droplet in a T-junction microfluidic device. AIChE Journal, 52(9), 3005–3010.

Yang, Y., & McClements, D. J. (2013). Vitamin E bioaccessibility: Influence of carrier oil type on digestion and release of emulsified α-tocopherol acetate. Food Chemistry, 141(1), 473–481.

Yoo, “Michelle” Ji Yeon, & Chen, X. D. (2006). GIT Physicochemical Modeling - A Critical Review. International Journal of Food Engineering, 2(4).

Yu, H., Shi, K., Liu, D., & Huang, Q. (2012). Development of a food-grade organogel with high bioaccessibility and loading of curcuminoids. Food Chemistry, 131(1), 48–54.

Žukauskas, A., Batavičiūtė, G., Ščiuka, M., Jukna, T., Melninkaitis, A., & Malinauskas, M. (2014). Characterization of photopolymers used in laser 3D micro/nanolithography by means of laser-induced damage threshold (LIDT). Optical Materials Express, 4(8), 1601.

3 MANUSCRIPTS OF SUBMITTED ARTICLES

In this part, all the experimental aspects, results and discussions are presented in the manuscripts of two articles (published in Food Chemistry).

The first article focuses on the methodology based on microfluidics and confocal fluorescence microscopy. A microfluidic device was developed and used to monitor the kinetics of lipid digestion and lipophilic micronutrient bioaccessibility simultaneously. Polydimethylsiloxane (PDMS) was chosen for the device fabrication due to several advantages. The PDMS is widely used and intensely studied in the microfluidic domain. Besides its low cost, the device fabrication protocols have become standard. The design of the microfluidic device was optimized for both the generation of the oil droplet and their trapping. The channel geometry of the junction for oil droplet generation was optimized using both simulation results and experimental results (shown in part 4.1). The optimized junction channel was used to obtain droplets of 100 µm allowing a sufficient number of droplets observed for the statistical analysis (7-8 droplets in the field of view of the confocal microscopy with 10x objective). The digestion monitoring was achieved using a confocal fluorescence microscope. Other conventional fluorescence microscopes were tested but were not usable for the tracking of micronutrients due to the lack of precise control of the laser exposition, resulting in bleaching.

In the second article, a systematic study was carried out to reveal the interplay between the kinetics of lipid digestion and of lipophilic micronutrient solubilization. Three different oils were used (tricaprylin C8:0, high oleic sunflower seed oil C18:1, fish oil C22:6). Those oils are very different in terms of FFA composition, both in the carbon chain length and the number of double bond. They were thus expected to yield different lipid digestion kinetics (cf. table 1). The oil droplets contained either beta-carotene or retinyl palmitate. Those two lipophilic micronutrients are very different regarding their average bioaccessibility in emulsion-based studies (15% for beta-carotene, 65% for retinyl palmitate) and also their partition coefficient logP (13 for beta-carotene, 6 for retinyl palmitate). Those two lipophilic micronutrients were also suitable for fluorescence imaging using appropriate laser wavelengths of the confocal microscope. For the digestion, the oil droplets with added lipophilic micronutrient were subjected to an intestinal phase alone or a gastric phase followed by an intestinal phase. All the digestive parameters (duration of gastric phase, pH values, digestive juice composition) were chosen based on the physiology of the fed state (Minekus et al. 2014). The flow rate value for the digestive fluid (50 µL/min) was chosen to obtain a shear rate (around the trapped droplets) of about 0.2 s^{-1} which is in the typical range of in vivo shear rate within the intestinal lumen.

Article 1 : Studying the real-time interplay between triglyceride digestion and lipophilic micronutrient bioaccessibility using droplet microfluidics. 1 Lab on a chip method

Hoang Thanh NGUYEN, Mélanie MARQUIS, Marc ANTON, Sébastien MARZE

Biopolymères Interactions Assemblages, INRA, 44300 Nantes, France

Abstract

This article is the first part of a series reporting on real-time digestion kinetics of triglyceride droplets containing different lipophilic micronutrients. This part focuses on the design, fabrication, and operation of a polydimethylsiloxane microfluidic device which enables the generation and digestion of oil droplets. The micro-channels were made hydrophilic to obtain oil droplets in an aqueous continuous phase. Optimized chip design and outlet control were implemented to provide efficient oil droplet generation, manipulation, and immobilization on a single chip. Highly monodisperse oil droplets were generated, immobilized in an array of traps and monitored in real time by fluorescence using a confocal microscopy method. The device was used to study the kinetics of beta-carotene release during tricaprylin digestion (intestinal lipolysis and micellar solubilization). The effect of the gastric phase on beta-carotene degradation was also investigated using the same method.

Introduction

Over the past decades, the development of technologies based on microfluidics has expanded in analysis and research domains (Huebner et al., 2009; Šalić, Tušek, & Zelić, 2012). Indeed, the use of micro-scale experimental devices involves small sample volumes with a high surface-volume ratio that allows reduction of costs and rapid kinetics study. In addition, the optical transmission of the materials commonly used in microfluidics (mostly polydimethylsiloxane (PDMS), poly(methyl methacrylate) (PMMA), and glass) provides high flexibility to use external light-based analysis techniques for real-time monitoring (Desai & Zaman, 2015; Heus et al., 2010; Mongersun et al., 2016; Windbergs & Weitz, 2011). With the trend of further reducing the sample volume, droplet microfluidics was developed. In this technique, each droplet is used as an independent micro-reactor of pico- to nano- litre scale (Huebner et al., 2009; Huebner, Abell, Huck, Baroud, & Hollfelder, 2011; Mongersun et al., 2016). However, most of the studies are based on water droplets, while oil droplets are rarely explored. In particular, lipid droplets containing lipophilic micronutrients or hydrophobic drugs were rarely investigated.

On the contrary, *in vitro* digestion of lipid and lipophilic bioactive molecules is extensively carried out using emulsions (Marze, 2015; Li, Kim, Park, & McClements, 2012). Nevertheless, even in a "simple" system such as emulsion, studying mechanisms is still challenging due to many interactions involved simultaneously. Emulsion digestion is indeed influenced by many physicochemical characteristics which are difficult to control. Moreover, real-time kinetics studies of lipid/lipophilic molecules digestion were rarely achieved using the conventional emulsion approach.

Those issues can be solved using droplet microfluidics. In that context, the use of the lipid droplet microfluidic digestion system recently developed by Marze et al. showed equivalent results to those obtained from static *in vitro* digestion of emulsions (Marze et al., 2014). Then, Scheuble et al. reported a similar approach based on lipid droplet digestion with multiple oil droplets trapping to study the coalescence effect (Scheuble et al., 2017). Using various lipid droplets in a microfluidic device can be seen as a potential screening approach not only for the digestion of lipids but also for the release of lipophilic bioactive molecules. However, several difficulties needed to be solved to make droplet microfluidics an experimental standard for lipid studies in micro-reactors. First, the micro-channel surface has to be hydrophilic to enable oil droplet generation and manipulation. As most microfluidic materials are natively hydrophobic, a chemical treatment is required to obtain a persistent hydrophilic surface (He et al., 2011; Marze et al., 2014; Tan, Xu, Li, & Luo, 2008; Wang, Lu, Xu, & Luo, 2009). The second difficultly is the control of the oil droplet generation, which may undergo flow instabilities due to the high viscosity of edible oils compared to that of water (Marze et al., 2014). Finally, a proper optical setup is needed to quantify the kinetics of lipophilic molecules in real time.

In this article, we present an optimized microfluidic platform to overcome these limitations. A single PDMS chip based on a microfluidic device with hydrophilic surface modification was developed to generate and manipulate monodisperse oil droplets that are immobilized in an array of traps. The hydrophilic treatment and device storage were optimized to obtain a long hydrophilicity persistency of the channel surface. The oil droplet generation and flow were stabilized by an open-close procedure of the outlets, with no extra devices or valves required. The use of this platform is illustrated by examples of single and multiple droplet trapping. Then, the implementation of a confocal fluorescence microscope setup for real-time monitoring is illustrated by the kinetics of beta-carotene release from tricaprylin droplets during digestion. The kinetics of beta-carotene degradation in gastric conditions is also presented, monitored in real time using this setup as well.

2. Experimental Section

2.1. Materials

The negative photoresist (SU8-2100) was from MicroChem Corp, PDMS (RTV615) was from Eleco Produits, polytetrafluoroethylene (PTFE) tubes (11919445) were from Fisher Scientific, stainless steel tubes (Coop 23G/15 mm) and Luer lock needles (LS22) were from Phymep. The other chemicals were provided by Sigma-Aldrich: propylene glycol methyl ether acetate (PGMEA), benzophenone, acrylic acid, pancreatic lipase (L3126, lipase from porcine pancreas type II, 1.6-8.3 U mg^{-1}), sodium glycodeoxycholate (G9910), tricaprylin (T9126), beta-carotene (22040), Amano lipase A (534781, fungal lipase from *Aspergillus niger*, 12 U mg^{-1}, protease activity $\leq$ 2.5 U mg^{-1}), pepsin (P7012, from porcine gastric mucosa, 2500 U mg^{-1}). β-lactoglobulin was purified from whey protein isolate in our laboratory. Milli-Q water with an electrical resistivity of 18.2 MΩ was used for all solution preparations.

2.2. Microfluidic Device

The preparation of the PDMS microfluidic device is based on soft lithography techniques using silicon wafer for the master (Whitesides, Ostuni, Takayama, Jiang, & Ingber, 2001).

2.2.1. Photomask design. We used the Adobe Illustrator software to draw the mask design which was then printed out as a photo mask by high resolution printing.

2.2.2. Master fabrication. The master was made using photolithography techniques. A thin layer of negative photoresist was coated on a silicon wafer using a spin-coater (SPIN150, SPSEurope). This was prebaked for 5 min at 65 ^{0}C followed with 20 min at 95 ^{0}C before being exposed to UV light (365 nm) for 40 s through the photomask by a UV LED masker (UV-KUB 2, Kloé). The post-baking was done for 5 min at 65 ^{0}C followed by 10 min at 95 ^{0}C. Finally, the master with microstructures of 120 µm in height was obtained by development with a solution of PGMEA for 20-30 min. Propanol was used to wash excess products of development, resulting in a clean master.

2.2.3. PDMS chip. The device was fabricated using similar techniques found in Marquis et al. (Marquis et al., 2012). One device is composed of two PDMS parts bonded by the gradient technique. First, two PDMS/crosslinker mixtures (10% or 5% crosslinker) were poured on the master and in a Petri dish, respectively. Then, both parts were degassed in a vacuum chamber (50 mbar). After the degassing step, both parts were cured at 70 ^{0}C for 30 min. The cured PDMS (10% crosslinker) was cut and peeled off the master before access holes for inlets and outlets were punched through PDMS. Then, this PDMS part was cleaned and assembled with the 5% crosslinker PDMS in the Petri dish by curing at 70 ^{0}C for 1 hour. Stainless steel tubes were inserted in the access holes, reinforced by plastic rings filled with cured PDMS (5% of crosslinker). Finally, the device was cured overnight at 70 ^{0}C and the

stainless steel tubes were replaced by new ones for the inlets/outlets of the device. The design of the chip is shown in fig. 1a.

2.2.4. Hydrophilic treatment. PDMS surface is natively hydrophobic (water contact angle > 100°) (Mata, Fleischman, & Roy, 2005). In this work, the PDMS device was used to generate and trap oil droplets in an aqueous continuous phase. Thus, the surface of PDMS channel needed to be modified. A hydrophilic treatment was achieved by UV-initiated graft polymerization of acrylic acid as proposed by Schneider et al. (Marc H. Schneider, Willaime, Tran, Rezgui, & Tabeling, 2010). The first step was the injection of a 10% benzophenone in acetone at a flow rate of 200 µL min^{-1} for 10 min. Then, the remaining solution was blown out by air flow and the device was placed under vacuum (85 mbar) for 35 min before the injection of a 20% acrylic acid aqueous solution at a flow rate of 200 µL min^{-1} for 5 min. Next, the acrylic acid solution was sealed into the device by closing access holes. The device was illuminated with UV for 5 min using the UV LED masker. Finally, the device was cleaned by successive flow of ethanol and water (pH 11) at 200 µL min^{-1} for 1 hour. After the hydrophilic treatment, the device was put inside a plastic bottle filled with distilled water (pH 11) and stored at 4 ^{o}C to maintain the hydrophilicity of the channel surface.

2.3. Droplet Generation and trapping

All fluid flows were generated and controlled by syringe pumps 11 elite (Harvard Apparatus) with glass syringes connected to the inlets of device by a Luer lock needle and PTFE tubes. During the device operation, the outlets and inlets of the device were temporarily blocked by a piece of PTFE tube filled with cured PDMS.

For droplet generation, the microfluidic device was placed under an IX51 inverted microscope (Olympus) with a 4× objective. First, the continuous phase (7.5 mg mL^{-1} β-lactoglobulin in 10 mM NaH_2PO_4 adjusted to pH 7.0) and the oil phase (tricaprylin) were injected into the micro-channels via inlet 1 at a flow rate of 150 µL min^{-1}, and via inlet 2 at a flow rate of 4 µL min^{-1}, respectively. Then, the flow rate was decreased to 50 µL min^{-1} for the continuous phase and to 1 µL min^{-1} for the oil phase to generate oil droplets of 100 µm. Initially, outlet 4 was blocked, leading the first oil droplets to the waste tank via outlet 3. When the desired oil droplet size was reached (100 µm), outlet 4 was opened and outlet 3 was blocked, leading the oil droplets to the chamber. When most of the chamber traps were filled with one oil droplet, the oil flow was stopped and the aqueous continuous phase flow was increased to 100 µL min^{-1} to wash out any untrapped droplets of the chamber. Next, outlet 3 was opened and outlet 4 was blocked to prevent any undesirable large oil droplets from entering the chamber.

2.4. Droplet digestion

Initially, monodisperse tricaprylin droplets (100 µm in diameter) with added 0.2 wt% beta-carotene were generated and trapped in the microfluidic device as described above. Then, all four access tubes were blocked and the device was stored inside an aluminium box in order to avoid chemical degradation due to ambient lights. The device containing the droplets was then moved to a hot plate set on a confocal microscope stage (fig. 1b). The temperature of the hot plate was set to 56 °C to maintain a measured temperature of 37 ^{0}C inside the chamber. Using PTFE tubes, inlet 1 and outlet 3 were connected to the aqueous continuous phase syringe (the same one used for droplet generation) and the digestive fluid syringe, respectively. Outlet 4 was connected to the waste tank. Before thermal equilibrium was reached, the continuous phase was injected into the chamber at a flow rate of 50 µL min^{-1} to prevent air bubble development due to temperature rising. Then, the flow of the continuous phase was stopped and the reaction in the droplets was initiated by injecting digestive fluid via outlet 3 at a flow rate of 50 µL min^{-1}. This flow rate was kept constant throughout the reaction so that the digestive fluid in the chamber was theoretically renewed every 6 s. In practice, we measured that a steady-state concentration was typically reached after 1 min when replacing one solution by another one (results not shown).

Digestion was carried out with an intestinal phase or a gastric phase. For the intestinal phase, 10 mL of buffer solution (100 mM NaH_2PO_4 adjusted to pH 7.0) was mixed with pancreatic lipase at 4 mg mL^{-1} and a bile salt (sodium glycodeoxycholate) at 5 mg mL^{-1} to prepare a fresh intestinal digestive fluid forming an aqueous micellar solution due to the bile salt. This fluid was centrifuged at 1000g for 15 min to remove large residues before injection into the chamber.

The gastric phase experiments were run for 2 hours with a gastric digestive fluid containing 0.03 mg mL^{-1} lipase from *Aspergillus niger* (lipase AN), and 0.6 mg mL^{-1} pepsin in a 100 mM KCl buffer adjusted to pH 3.0. In order to get insights into the mechanisms of BC degradation during the gastric phase, three compositions of the gastric fluid were tested: i) lipase AN and pepsin, ii) lipase AN without pepsin, iii) only buffer with no enzymes.

2.5. Lipid monitoring

Tricaprylin (TC) droplets containing beta-carotene (BC) were observed during the digestion using a confocal microscope (Nikon A1+) with a 10× objective. The pinhole was set so that the thickness of the optical section was larger than the droplet initial diameter. Seven trapped droplets were monitored simultaneously in the field of view. A laser with an excitation wavelength of 488 nm and an emission window of 500-530 nm was used to obtain the autofluorescence image of BC contained in the oil droplets. A transmitted light image for the droplet size was obtained simultaneously using the same excitation beam (Paddock, 2000).

For quantitative analysis, a calibration curve was constructed with five points. TC droplets with various BC concentrations (0 wt% as the negative control, 0.05, 0.2, 0.4, 0.5 wt%) were trapped in five different microfluidic devices to measure the fluorescence intensity due to BC autofluorescence (no dye is used in the experiments). The degradation of BC was also checked as a function of time for TC droplets containing BC. In those tests, the conditions were the same than for intestinal digestion, except only the buffer solution (pH 7.0) was injected instead of the digestive fluid. The measured fluorescence intensity was found to be proportional to the BC concentration inside the oil droplets, independently on the droplet size, and the degradation was found to be negligible (supplementary material S1).

Images were recorded automatically with an interval of 2 min or 5 min for intestinal or gastric digestion, respectively. Then, image analysis was performed to measure the size of the seven droplets in the field of view and their average fluorescence intensity. The droplet size was converted to the droplet volume, and the average fluorescence intensity was converted to BC concentration inside the oil droplet.

Note that the analysis was developed using pure chemicals (pure tricaprylin and a single bile salt) to avoid autofluorescence of undesirable molecules. As lipophilic micronutrients have specific fluorescent properties, it was found that real edible oils could be used with no fluorescence overlapping. In contrast, bile extract was difficult to use because it contains many unidentified molecules, resulting in fluorescence over a wide wavelength range (see the second article of this series).

For each system, two to three independent digestions were conducted with the monitoring of seven individual droplets for each digestion. A distinct microfluidic device was used for each digestion to ensure identical initial conditions. The variability of the measurements was very low between the seven droplets monitored during one digestion, so the error bar (plotted as the standard deviation) represents the variability of the two to three independent digestions.

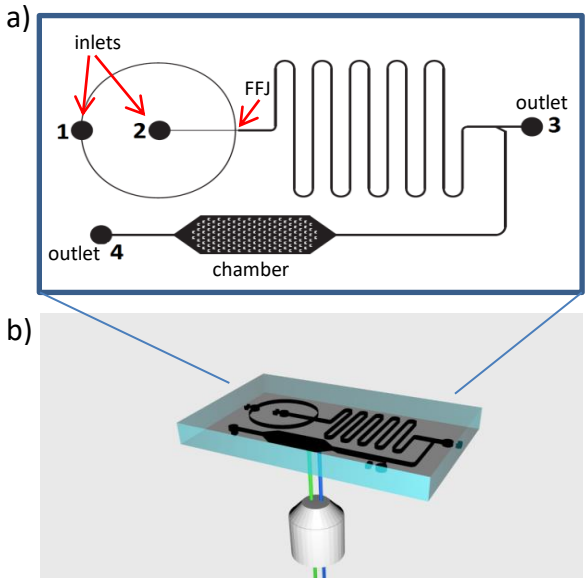

Fig. 1 a) Design of the PDMS microfluidic device for the generation, immobilization, and digestion of oil droplets. b) Real-time reactivity monitoring using confocal fluorescence microscopy.

3. Results and discussion

3.1. PDMS device fabrication

The PDMS device was constructed using two PDMS layers with different crosslinker concentrations (gradient technique). This technique resulted in a better association between the two PDMS parts compared to the plasma treatment method, eliminating the leakage during device operation while simplifying device fabrication. Moreover, this enabled the fabrication of 100% PDMS devices, which are lighter and easier to shape compared to devices made of PMMA, or using glass as the bottom part (Desai & Zaman, 2015; Huebner et al., 2009). In addition, PDMS has a broader transmission range (transmittance > 85%) than that of glass and PMMA, what is an advantage for the fluorescence analysis (Žukauskas et al., 2014).

3.2. PDMS surface modification

For the generation of oil droplets, the PDMS surface was rendered hydrophilic using the method proposed by Schneider et al. (Marc H. Schneider et al., 2010). In this method, the benzophenone molecules diffuse into the PDMS matrix and play the role of the photoinitiator of UV polymerization, turning acrylic acid (pre-absorbed in the PDMS) into grafted hydrophilic poly(acrylic acid). The advantages of this method are to keep the geometry of the channel unchanged and to provide a long persistency of the surface channel hydrophilicity. The post-

treated devices still have an operational hydrophilic surface after one month of storage in pH 11 water at 4 °C. On the contrary, the layer coating technique changed the PDMS device geometry (Abate et al., 2008), and the hydrophilicity obtained via the plasma treatment method was only stable within 24 hours (Marze et al., 2014). The hydrophilic persistency we obtained enabled a systematic preparation of microfluidic devices that could be stored for later experiments.

3.3. Oil droplet immobilization

Oil droplets were generated in the flow focusing junction (FFJ) and trapped in the chamber of the microfluidic device (see fig. 1a). At the FFJ, the aqueous continuous phase entered perpendicularly to the oil disperse phase, facilitating the formation of oil droplets (supplementary video 1). Due to fluid handling limitation and instabilities, oil droplet size could not be modulated in our previous work (Marze et al., 2014). Here, the flow of initial polydisperse large oil droplets was led to the waste tank. When the desired droplet size was reached, the flow was switched to the chamber. Supplementary video 2 shows that this flow switch does not change the droplet size and the monodispersity. Thus, our new design with the chamber part and the FFJ part on the same chip leads to stable flows and enables droplet sorting so that only size-controlled ones enter the chamber. Moreover, its operation is more reliable, as the connection between the FFJ device and the chamber was a source of air/liquid leakage, flow disturbance, and droplet coalescence in the previous design (Marze et al., 2014). Nevertheless, one aspect needs to be discussed for this droplet generation approach. During the flow switch, the difference of hydrodynamic resistances between the two paths could disturb flow equilibrium. We optimized the geometry of the chip so that no droplet flow interruption was observed. Then, the continuous phase flow rate is only 50-fold higher than the oil flow rate, what is low compared to typical values required for viscous oils (200-fold higher). Indeed, the disturbance of the flow equilibrium comes from the disturbance of the pressure $\Delta P=R_h.Q$, (ΔP: applied pressure, R_h: hydrodynamic resistance, Q: flow rate). Thus, in the case of a low flow rate Q, the change in R_h will only have a small effect on the pressure ΔP. On the contrary, in the case of a high flow rate, the flow equilibrium would be more susceptible to the change in the hydrodynamic resistance. So the geometry (width, height and length of the channel) of the two branches has to be calculated carefully to suppress any hydrodynamic resistance difference.

Supplementary video 3 shows the trapping process of the oil droplets in the chamber. Most of the traps are filled with oil droplets. The number of traps was made large enough (150 traps) so that several droplet-free traps do not compromise the experiment. The average diameter of the oil droplets was manipulated to be 100 ± 5 µm in the different experiments. The monodispersity of the droplet size in the same experiment is about 0.8%, crucial for

repeatable measurements in the case of surface-dependent reactions. The total volume of the oil droplets represents approximately 0.7% of the total volume of the chamber. The oil droplets kept their spherical shape with no sign of surface deformations that could be caused by local defects of the hydrophilic treatment at the internal surface of the traps (Marze et al., 2014). The absence of hydrophilicity defects minimizes the contact between the oil droplets and the trap, maximizing the accessible droplet surface area. This validates this passive immobilization method by obstacles, which gives a high accessible droplet surface area and a high trapping efficiency compared to active trapping methods (optical tweezers, dielectrophoresis, acoustic trapping), which give a full accessible surface area but a low trapping efficiency (Hunt et al., 2007; Lee et al., 2009; Park & Chiou, 2011).

During device operation, the order of opening and blocking of outlets 3 and 4 must be respected to achieve monodisperse oil droplets trapping in the chamber. In this condition, neither air bubbles nor droplet coalescence are observed inside the device during oil droplet generation and trapping. This open-close procedure for the outlets is a very efficient method to control the flow of oil droplets while simplifying the device structure, avoiding the use of pneumatic valves (Unger et al., 2000), or torque-actuated valves as proposed by Weibel et al. (Weibel et al., 2005). Also, our method does not require infusion-withdraw pumps to control the droplet flow (Huebner et al., 2009).

Our device was also used to obtain multiple droplets trapped in a single trap for coalescence studies. Monodisperse TC droplets of 90 µm diameter were generated and trapped. In this case, the droplet size was smaller than that of the trapping space, resulting in two droplets per trap. This configuration was used to study the effect of droplet coalescence during the gastric phase on the subsequent intestinal droplet digestion (supplementary material S2).

Similar PDMS devices were proposed to immobilize aqueous droplets for enzymatic reactions (Huebner et al., 2009), or oil droplets for lipid digestion (Marze et al., 2014). In this work, oil droplets containing BC were used to study the release (or degradation) kinetics of BC during the intestinal phase (or the gastric phase), as reported in the following section.

3.4. Kinetics of beta-carotene release during intestinal digestion

In order to illustrate the application of the device for release kinetics of lipophilic molecules, immobilized TC droplets with added 0.2 wt% BC were generated (single droplet trapping) and then submitted to intestinal digestion conditions. The kinetics of lipid digestion and beta-carotene release were monitored simultaneously in real time with a confocal fluorescence microscope setup.

Figs. 2 and supplementary video 4 show the evolution of oil droplet size and BC concentration as a function of digestion time. The droplet volume and BC concentration are reported as normalized values (relative to the initial values) in order to simplify the

comparisons. Droplet volume is reduced over time (fig. 2a) because triglyceride lipolysis produces fatty acids and monoglycerides that exit the droplet as they are soluble in the aqueous micellar phase. The kinetics is similar to the one reported by Marze et al. (Marze et al., 2014). A discussion of the effect of lipase concentration on digestion kinetics is found in the supplementary material S3.

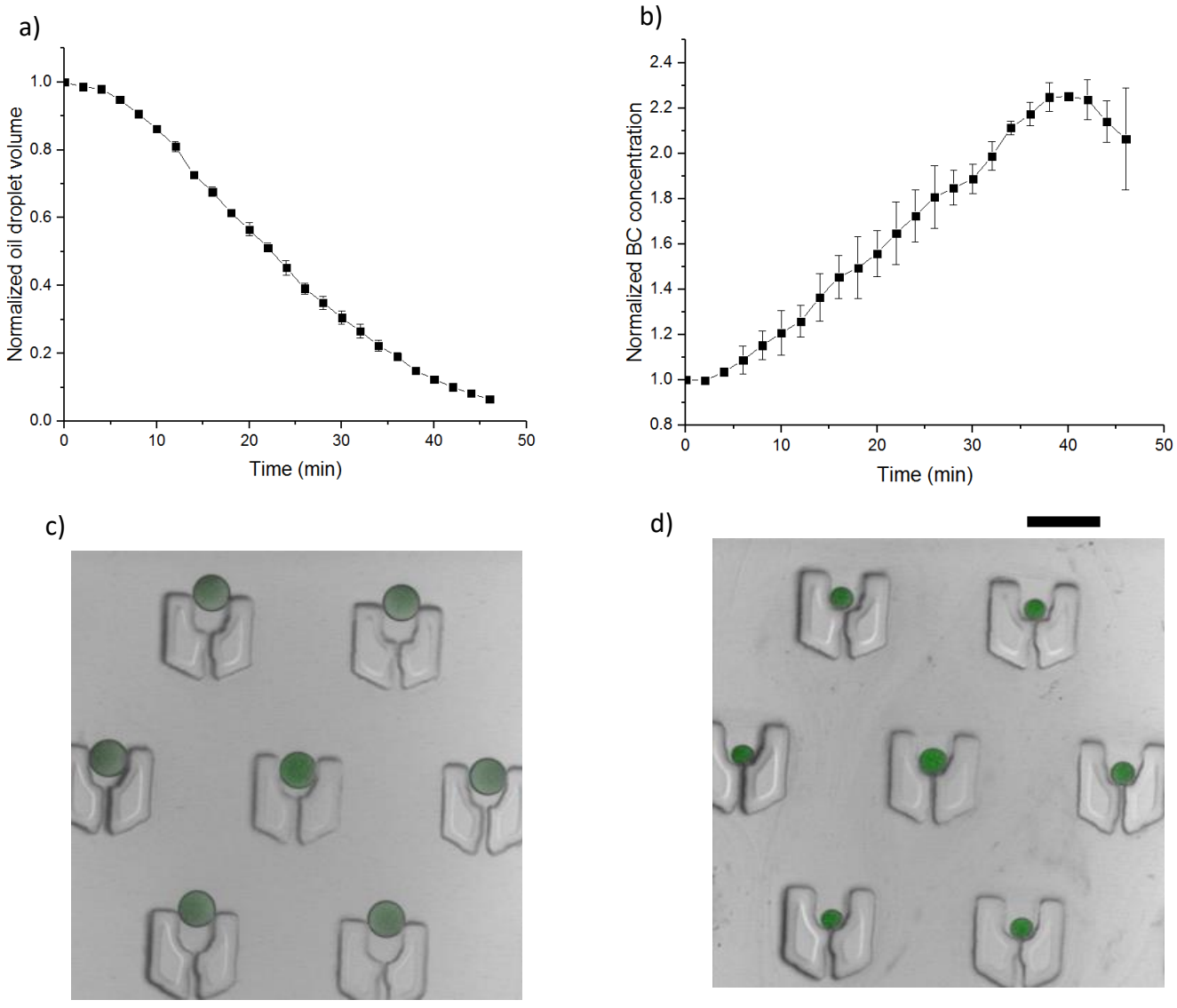

Fig. 2 a) Evolution of the normalized volume of TC droplets during intestinal digestion. b) Evolution of the normalized beta-carotene concentration inside TC droplet during intestinal digestion. c) d) Images of TC droplets containing beta-carotene at digestion times: 0, 24 min, respectively. The scale bar represents 200 µm.

As evidenced in fig. 2b, a trend for BC concentration in oil droplets is observed. Indeed, BC concentration mainly increases during digestion, although it reaches a maximum and then decreases near the end of the digestion. This means that the reduction rate of oil droplet volume is faster than the solubilizing rate of BC out of the droplets. Thus, BC concentrates inside the reducing droplets. At the end of the digestion, triglyceride digestion rate slows down but not the BC release rate (fig. 3), resulting in the decreasing trend for BC concentration.

From the data presented in figs. 2a and 2b, BC quantity released out of the droplets (incorporated in the micellar phase) can be calculated for quantitative analysis, using the mass balance:

$$m_{RL} = m_{Di} - m_D \quad \text{with} \quad m_D = V_D C \qquad (1)$$

Here m_{RL} is the mass of BC released from the oil droplet, m_{Di} is the initial mass of BC inside the oil droplet, m_D is the mass of BC inside the oil droplet, V_D is the volume of the oil droplet and C is the concentration of BC inside the oil droplet, determined from the fluorescence intensity using the calibration curve. All values are presented in normalized form.

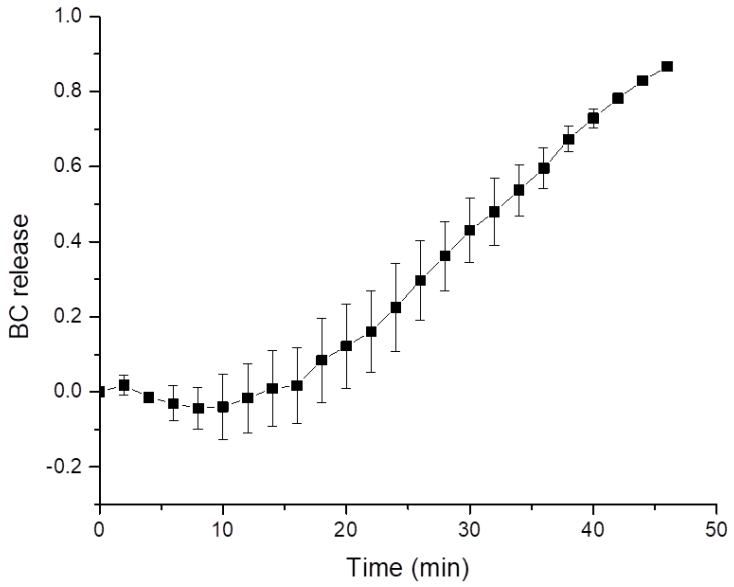

Fig. 3 Evolution of the BC proportion released from TC droplets during intestinal digestion (bioaccessibility).

Kinetics of BC release during intestinal digestion is shown in fig. 3. Note that negative values can be obtained at the beginning of the digestion where both kinetics are slow. Due to these

initial low releases, the determination of BC concentration is indeed sensitive to the precision of the calibration curve, and to fluctuations of the laser intensity. Nevertheless, the error bars in fig. 3 show that these values are not significantly different from zero.

In the current non-static digestion conditions with continuous renewal of the intestinal digestive fluid, bile salt micelles come in large excess compared to the digestion products and BC to solubilize. That explains the higher release of BC (almost 90% bioaccessibility) than those typically reported for static digestion of emulsions in the literature (Nik, Corredig, & Wright, 2011; Mutsokoti et al., 2017; Salvia-Trujillo et al., 2017).

Fig. 4 shows the relation between the micellar solubilization of BC and of the lipolytic products during intestinal digestion, providing a better view of their kinetic interplay. The black dash line represents the “balance” case of identical BC and lipid release rate. In order to analyze the curves in fig. 4 in terms of relative kinetics, three tangent lines are added, representing different BC release regimes. The first order derivative of the curve $\frac{dRL_{BC}}{dRL_{LP}}$ (slope of the tangent line) is equal to the release rate ratio between BC and lipids:

$$\frac{dRL_{BC}}{dRL_{LP}} = \frac{\frac{dRL_{BC}}{dt}}{\frac{dRL_{LP}}{dt}} = \frac{\text{BC release rate}}{\text{Lipid release rate}} \qquad (2)$$

In which, $\frac{dRL_{BC}}{dt}$ and $\frac{dRL_{LP}}{dt}$ are the first order derivative of BC and lipid release as a function of digestion time, respectively.

The slopes on the non-linear curve reveal three different kinetic regimes. In the first part (beginning of the digestion), the slope of the tangent line is smaller than 1 ($\frac{dRL_{BC}}{dRL_{LP}}$<1), showing that BC release rate is slower than that of lipids. This caused the increase of BC concentration inside the oil droplets. In the middle part, a balanced regime can be observed. In the third part (end of the digestion), the release rate of BC becomes faster than that of the lipids ($\frac{dRL_{BC}}{dRL_{LP}}$ >1), explaining the decrease trend of BC concentration observed near the end of the digestion (fig. 2b).

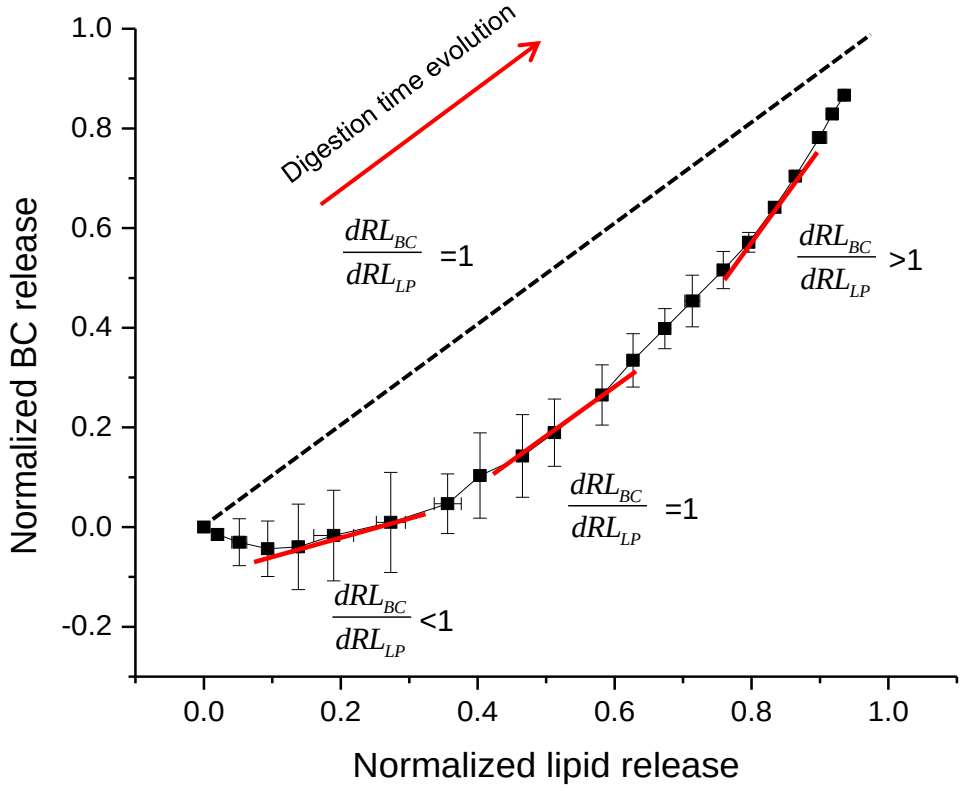

Fig. 4 Relation between the normalized mass release of BC and of lipids.

3.5. Beta-carotene degradation in gastric conditions

For this study, the same protocols (as in section 3.4.) were used except the intestinal fluid was replaced by a gastric fluid. Fig. 5a shows the evolution of the droplet volume in gastric conditions using various gastric fluid compositions. The decrease of the TC droplet volume was only seen with the gastric fluid containing both lipase AN and pepsin. This decrease reached up to 50% of the initial droplet volume, what is higher than the usual lipolysis degree (10-30%) measured during the gastric phase *in vivo* (Favé et al., 2004). This difference could be explained by the absence of droplet coalescence, that has an essential effect in the stomach *in vivo* (Y. Li et al., 2012). Marze et al. reported 10-20% TC droplet volume reduction (initial size of 137 µm) obtained after 55 min of gastric digestion using a similar device (Marze et al., 2014). The larger initial droplet size, shorter duration of the gastric phase, and the absence of pepsin in the gastric fluid could explain the lower lipolysis degree of tricaprylin. Fig. 5a also shows the role of pepsin, as no reduction of the droplet volume was obtained in the absence of pepsin in the gastric fluid. Indeed, pepsin hydrolyses the β-lactoglobulin protein initially coating the droplet surface, facilitating the adsorption and activity of lipase AN for triglyceride lipolysis.

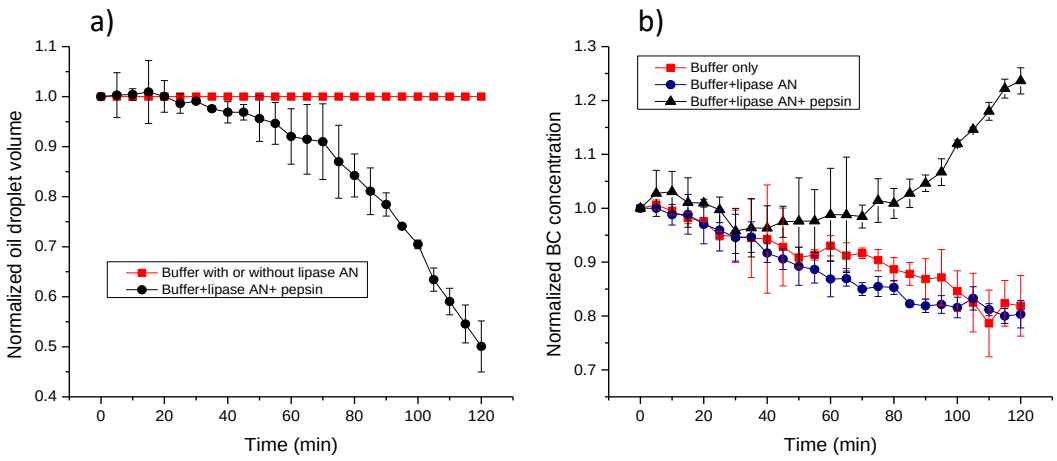

Fig. 5 a) Evolution of the normalized volume of TC droplets, and b) evolution of the normalized BC concentration inside TC droplets during gastric digestion with different gastric fluid compositions. In the cases of buffer with or without lipase AN, no change in droplet volume was observed.

Fig. 5b shows the evolution of BC concentration inside the TC droplets during the gastric phase. In the absence of pepsin (lipase AN or buffer only), as there was no change in droplet volume, the 20% decrease of BC concentration reveals a 20% degradation of BC. This result shows that this degradation is mostly due to the low pH condition (pH 3.0) during the gastric phase, as the addition of lipase AN has no significant effect on BC degradation. A 25% degradation of BC in emulsions during the gastric phase was reported by Kopec et al. (Kopec, Gleize, Borel, Desmarchelier, & Caris-Veyrat, 2017), regardless of the presence or absence of pepsin. In the case with lipase AN and pepsin, two different regions are observed, with a BC concentration decreasing trend during the first 40 min, followed by an increasing trend until the end of the gastric phase. During the first 40 min, there is almost no reduction of the droplet volume, thus the decrease of the BC concentration reveals the degradation of BC inside the oil droplet. The kinetics of BC degradation is similar than in the absence of pepsin, confirming the limited effect of pepsin on BC degradation. The region of increasing BC concentration is observed during the reduction of the droplet volume. In this region, it is likely that both BC degradation and BC release contribute to the kinetics.

In order to discriminate each contribution, we assumed that the degradation of BC in the presence of pepsin is similar to the case without pepsin (buffer+lipase AN). Thus, both BC degradation and BC total loss (degradation+release) could be calculated from the data presented in figs. 5a and 5b. Then, the BC release could be deduced. The evolutions of the normalized total loss and release of BC during the gastric phase are shown in fig. 6. This

result shows that BC release during the gastric phase is low (about 20%), occurring significantly only after 100 min. This was not expected as BC is highly hydrophobic and should only release in the presence of bile salt micelles. However, a similar result (up to 30% BC release) was reported in the case of highly stable MCT emulsions using decaglycerol monolaurate as the emulsifier (Liu, Hou, Lei, Chang, Gao, 2012). The absence of coalescence might explain the efficiency of the release, although another factor is needed, such as the possibility of tricaprylin lipolytic products (or decaglycerol monolaurate in Liu, Hou, Lei, Chang, Gao, 2012) to form micelles able to solubilize BC.

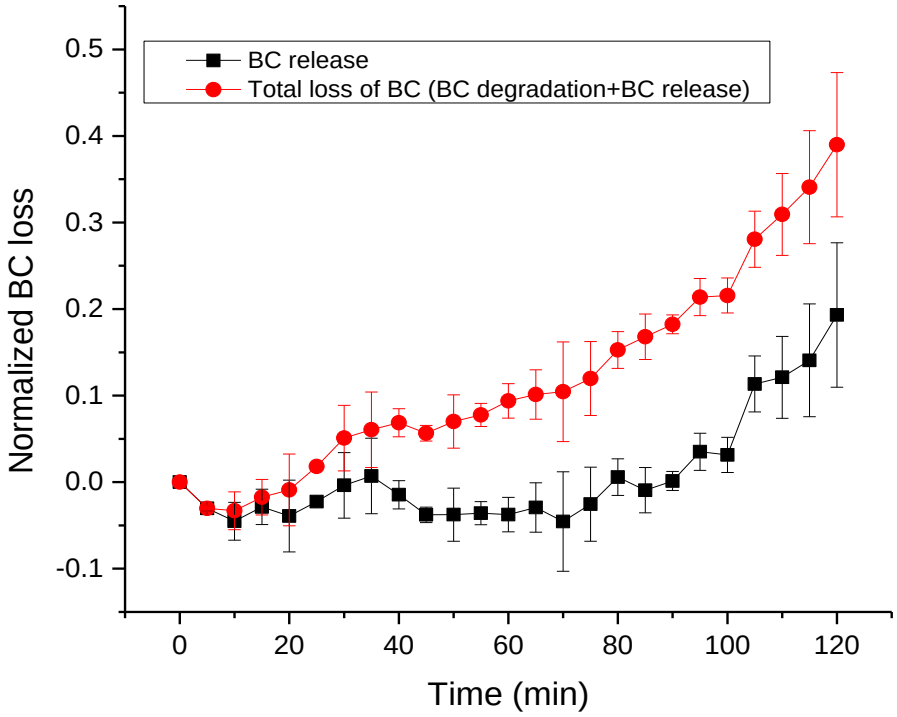

Fig. 6 Normalized BC total loss (BC degradation+BC release) and BC release during gastric digestion, in the case of buffer+ lipase AN+pepsin.

4. Conclusion

This work shows that the real-time kinetics of lipophilic bioactive molecules can be studied using droplet microfluidics, as monitored by confocal fluorescence microscopy. The design and fabrication of the setup were optimized to obtain a long hydrophilicity persistency of the channel surface, and to facilitate the oil droplet generation and trapping. The development of an open-close procedure of the outlets enabled the generation and trapping of oil droplets on a single chip, and solved the issue of flow instabilities by compensating for the high oil

viscosity. These results show the potential of immobilized oil droplets to screen the reactivity of lipophilic molecules. In the second article of this series and in subsequent works, the use of this lab on a chip platform will be extended to different edible oils and fat-soluble micronutrients. A comprehensive study of the degradation of antioxidant lipophilic molecules during the gastric phase will be carried out as well. The whole approach can be generalized to screen the reactivity of lipophilic molecules in the context of bioavailability studies which are conducted in nutrition, pharmacology, and toxicology.

References

Abate, A. R., Lee, D., Do, T., Holtze, C., & Weitz, D. A. (2008). Glass coating for PDMS microfluidic channels by sol-gel methods. *Lab on a Chip*, *8*(4), 516–518.

Desai, D., & Zaman, M. H. (2015). Continuous flow microfluidic solution for quantitative analysis of active pharmaceutical ingredient content and kinetic release. *Analytical Methods*, *7*(5), 1914–1923.

Favé, G., Coste, T. C., & Armand, M. (2004). Physicochemical properties of lipids: new strategies to manage fatty acid bioavailability. *Cellular and Molecular Biology (Noisy-Le-Grand, France)*, *50*(7), 815–831.

He, T., Liang, Q., Zhang, K., Mu, X., Luo, T., Wang, Y., & Luo, G. (2011). A modified microfluidic chip for fabrication of paclitaxel-loaded poly(l-lactic acid) microspheres. *Microfluidics and Nanofluidics*, *10*(6), 1289–1298.

Heus, F., Giera, M., De Kloe, G. E., Van Iperen, D., Buijs, J., Nahar, T. T., … Kool, J. (2010). Development of a microfluidic confocal fluorescence detection system for the hyphenation of nano-LC to on-line biochemical assays. *Analytical and Bioanalytical Chemistry*, *398*(7–8), 3023–3032.

Huebner, A., Bratton, D., Whyte, G., Yang, M., Demello, A. J., Abell, C., & Hollfelder, F. (2009). Static microdroplet arrays: A microfluidic device for droplet trapping, incubation and release for enzymatic and cell-based assays. *Lab on a Chip*, *9*(5), 692–698.

Huebner, A. M., Abell, C., Huck, W. T. S., Baroud, C. N., & Hollfelder, F. (2011). Monitoring a Reaction at Submillisecond Resolution in Picoliter Volumes. *Analytical Chemistry, 83*, 1462–1468.

Hunt, T. P., Issadore, D., & Westervelt, R. M. (2007). Integrated circuit/microfluidic chip to

programmably trap and move cells and droplets with dielectrophoresis. *Lab on a Chip*, *8*(1), 81–87.

Kopec, R. E., Gleize, B., Borel, P., Desmarchelier, C., & Caris-Veyrat, C. (2017). Are lutein, lycopene, and β-carotene lost through the digestive process? *Food and Function*, *8*(4), 1494–1503.

Lee, J., Teh, S. Y., Lee, A., Kim, H. H., Lee, C., & Shung, K. K. (2009). Single beam acoustic trapping. *Applied Physics Letters*, *95*(7), 2–4.

Li, Y., Kim, J., Park, Y., & McClements, D. J. (2012). Modulation of lipid digestibility using structured emulsion-based delivery systems: Comparison of in vivo and in vitro measurements. *Food and Function*, *3*(5), 528–536.

Liu,Y., Hou, Z., Lei, F., Chang, Y., & Gao, Y. (2012). Investigation into the bioaccessibility and microstructure changes of β-carotene emulsions during in vitro digestion. *Innovative Food Science and Emerging Technologies, 15*, 86–95.

Marquis, M., Renard, D., & Cathala, B. (2012). Microfluidic generation and selective degradation of biopolymer-based Janus microbeads. *Biomacromolecules*, *13*(4), 1197–1203.

Marze, S., Algaba, H., & Marquis, M. (2014). A microfluidic device to study the digestion of trapped lipid droplets. *Food Funct.*, *5*(7), 1481–1488.

Marze, S. (2015). Bioaccessibility of lipophilic micro-constituents from a lipid emulsion. *Food and Function*, *6*(10), 3218–3227.

Mata, A., Fleischman, A. J., & Roy, S. (2005). Characterization of polydimethylsiloxane (PDMS) properties for biomedical micro/nanosystems. *Biomedical Microdevices*, *7*(4), 281–293.

Mongersun, A., Smeenk, I., Pratx, G., Asuri, P., & Abbyad, P. (2016). Droplet Microfluidic Platform for the Determination of Single-Cell Lactate Release. *Analytical Chemistry*, *88*(6), 3257–3263.

Mutsokoti, L., Panozzo, A., Pallares Pallares, A., Jaiswal, S., Van Loey, A., Grauwet, T., & Hendrickx, M. (2017). Carotenoid bioaccessibility and the relation to lipid digestion: A kinetic study. *Food Chemistry*, *232*, 124–134.

Nik, A. M., Corredig, M., & Wright, A. J. (2011). Release of lipophilic molecules during in vitro digestion of soy protein-stabilized emulsions. *Molecular Nutrition and Food Research*,

55(SUPPL. 2), 278–289.

Paddock, S. W. (2000). Principles and Practices of Laser Scanning Confocal Microscopy. *Molecular Biotechnology*, *16*(2), 127–150.

Park, S. Y., & Chiou, P. Y. (2011). Light-driven droplet manipulation technologies for lab-on-a-chip applications. *Advances in OptoElectronics*, *2011*(1).

Šalić, A., Tušek, A., & Zelić, B. (2012). Application of microreactors in medicine and biomedicine. *Journal of Applied Biomedicine*, *10*(3), 137–153.

Salvia-Trujillo, L., Verkempinck, S. H. E., Sun, L., Van Loey, A. M., Grauwet, T., & Hendrickx, M. E. (2017). Lipid digestion, micelle formation and carotenoid bioaccessibility kinetics: Influence of emulsion droplet size. *Food Chemistry*, *229*, 653–662.

Scheuble, N., Iles, A., Wootton, R. C. R., Windhab, E. J., Fischer, P., & Elvira, K. S. (2017). Microfluidic Technique for the Simultaneous Quantification of Emulsion Instabilities and Lipid Digestion Kinetics. *Analytical Chemistry*, *89*(17), 9116–9123.

Schneider, M. H., Willaime, H., Tran, Y., Rezgui, F., & Tabeling, P. (2010). Wettability patterning by UV-initiated graft polymerization of poly(acrylic acid) in closed microfluidic systems of complex geometry. *Analytical Chemistry*, *82*(21), 8848–8855.

Tan, J., Xu, J. H., Li, S. W., & Luo, G. S. (2008). Drop dispenser in a cross-junction microfluidic device: Scaling and mechanism of break-up. *Chemical Engineering Journal*, *136*(2–3), 306–311.

Unger, M. A., Chou, H. P., Thorsen, T., Scherer, A., & Quake, S. R. (2000). Monolithic microfabricated valves and pumps by multilayer soft lithography. *Science*, *288*(5463), 113–116.

Wang, K., Lu, Y. C., Xu, J. H., & Luo, G. S. (2009). Determination of dynamic interfacial tension and its effect on droplet formation in the T-shaped microdispersion process. *Langmuir*, *25*(4), 2153–2158.

Weibel, D. B., Kruithof, M., Potenta, S., Sia, S. K., Lee, A., & Whitesides, G. M. (2005). Torque-actuated valves for microfluidics. *Analytical Chemistry*, *77*(15), 4726–4733.

Whitesides, G. M., Ostuni, E., Takayama, S., Jiang, X., & Ingber, D. E. (2001). Soft Lithography in Biology and Biochemistry. *Annual Review of Biomedical Engineering*, *3*(1), 335–373.

Windbergs, M., & Weitz, D. A. (2011). Drug Dissolution Chip (DDC): A microfluidic approach for drug release. *Small*, *7*(21), 3011–3015.

Žukauskas, A., Batavičiūtė, G., Ščiuka, M., Jukna, T., Melninkaitis, A., & Malinauskas, M. (2014). Characterization of photopolymers used in laser 3D micro/nanolithography by means of laser-induced damage threshold (LIDT). *Optical Materials Express*, *4*(8), 1601.

Supplementary material 1: Calibration curve for beta-carotene concentration and degradation due to the intestinal buffer at pH 7.0

A factor that may have an effect on the real-time measurement of fluorescence is BC degradation due to the repeated laser excitation at 488 nm. This figure shows the effect of a pulse excitation (500 ms pulse duration) repeated every 2 min on the fluorescence intensity of TC droplets with added 0.2 wt% BC. The measured fluorescence intensity decreased by 1% and 5% after 25 and 60 excitations (corresponding to 50 and 120 min), respectively. About 25 time points were used to cover the digestion kinetics, so by the end of the experiment, only 1% of the variation of the fluorescence intensity could be attributed to degradation, which was neglected.

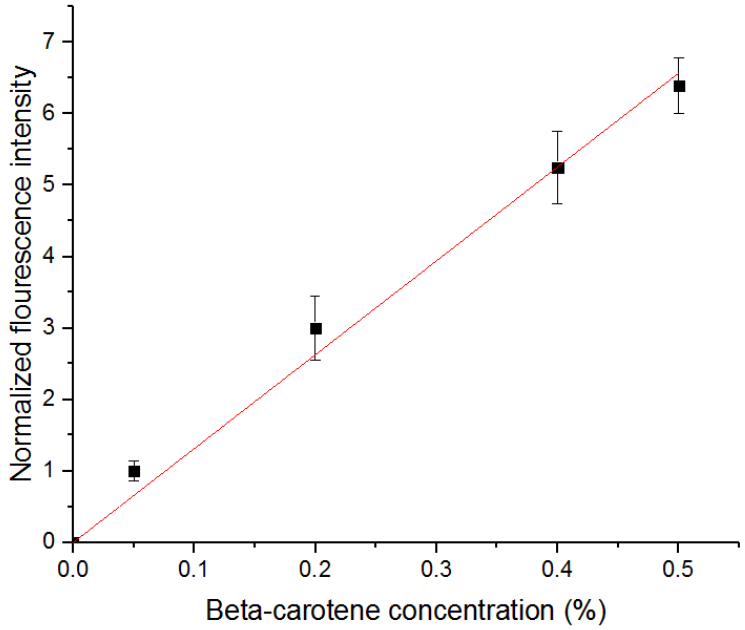

Calibration curve of the average fluorescence intensity in the TC droplets as a function of BC concentration (R^2=0.9902).

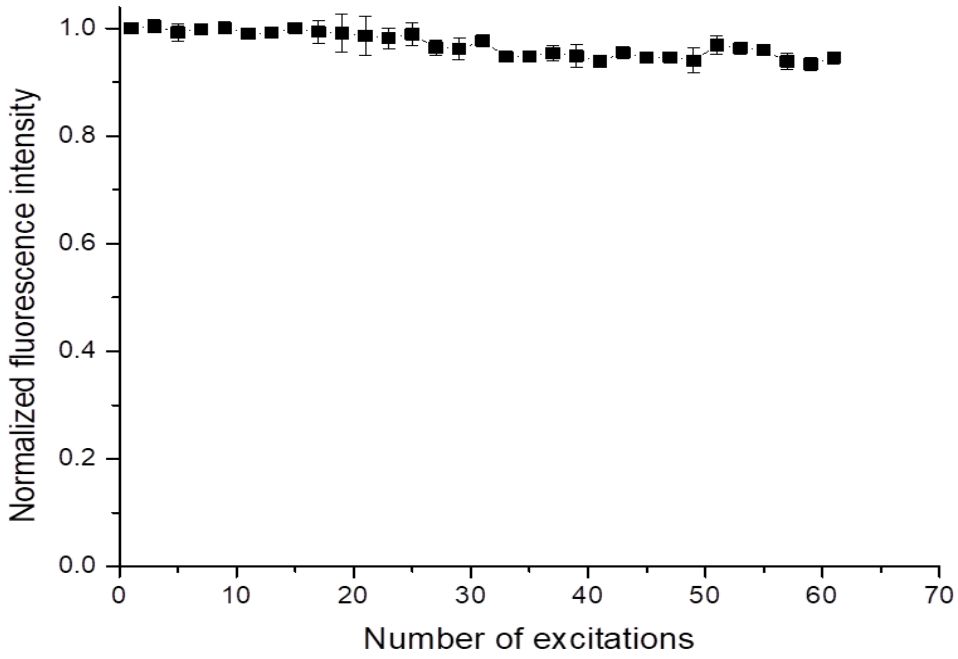

Evolution of the average fluorescence intensity in the TC droplets exposed to the intestinal buffer at pH 7.0 as a function of the number of laser excitations.

Supplementary material 2: Gastric coalescence effect on intestinal digestion

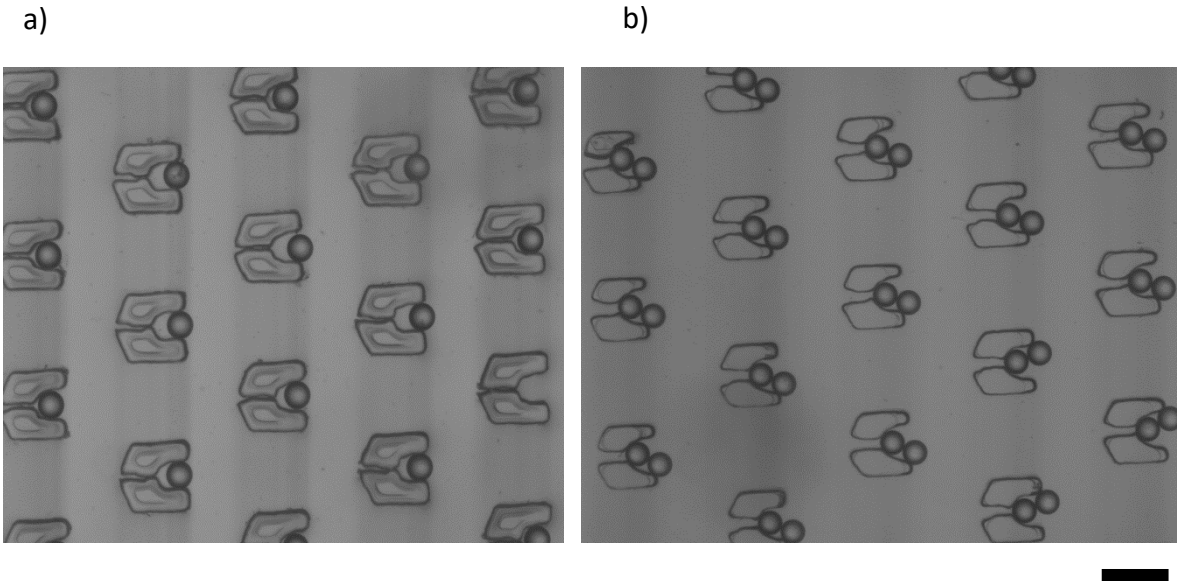

Fig. 1 Oil droplets trapped inside the chamber: a) Single droplet trapping, b) double droplet trapping. The scale bar represents 200 µm.

For this experiment, two droplets of 90 µm per trap were subjected to gastrointestinal digestion to test the effect of coalescence. A gastric phase (buffer+lipase AN+pepsin) of 60 min preceded the intestinal phase. Fig. 2a) shows the droplets at different times of gastrointestinal digestion. Coalescence occurred in some but not all traps near the end of the gastric phase. Thus intestinal digestion could be monitored simultaneously for both uncoalesced (diameter 90 µm) and coalesced (diameter 112 µm) droplets. Fig. 2b) shows the different kinetics of intestinal digestion in these two cases. The rate of volume decrease for the uncoalesced droplets is higher than that for the coalesced droplet (rate ratio of about 1.28). This is likely a surface area effect, as gastric coalescence caused the fusion of two droplets into a single larger droplet, reducing the surface area compared to separate droplets. The surface area is indeed reduced by a factor $2*(90/112)^2$, that is about 1.29, explaining the ratio between the rates of volume decrease.

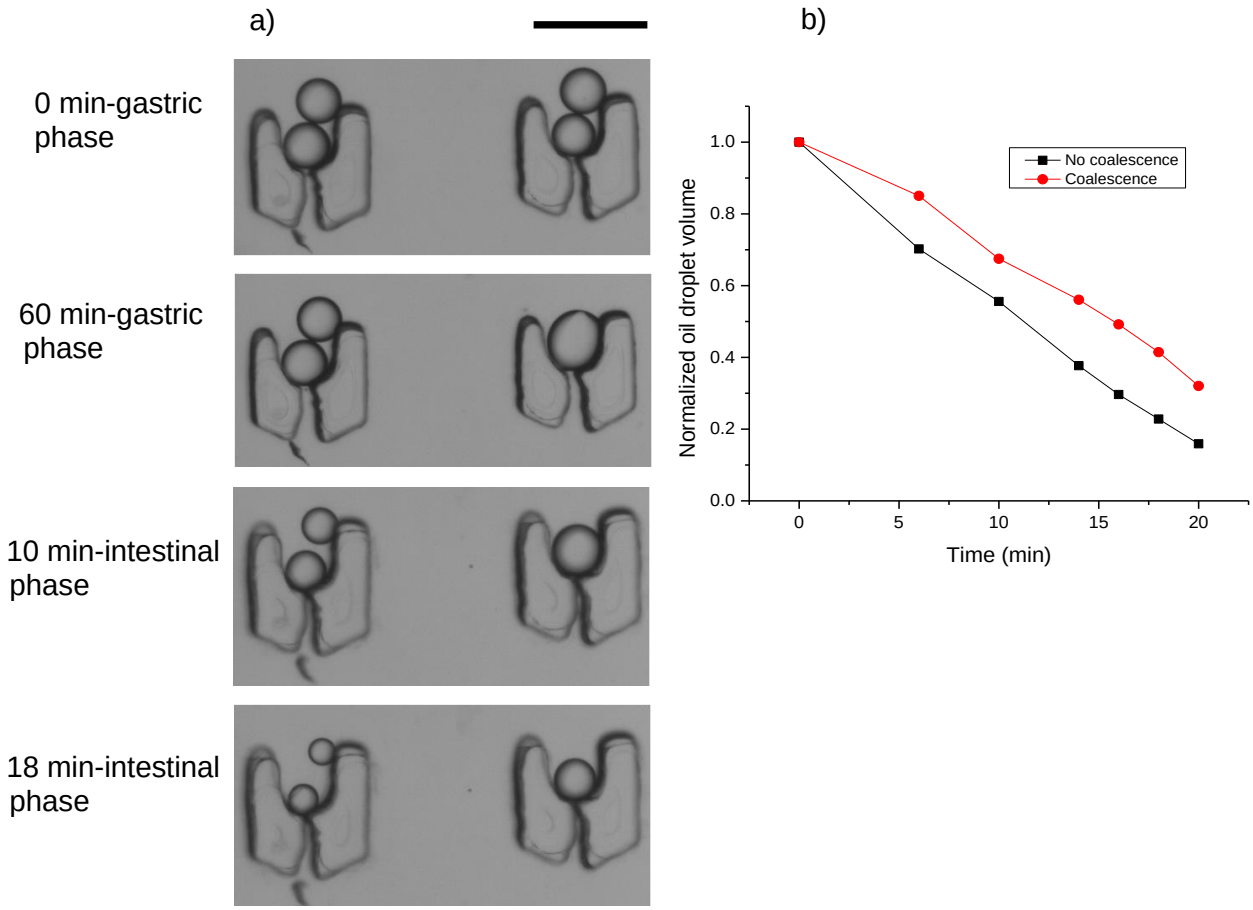

Fig. 2 a) Images of uncoalesced and coalesced droplets during gastrointestinal digestion, b) Evolution of the normalized volume of TC droplets during intestinal digestion (with or without coalescence during the gastric phase). The black scale bar is 200 µm.

Supplementary material 3: Effect of lipase concentration on the intestinal digestion of oil droplets

Oil droplets were subjected to intestinal digestion with lower lipase concentrations (0.1 mg mL^{-1}) to compare with the normal case of lipase concentration 4 mg mL^{-1}. Tricaprylin digestion with the two lipase concentrations is shown below. In the case of the low lipase concentration (0.1 mg mL^{-1}), a longer lag phase is observed at the beginning of the digestion. This lag phase likely represents the time needed to saturate the oil droplet surface with lipase. Thus, a lower lipase concentration results in a longer lag phase. When the curve for the lower lipase concentration (0.1 mg mL^{-1}) is shifted by 10 min (lag phase), both curves superimpose (see figure). This result means that as long as lipase saturates the droplet surface, lipid digestion proceeds with the same kinetics regardless of the lipase concentration in the digestive fluid.

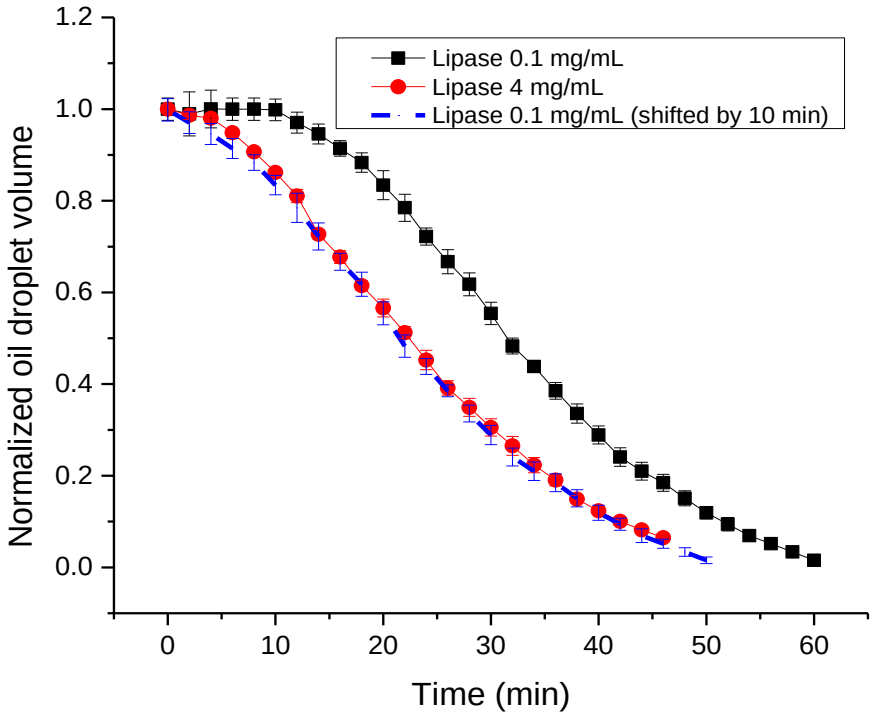

Effect of lipase concentration on intestinal digestion of TC oil droplets

Article 2: Studying the real-time interplay between triglyceride digestion and lipophilic micronutrient bioaccessibility using droplet microfluidics. 2 Application to various oils and (pro)vitamins

Hoang Thanh NGUYEN, Mélanie MARQUIS, Marc ANTON, Sébastien MARZE

Biopolymères Interactions Assemblages, INRA, 44300 Nantes, France

Abstract

The kinetics of micellar solubilization of lipophilic micronutrients (bioaccessibility) in relation with triglyceride digestion remains poorly known. To study this interplay in real-time, a droplet microfluidic method was designed and used as reported in the first part of this article series. In this second part, the interplay between the micellar solubilization of (pro)vitamins (beta-carotene or retinyl palmitate) and the digestion of triglyceride oils (tricaprylin TC, or high-oleic sunflower seed oil HOSO, or fish oil FO) during simulated gastrointestinal digestion was investigated. The relation between the release of both micronutrients and of triglyceride lipolytic products was found to be non-linear. The kinetics of beta-carotene was found to follow the kinetics of lipolytic products, depending on the oil type (TC > HOSO > FO). The effect of the gastric phase on the intestinal phase was also found to follow this order, mostly due to partial lipolysis during the gastric phase.

1. Introduction

Micronutrients (minerals, vitamins) are essential to maintain normal functions of human body. However, their absorption, especially that of lipophilic vitamins and carotenoids, is much more variable than that of macronutrients, due to biological and physicochemical factors (Patrick Borel, 2003). In the fat-soluble micronutrient class, vitamin A has received an intensive research attention due to its multiple functions in normal growth and development of human body. Vitamin A is notably involved in immune system maintenance, vision health and regulation of cell division (Grune et al., 2010; Haskell, 2012). Vitamin A is present in food in two forms: pre-formed vitamin A (mostly as retinyl palmitate) from animal sources, and provitamin A carotenoids (carotenes, beta-cryptoxanthin) from plant sources. Among provitamin A carotenoids, beta-carotene has the highest vitamin A activity thanks to its unique symmetrical structure (Grune et al., 2010; Haskell, 2012). Nevertheless, in order to achieve their vitamin activity, they need to be available in tissues (bioavailability), what requires many processes: i) release from the food matrix and incorporation in triglyceride droplets, ii) co-digestion with triglycerides, then co-solubilization into mixed micelles (bioaccessibility), iii) transport, processing, and secretion by intestinal cells iv) circulation in the lymph or blood system in lipoprotein. Among these processes, the micellar solubilization is an important prerequisite for transport. However, because fat-soluble micronutrients are

poorly soluble in the aqueous gastrointestinal environment, their bioaccessibility may be low and variable depending on many factors involving the food matrix structure and composition (Patrick Borel, 2003). Improving bioaccessibility is thus a strategy to enhance the bioavailability of these lipophilic micronutrients.

For the last couple of decades, many works based on *in vitro* digestion were carried out to study the bioaccessibility of beta-carotene in relation with triglyceride digestion (Huo, Ferruzzi, Schwartz, & Failla, 2007; Yi, Zhong, Zhang, Yokoyama, & Zhao, 2015). However, the interplay between the micellar solubilization of lipophilic micronutrients and of lipolytic products remains poorly known. For that matter, emulsion kinetic studies provided insights into the mechanisms of micellar solubilization of beta-carotene (Borel et al., 1996; Nik, Corredig, & Wright, 2011; Mutsokoti et al., 2017; Verkempinck et al., 2017). Better than a single end-point measurement, the release profile of bioactive molecules can be obtained by analyzing different incubation time points, but this is challenging due to difficulties in the control of experimental parameters using emulsion, the amount of materials needed, and the required high number of time points. Alternative approaches are scarce and the simultaneous real-time kinetics were established only once, using multiplex coherent Anti-Stokes Raman scattering microspectroscopy (Day, Rago, Domke, Velikov, & Bonn, 2010).

These issues can also be solved using droplet microfluidics. In the first part of this article series, we proposed a lab on a chip method enabling the simultaneous monitoring of beta-carotene and of tricaprylin lipolytic products in real time. In this second part, we extend this microfluidic approach to other oils and lipophilic micronutrients in order to understand their roles on the kinetic solubilization interplay. Three oils and two (pro)vitamins were tested separately, among which 5 systems were investigated. The full relation between the micellar solubilization of oil lipolytic products and of these micronutrients was established. The effect of the gastric phase on the subsequent intestinal phase was investigated as well.

2. Experimental Section

2.a. Materials

Pancreatic lipase (L3126, lipase from porcine pancreas type II, 1.7-8.3 U mg^{-1}), Amano lipase A (534781, lipase from Aspergillus niger, 12 U mg^{-1}, protease activity $\leq$ 2.5 U mg^{-1}), pepsin (P7012, pepsin from porcine gastric mucosa, 2500 U mg^{-1}), sodium glycodeoxycholate (G9910), tricaprylin TC (T9126), beta-carotene (22040), retinyl palmitate RP (R1512) were provided by Sigma-Aldrich. High-oleic sunflower seed oil HOSO was provided by Vandamme (Belgium). Fish oil FO (1050 TG) was provided by Polaris (France).

2.b. Droplet digestion and lipid monitoring

In this work, digestion of oil droplets containing an added micronutrient was performed using the same microfluidic method described in detail in the first part of this article series. Briefly, monodisperse oil droplets of 100 µm containing an added micronutrient were generated/immobilized in a lab on chip device and then subjected to a semi-dynamic gastrointestinal digestion in the same chip, with a continuous flow (and thus renewal) of the digestive fluids at a flow rate of 50 µL min^{-1}. The digestion of the trapped oil droplets was carried out under controlled temperature of 37 °C inside the digestion chamber, and monitored in real-time (2 min time steps) using a confocal fluorescence microscope (Nikon A1+) with a 10× objective. All optical parameters were optimized to obtain auto fluorescence intensity of the different micronutrients for quantitative analysis. A laser with an excitation wavelength of 488 nm and a channel with emission window of 500-530 nm were used to obtain the autofluorescence image of BC inside the oil droplets. A transmitted light image for the droplet size was obtained simultaneously using the same excitation beam. Due to its different absorption and emission properties compared to those of BC, a laser with an excitation wavelength of 375 nm and a channel with an emission window of 425-475 nm were used to obtain the autofluorescence image of RP. A transmitted light image for the droplet size was obtained simultaneously using the 488 nm laser already used for BC. The droplet size and fluorescence were measured by image analysis. Micronutrient concentration and release were calculated from these values using a fluorescence calibration curve as explained in the first part of this series.

The digestion was run with either an intestinal phase alone or a gastric phase followed by an intestinal phase. The intestinal fluid was prepared by mixing a buffer solution (100 mM NaH_2PO_4 adjusted to pH 7.0) with pancreatic lipase at 4 mg mL^{-1} and a bile salt (sodium glycodeoxycholate) at 5 mg mL^{-1}. When a gastric phase was performed prior to the intestinal phase, it was carried out for 2 hours with a gastric fluid prepared by mixing 0.03 mg mL^{-1} lipase from *Aspergillus niger* (lipase AN), and 0.6 mg mL^{-1} pepsin in a 100 mM KCl buffer adjusted to pH 3.0.

Three triglycerides composed of different fatty acids were tested: pure tricaprylin (TC, C8:0), or high-oleic sunflower seed oil (HOSO, mainly C18:1), or a fish oil rich in DHA (FO, mainly C22:6). Two micronutrients were tested separately (same initial concentration of 0.2 wt% in the oils): beta-carotene (provitamin A) or retinyl palmitate (preformed vitamin A). For each system, two to three independent digestions were conducted with the monitoring of seven individual droplets for each digestion. A distinct microfluidic device was used for each digestion to ensure identical initial conditions. The variability of the measurements was very low between the seven droplets monitored during one digestion, so the error bar (plotted as the standard deviation) represents the variability of the two to three independent digestions.

3. Results and discussion

3.a. Intestinal phase

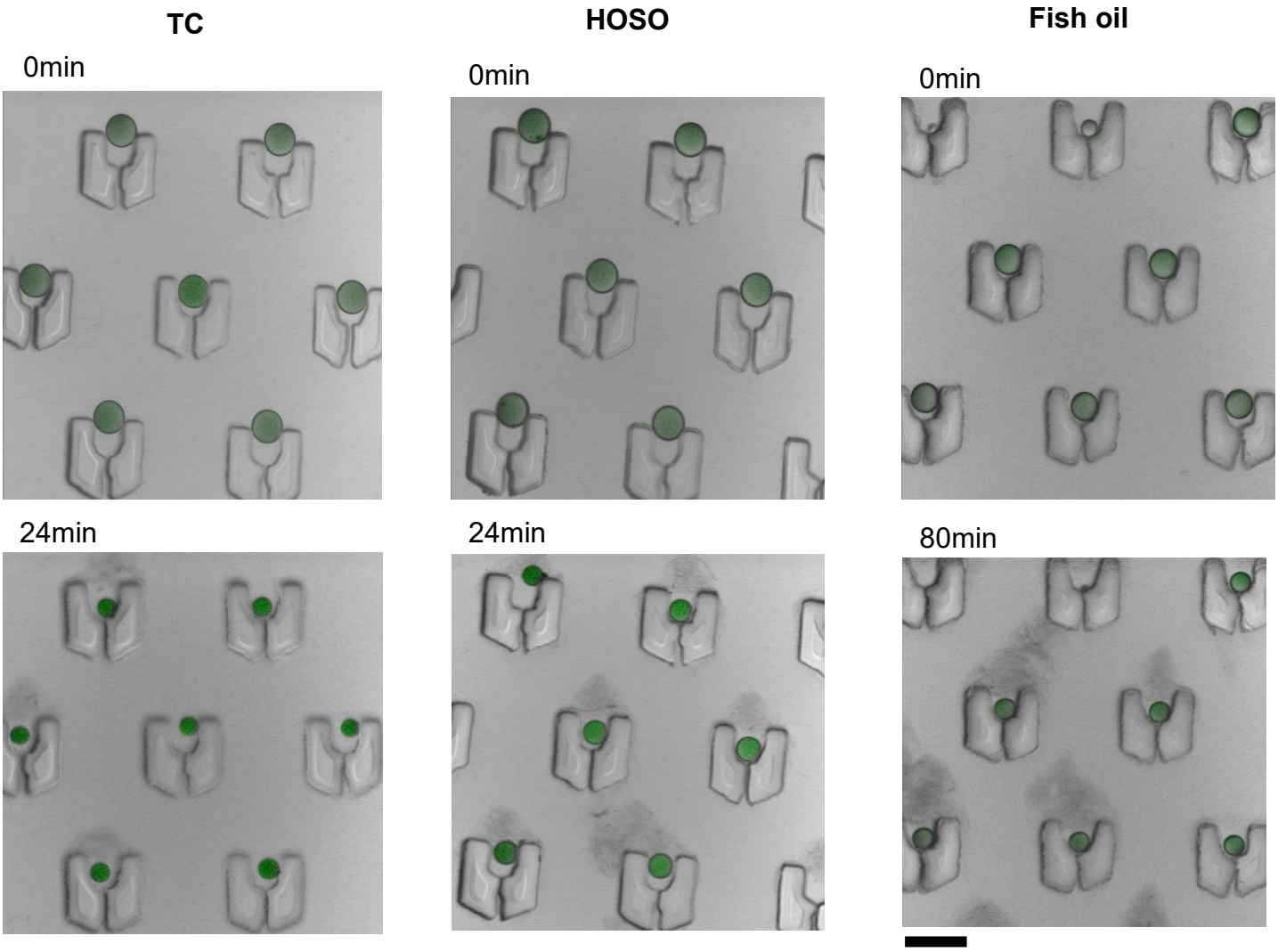

Fig. 1 Images of droplets containing beta-carotene for different oils (TC, HOSO, fish oil) at various intestinal digestion times. The scale bar represents 200 µm.

Digestion of TC, HOSO, and fish oil containing the same initial BC concentration (0.2 wt%) were conducted. Fig. 1 shows the evolution of droplet size and fluorescence for different oils during the intestinal digestion. The reduction of the droplet size comes from the lipolysis of triglycerides into free fatty acids and monoglycerides, which exit the droplet as they can solubilize in the aqueous bile salt micelles.

The digestion kinetics of the three oils is shown in fig. 2a. The fastest rate is found for TC and the slowest rate for fish oil. This is due to higher lipase activity and bile salt solubilization capacity for short saturated fatty acid chains (TC) compared to long polyunsaturated fatty acid chains (fish oil), as already reviewed (Marze, 2014). Calculations were done to quantify the free fatty acid (FFA) release rate during the intestinal digestion. The mathematical model is detailed in the supplementary material S1. Assuming the FFA release rate is proportional to the surface area of the oil droplet (Li & Mcclements, 2010; Marze & Choimet, 2012; Gaucel, Trelea, & Le Feunteun, 2015), the equation we used reads:

$$R(t) = R_0 \left(1 - \frac{k_S M_W}{2R_0 \rho} t\right) \qquad (1)$$

where k_s is the FFA release rate per unit droplet surface area (mol s^{-1} m^{-2}), ρ is the density of the triglyceride oil droplet (g m^{-3}), M_W is the molecular weight of the triglyceride oil (g mol^{-1}), t is the time (s), and R_0 is the initial radius of the oil droplet (m).

Note that a similar equation accounting for the total reaction volume is derived in the supplementary material S1. These models were systematically applied to pH-stat measurements of emulsion lipolysis. The comprehensive fitted release rates for microfluidic droplets and for emulsions are compared in the supplementary material S2.

The FFA release rate per droplet surface area was determined using eq. (1). The rates were of 41.2 ± 1.4, 13.2 ± 0.2, and 3.08 ± 0.01 µmol s^{-1} m^{-2} for TC, HOSO, and fish oil, respectively. These values are about 35% lower than those obtained previously using droplet microfluidics (Marze, Algaba, & Marquis, 2014), but when the rates are normalized to HOSO, the ratios are of 3.1 and 0.23 for TC and fish oil, respectively, which are close to the ratios of 2.5 and 0.21 normalized to olive oil (Marze et al., 2014). The absolute rate values are about one-two orders of magnitude higher than those for emulsions (Li, & McClements, 2010, Marze, & Choimet, 2012, supplementary material S2). This difference is likely due to the absence of coalescence in our droplet microfluidic approach, whereas coalescence reduces the surface area available for lipolysis and solubilization in the case of emulsions, what is not accounted for in the models (supposing no coalescence).

The digestion rate also depends on both the lipase specificity for the triglycerides and the capacity of the bile salt to remove the lipolytic products from the droplet surface (solubilization of lipolytic products). In general, the longer the fatty acid chain, the lower the lipase activity and the lower the solubilization capacity for the lipolytic products (Marze, 2014). Lipase activity is actually dependent on solubilization capacity, as lipolytic products accumulating at the droplet surface are known to inhibit further lipolysis (Pafumi et al., 2002). Hence, a lower solubilization capacity will induce a lower apparent lipolysis rate. In these microfluidic experiments, the continuous renewal of the intestinal fluid results in a large

excess of bile salts, thus lipolysis is likely the limiting step. This is confirmed by comparing the results of this single droplet study to emulsion lipolysis experiments with optimized bile salt concentrations (Marze, 2014). The relative rates normalized to HOSO (3.1 and 0.23 for TC and fish oil, respectively) are indeed in the same range.

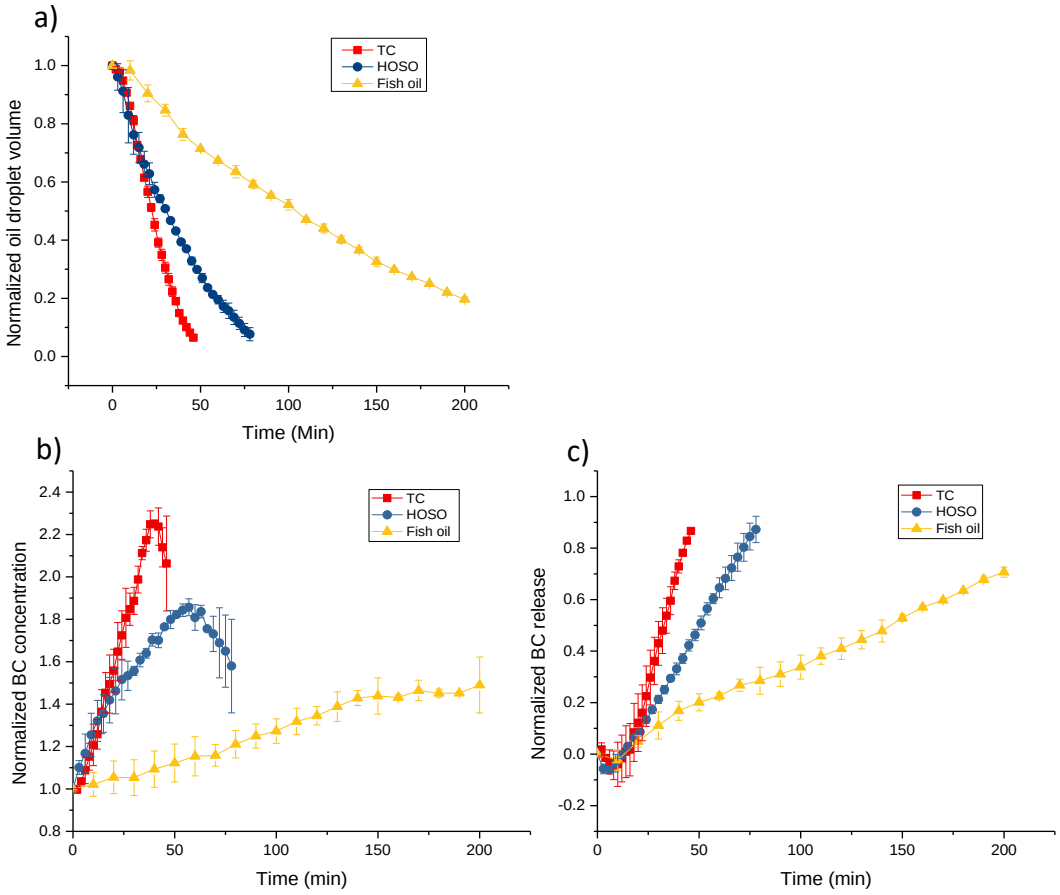

Fig. 2 a) Evolution of the normalized droplet volume, b) evolution of the normalized BC concentration inside the droplets, and c) evolution of BC proportion released from the droplets for different oils (TC, HOSO, Fish oil) during intestinal digestion.

In fig. 2b, the concentration of BC in the droplets during intestinal digestion for the three oils is reported. For TC and HOSO, BC concentration mainly increases during digestion, reaching a maximum and then decreases near the end of the digestion. For fish oil, the decreasing part was not observed due to a much longer digestion time. Such increasing trend for vitamin D3 concentration inside TC droplets was reported for emulsions, but no decrease was observed because the digestions were incomplete (Day et al., 2010). The increase of BC inside the oil droplets could be explained by the competition between BC and lipolytic products for solubilization into the bile salt micelles, knowing that their solubilization

capacity is much lower for beta-carotene and retinol (about 5.10^{-4} and 6.10^{-3} mol/mol, respectively) (El-Gorab, & Underwood, 1973), compared to fatty acids and monoglycerides (range 4.10^{-2} – 3.5) (Marze, 2014). Differences in the kinetics of BC concentration for the three oils are observed, as BC concentrates more in the droplets in the case of oils undergoing faster lipolysis.

The evolution of BC release as a function of intestinal digestion time is presented in fig. 2c. These results show that although BC concentration increases in the droplets, it is nevertheless significantly released in all cases. Thus the concentration increase is due to a slower BC release rate compared to the lipolytic products release rate. The maximal rates of BC release from the oil droplet per unit droplet surface area were calculated from the BC release and the droplet size data, of 0.57 ± 0.04, 0.25 ± 0.03, and 0.035 ± 0.008 µmol s^{-1} m^{-2} for TC, HOSO, and fish oil, respectively. The BC release rates were found to follow the same order as the lipolytic products release rates (TC > HOSO > FO). This is in agreement with many studies showing higher bioaccessibility of various lipophilic compounds from medium-chain triglycerides compared to long-chain triglycerides (Marze, 2015). For all three oils, much higher final BC bioaccessibility values (about 90% in the cases of the fully digested TC and HOSO) were found compared to values obtained for the static digestion of emulsions in the literature (Nik et al., 2011; Mutsokoti et al., 2017; Verkempinck et al., 2017). This is likely explained by the continuous renewal of the intestinal digestive fluid (semi-dynamic method), providing bile salt micelles that are not saturated with lipolytic products and BC constantly, in contrast with the static methods in which saturated bile salt micelles are not replaced. Note that a porcine bile extract containing various bile salts was also tested instead of the single bile salt, at the same total bile salt concentration. The kinetics were found to be significantly faster only in the case of TC, probably because all bile salts formed mixed micelles efficiently with medium-chain fatty acids and monoglycerides, as compared to long-chain ones (Marze, 2014).

As in the first article of this series, the relation between the micellar solubilization of BC and of the lipolytic products is shown in fig. 3. First, we observe that this relation is almost linear in the case of fish oil, but can be highly non-linear in the cases of TC and HOSO. The added black dash line represents the “balance” case in which the BC release equals the lipolytic products release (also named lipid release). All three curves lie below this black dash line, so the relative mass release of BC is always lower compared to that of lipids, hence the increase of the BC concentration inside the oil droplets observed in fig. 2b. Although the BC release rate ranks like the lipid release rate, that is TC > HOSO > FO, the reverse is true when BC mass release is compared to the lipid mass release. The curve of fig. 3 can be seen as a micronutrient release efficiency curve, where the closer the curve from the black dash line, the more efficient the triglyceride digestion is for BC release.

For retinyl palmitate, RP concentration trends inside the oil droplets and RP release were very similar to those for BC shown in figs. 2. The final RP release efficiency curves for two oils are compared to the case of BC in figs. 3b and 3c. The results show similar non-linear relations. A higher RP release efficiency compared to BC is observed in the first part of the digestion. However, this is only statistically significant in the case of HOSO due to much larger error bars for RP. These variations were explained by much larger fluctuations in the intensity of the 375 nm laser as compared to the 488 nm laser.

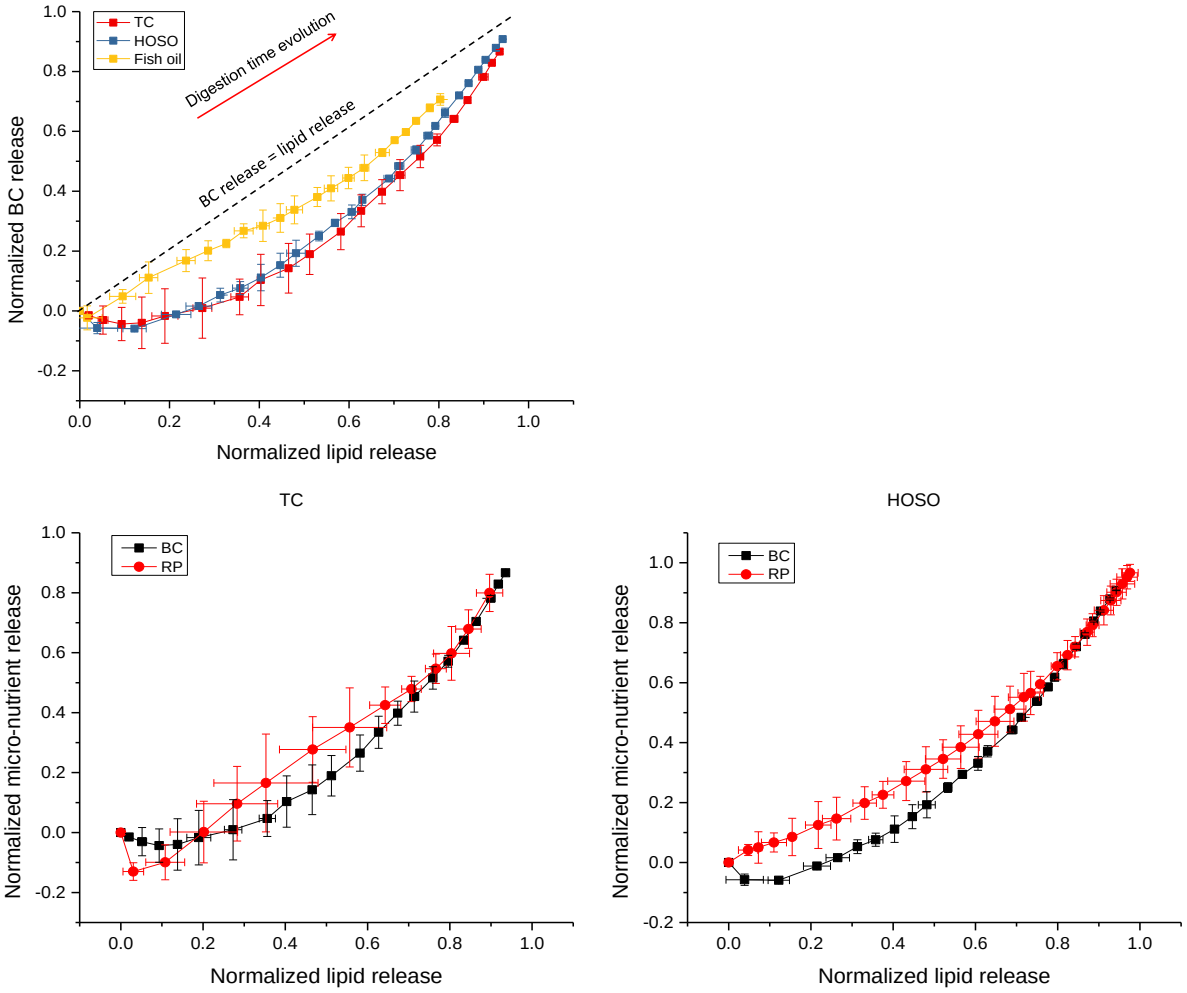

Fig. 3 a) Relation between the normalized mass release of BC and of lipids for different oils (TC, HOSO, fish oil), b) comparison between BC and RP release for TC, and c) comparison between BC and RP release for HOSO.

In the case of a fast initial lipolysis (TC and HOSO), the micronutrients must compete with more lipolytic products for solubilization in bile salt micelles. Thus, it leads to a low initial BC mass release. The curve for the fish oil is significantly different, showing that a slower initial lipolysis can induce a high initial BC mass release. In this case, there is more interplay between micronutrient release and lipid digestion, suggesting that cooperation prevails over competition. This is in agreement with the enhancement of the solubilization capacity of bile salt micelles by the formation of mixed micelles containing fatty acids and monoglycerides. This enhancement is indeed known to be much more efficient in the case of long polyunsaturated lipids compared to short saturated ones (Kossena, 2004). This could be understood on the basis of the formation of highly swollen mixed micelles accommodating large lipophilic molecules, or poorly swollen mixed micelles with lower solubilization capacity, respectively (Colle, 2012).

Similar to the case for TC discussed in the first article of the series, the BC release efficiency curve for HOSO was found to be non-linear with three different kinetic regimes. In contrast, strictly linear relations are often reported in emulsion digestion studies (Borel et al., 1996; Nik et al., 2011; Mutsokoti et al., 2017). This is likely due to the limited number of time points monitored using the emulsion approach. Indeed, most portions of the full efficiency curve will appear linear with scarce data points. In the contrary, very similar non-linear curves were obtained from agent-based simulations (Marze, 2014). In addition to the competition/cooperation interpretation, these simulations revealed that highly lipophilic molecules slowly diffuse inside the droplet. When the triglyceride digestion rate is slow, they statistically have enough time to reach the interface at the beginning of the digestion (ideal balance case and fish oil). When the triglyceride digestion rate is fast, they statistically reach the interface towards the end of the digestion, when the droplet size is small, hence the higher release in this regime.

3.b. Effect of the gastric phase

A gastric phase was added prior to the intestinal phase in order to investigate its effect. Fig. 4 shows the evolution of the normalized droplet volume as a function of digestion time during the gastric phase followed by the intestinal phase for the three oils. During the gastric phase, a decrease in the droplet volume was only observed for TC. Using eq. (1), the release rate of FFA per unit droplet surface area was calculated to be 9.7 ± 2.8 µmol s^{-1} m^{-2}, which is much lower than that during the intestinal phase (41.2 ± 1.4 µmol s^{-1} m^{-2}). These results are consistent with those reported by Marze et al., 2014 and can be explained by the much lower concentration of lipase AN compared to pancreatic lipase, and by the absence of bile salts in the gastric phase. The lipolytic products of TC have a sufficiently high aqueous solubility to be removed from the interface in the absence of bile salt micelles, allowing interfacial lipase

activity. In the contrary, the poorly water soluble lipolytic products of long-chain triglycerides (HOSO and fish oil) can actually not be solubilized in the aqueous phase and hence saturate the interface, allowing only partial lipolysis by inhibiting further lipase activity (Pafumi et al., 2002).

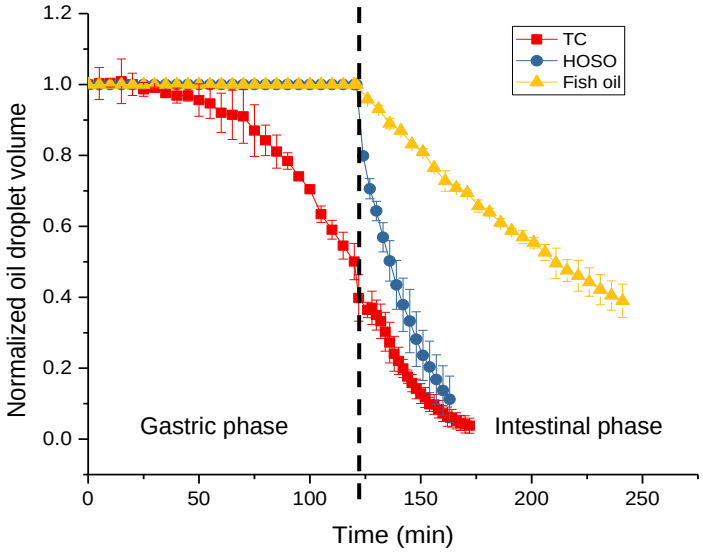

Fig. 4 Evolution of the normalized droplet volume for different oils (TC, HOSO, fish oil) as a function of digestion time, with a gastric phase before the intestinal phase.

In figs. 5, the evolution of the droplet volume during the intestinal phase (with or without a preceding gastric phase) is presented. It shows that the effect of the gastric phase depends on the oil. The shorter the chain length of the triglycerides is, the greater the effect. In the case of TC, the gastrointestinal digestion extent was always higher than the intestinal digestion alone, mainly due to the solubilization during the gastric phase. Indeed, when the droplet volume is renormalized at the start of the intestinal phase, the kinetics is only significantly faster at the beginning of the intestinal phase, with an initial steep decrease in the droplet volume. In the case of HOSO, an even steeper decrease is observed at the beginning of the intestinal phase following the gastric phase. This confirms that partial lipolysis occurred and lipolytic products accumulated at the droplet interface during the gastric phase, immediately removed by the bile salt micelles at the start of the intestinal phase, causing the steep decrease in the droplet volume. In the contrary, the gastric phase has almost no effect in the case of the fish oil. Those results are different from the ones reported by Marze et al., 2014, in which the gastric phase had no effect on the following intestinal phase. This contradiction can be explained by different experimental parameters

regarding the initial droplet size, the gastric fluid composition, and the gastric phase duration. In the current experiments, the initial droplet size was smaller (higher surface to volume ratio), pepsin was present in the gastric fluid, hydrolyzing the initial layer of beta-lactoglobulin, and the gastric phase duration was longer.

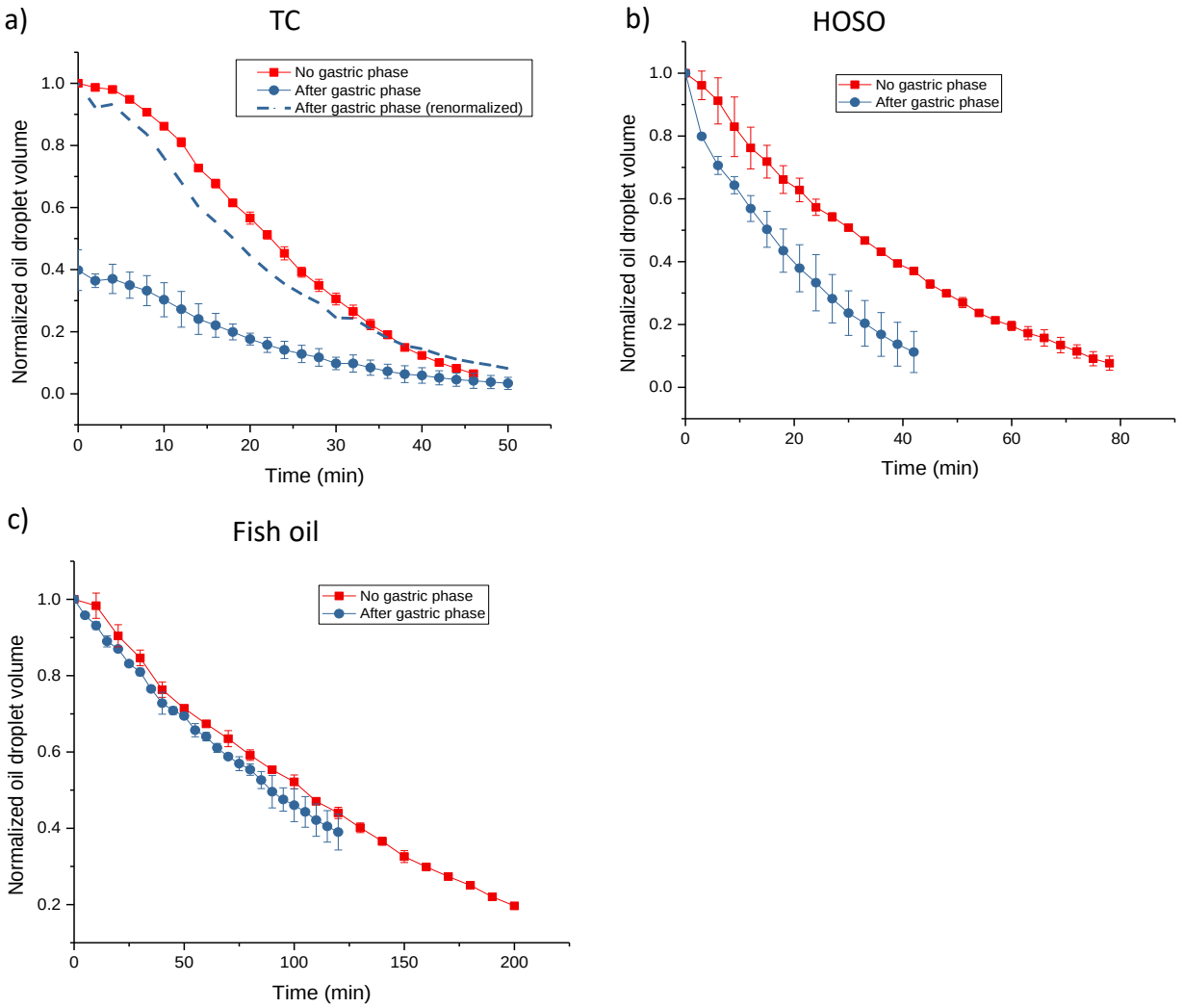

Fig. 5 Effect of the gastric phase on the intestinal phase of digestion for different oils: a) TC, b) HOSO, c) fish oil.

Figs. 6 show the effect of the gastric phase on the BC release from the oil droplets during the intestinal phase. For TC and HOSO, the BC release is significantly faster at the beginning of the intestinal phase when a preceding gastric phase was performed. For TC, this is likely due to the smaller size of the droplets, as discussed above. For HOSO, BC molecules could localize in clusters of lipolytic products at the droplet surface, as postulated by Pafumi et al., 2002 for long-chain lipids. When the intestinal phase starts, the bile salt micelles would

quickly solubilize these clusters, resulting in a fast release of both lipids and BC. For fish oil, no effect of the gastric phase on the BC release during the intestinal phase was observed.

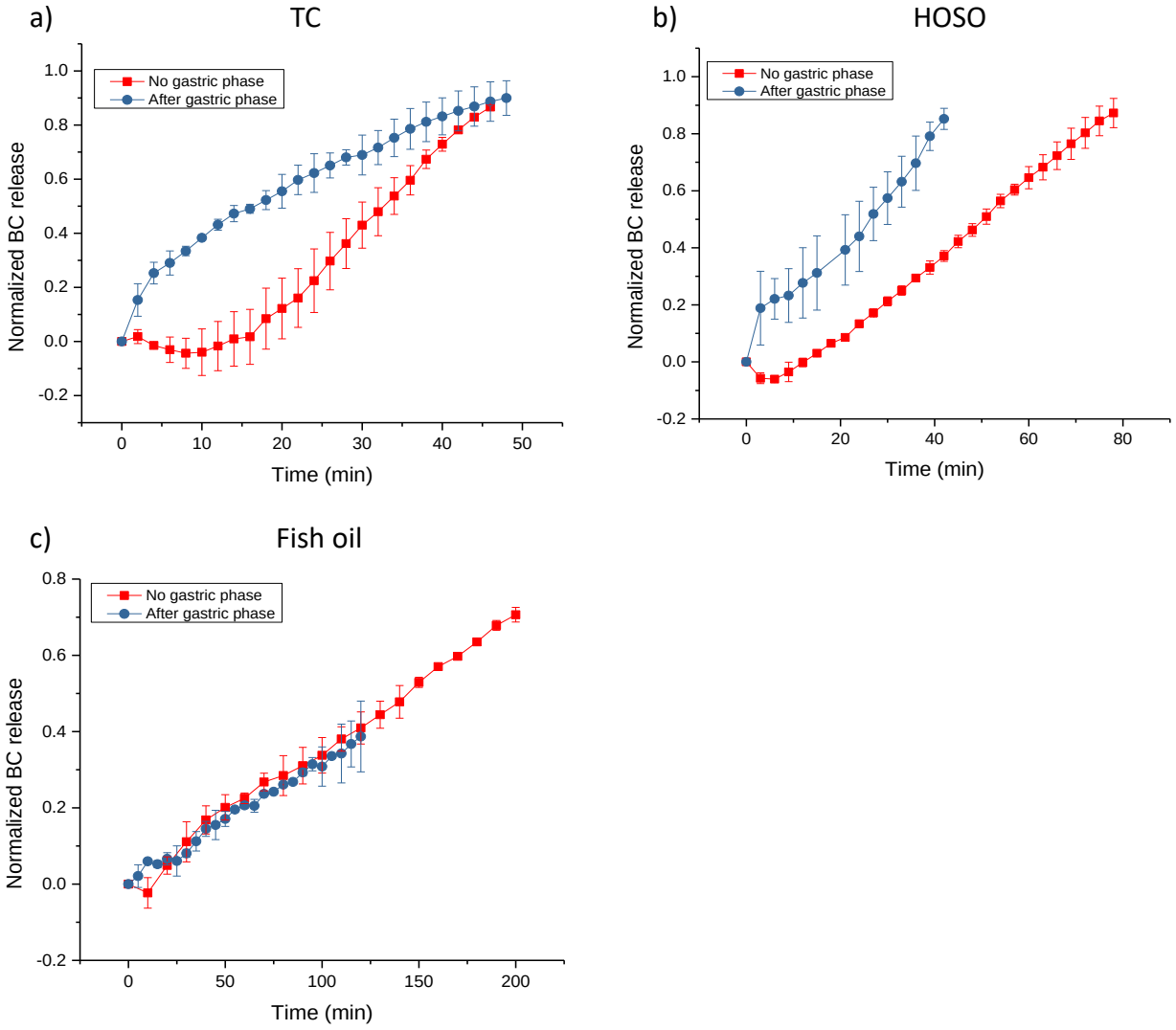

Fig. 6 Effect of the gastric phase on BC release from the droplets during the intestinal phase of digestion for different oils: a) TC, b) HOSO, c) fish oil.

Conclusion

The full kinetic relation between the release of micronutrients and the release of lipolytic products was found to be non-linear for both BC and RP. The bioaccessibility kinetics of both micronutrients depended on the type of fatty acid. BC added to the quickly digested oil (TC, with a short saturated fatty acid chain) presented a lower release efficiency compared to BC added in the slowly digested oil (fish oil, with long polyunsaturated fatty acid chains). The interplay between the bioaccessibility of micronutrients and the lipolysis of triglycerides was

interpreted on the basis of micellar solubilization competition/cooperation and of digestion/diffusion time comparisons. The effect of the gastric phase before the intestinal phase was also found to depend on the fatty acid type.

These results could be used to design delivery systems with controlled release properties based on the oil-micronutrient association. Overall, these results show the need for real-time kinetics studies of lipophilic micronutrients to provide insights about their fate in the gastrointestinal tract. This knowledge will enable a better understanding and improvement of the bioaccessibility of lipophilic micronutrients, and in turn could prove essential to control their bioavailability.

References

Borel, P. (2003). Factors affecting intestinal absorption of highly lipophilic food microconstituents (fat-soluble vitamins, carotenoids and phytosterols). *Clinical Chemistry and Laboratory Medicine*, *41*(8), 979–994.

Borel, P., Grolier, P., Armand, M., Partier, A., Lafont, H., Lairon, D., & Azais-Braesco, V. (1996). Carotenoids in biological emulsions: Solubility, surface-to-core distribution, and release from lipid droplets. *Journal of Lipid Research*, *37*(2), 250–261.

Colle, I. J. P., Van Buggenhout, S., Lemmens, L., Van Loey, A. M., & Hendrickx, M. E. (2012). The type and quantity of lipids present during digestion influence the in vitro bioaccessibility of lycopene from raw tomato pulp. *Food Research International*, *45*(1), 250–255.

Day, J. P. R., Rago, G., Domke, K. F., Velikov, K. P., & Bonn, M. (2010). Label-free imaging of lipophilic bioactive molecules during lipid digestion by multiplex coherent anti-stokes raman scattering microspectroscopy. *Journal of the American Chemical Society*, *132*(24), 8433–8439.

El-Gorab, M., & Underwood, B. A. (1973). Solubilization of beta-carotene and retinol into aqueous solutions of mixed micelles, *306*, 58–66.

Giang, T. M., Gaucel, S., Brestaz, P., Anton, M., Meynier, A., Trelea, I. C., & Le Feunteun, S. (2016). Dynamic modeling of in vitro lipid digestion: individual fatty acid release and bioaccessibility kinetics. *Food Chemistry*, *194*, 1180–1188.

Grune, T., Lietz, G., Palou, A., Ross, A. C., Stahl, W., Tang, G., … Biesalski, H. K. (2010). Beta-carotene is an important vitamin A source for humans. *The Journal of Nutrition*, *140*(12), 2268S–2285S.

Haskell, M. J. (2012). The challenge to reach nutritional adequacy for vitamin A: β-carotene bioavailability and conversion - Evidence in humans. *American Journal of Clinical Nutrition*, *96*(5), 1193S-1203S.

Huo, T., Ferruzzi, M. G., Schwartz, S. J., & Failla, M. L. (2007). Impact of fatty acyl

composition and quantity of triglycerides on bioaccessibility of dietary carotenoids. *Journal of Agricultural and Food Chemistry*, *55*(22), 8950–8957.

Kossena, G. A., Charman, W. N., Boyd, B. J., Dunstan, D. E., & Porter, C. J. H. (2004). Probing Drug Solubilization Patterns in the Gastrointestinal Tract after Administration of Lipid-Based Delivery Systems: A Phase Diagram Approach. *Journal of Pharmaceutical Sciences*, *93*(2), 332–348.

Li, Y., & Mcclements, D. J. (2010). New mathematical model for interpreting ph-stat digestion profiles: Impact of lipid droplet characteristics on in vitro digestibility. *Journal of Agricultural and Food Chemistry*, *58*(13), 8085–8092.

Marze, S., & Choimet, M. (2012). In vitro digestion of emulsions: Mechanistic and experimental models. *Soft Matter*, *8*(42), 10982–10993.

Marze, S. (2014). A coarse-grained simulation to study the digestion and bioaccessibility of lipophilic nutrients and micronutrients in emulsion. *Food Funct.*, *5*(1), 129–139.

Marze, S., Algaba, H., & Marquis, M. (2014). A microfluidic device to study the digestion of trapped lipid droplets. *Food Funct.*, *5*(7), 1481–1488.

Mutsokoti, L., Panozzo, A., Pallares Pallares, A., Jaiswal, S., Van Loey, A., Grauwet, T., & Hendrickx, M. (2017). Carotenoid bioaccessibility and the relation to lipid digestion: A kinetic study. *Food Chemistry*, *232*, 124–134.

Nik, A. M., Corredig, M., & Wright, A. J. (2011). Release of lipophilic molecules during in vitro digestion of soy protein-stabilized emulsions. *Molecular Nutrition and Food Research*, *55*(SUPPL. 2), 278–289.

Pafumi, Y., Lairon, D., De La Porte, P. L., Juhel, C., Storch, J., Hamosh, M., & Armand, M. (2002). Mechanisms of inhibition of triacylglycerol hydrolysis by human gastric lipase. *Journal of Biological Chemistry*, *277*(31), 28070–28079.

Yi, J., Zhong, F., Zhang, Y., Yokoyama, W., & Zhao, L. (2015). Effects of Lipids on in Vitro Release and Cellular Uptake of β-Carotene in Nanoemulsion-Based Delivery Systems. *Journal of Agricultural and Food Chemistry*, *63*(50), 10831–10837.

Supplementary material 1: Mathematical models for the FFA release

Calculations were done to quantify the free fatty acid (FFA) release rate during the intestinal digestion. Assuming the FFA release rate is proportional to the surface area of the oil droplet (Li & Mcclements, 2010; Marze & Choimet, 2012; Gaucel et al., 2015), the number of moles of FFA released from the droplet per unit time (mol s^{-1}) is written:

$$\frac{dN_{FFA}}{dt} = k_S S \quad (1)$$

where S is the droplet surface area (m^2), and k_s is the FFA release rate per unit droplet surface area (mol s^{-1} m^{-2}).

As the lipolysis of one triglyceride (TG) molecule releases two molecules of free fatty acid (and one molecule of monoglyceride):

$$\frac{dN_{FFA}}{dt} = -2\frac{dN_{TG}}{dt} \quad (2)$$

where $\frac{dN_{TG}}{dt}$ is the number of moles of TG lost from the oil droplet per unit time due to lipolysis and solubilization, with N_{TG} the number of TG moles in the oil droplet (mol).

From eqs (1), (2) we have

$$k_S S = -2\frac{dN_{TG}}{dt} \quad (3)$$

The number of TG moles can be related to the droplet volume as:

$$N_{TG} = \frac{V\rho}{M_W} \quad (4)$$

where V is the volume of the triglyceride oil droplet (m^3), ρ is the density of the triglyceride oil droplet (g m^{-3}), assumed to be constant throughout digestion, and M_W is the molecular weight of the triglyceride oil (g mol^{-1}).

From eqs. (3) and (4), we have:

$$k_S S = -2\frac{\rho}{M_W}\frac{dV}{dt} \quad (5)$$

as $S = 4\pi R^2$ and $V = \frac{4}{3}\pi R^3$, R being the radius of the oil droplet (m). Substituting S and V in eq. (5) leads to:

$$k_S 4\pi R^2 = -2\frac{\rho}{M_W}\frac{dV}{dR}\frac{dR}{dt} = -2\frac{\rho}{M_W}4\pi R^2\frac{dR}{dt} \qquad (6)$$

Simplifying eq. (6) leads to:

$$k_S = -2\frac{\rho}{M_W}\frac{dR}{dt} \qquad (7)$$

for which a solution can be calculated to be:

$$R(t) = R_0\left(1 - \frac{k_S M_W}{2R_0\rho}t\right) \qquad (8)$$

For N_{FFA} (t), a solution was calculated in the literature (Li & Mcclements, 2010; Marze & Choimet, 2012; Gaucel et al., 2015):

$$N_{FFA}(t) = 2N_{TG,total}\left[1 - \left(1 - \frac{k_S M_W}{2R_0\rho}t\right)^3\right] \qquad (9)$$

Assuming the FFA release rate is proportional to the surface area of the oil droplet per unit total reaction volume (specific surface area), eqs. (8) and (9) can be rewritten as:

$$R(t) = R_0\left(1 - \frac{k_{SV} M_W}{2R_0\rho V_T}t\right) \qquad (10)$$

$$N_{FFA}(t) = 2N_{TG,total}\left[1 - \left(1 - \frac{k_{SV} M_W}{2R_0\rho V_T}t\right)^3\right] \qquad (11)$$

where V_T is the total reaction volume (m^3), that is the volume of both the oil and the aqueous phases, and k_{sv} is the FFA release rate per unit specific droplet surface area (mol m s^{-1}).

References

Li, Y., & Mcclements, D. J. (2010). New mathematical model for interpreting ph-stat digestion profiles: Impact of lipid droplet characteristics on in vitro digestibility. Journal of Agricultural and Food Chemistry, 58(13), 8085–8092.

Marze, S., & Choimet, M. (2012). In vitro digestion of emulsions: Mechanistic and experimental models. Soft Matter, 8(42), 10982–10993.

Gaucel, S., Trelea, I. C., & Le Feunteun, S. (2015). Comment on New Mathematical Model for Interpreting pH-Stat Digestion Profiles: Impact of Lipid Droplet Characteristics on in Vitro Digestibility, 3(4), 4–5.

Supplementary material 2: pH-stat measurements for emulsions

The digestion degree of emulsions was measured by the pH-stat method with buffer and ionization corrections (Chatzidaki et al., 2016).

Emulsions (2 wt% oil) of different oils (TC or HOSO or fish oil) were prepared. The aqueous phase (2 mg mL^{-1} beta-lactoglobulin) was prepared by mixing the protein in 10 mM NaH_2PO_4 buffer solution (pH 7.0) for 30 min at room temperature. A rotor-stator homogenizer (Silent Crusher M, Heidolph Instruments, Germany) was used for a pre-emulsification step (2 min, 16000 rpm). Then, a fine emulsion was obtained by sonication (Misonix Sonicator 4000, Qsonica, USA) applied for 3 cycles of 1 min (total energy 2100 J). A 2 min cooling time was applied between each cycle. The droplet size distributions of the emulsions were measured using dynamic light scattering (Zetasizer Nano ZS, Malvern Instruments, UK) equipped with a He-Ne laser of wavelength 633 nm. The volume-based mean droplet diameters were found to be of 265±38, 313±43, and 351±48 nm for TC, HOSO, and fish oil emulsions, respectively.

Emulsions were diluted 2 fold with a gastric buffer solution (130 mM NaCl, 1.6 mM $CaCl_2.(H_2O)_2$, pH 3.0) to mimic the gastric dilution. The digestion was started by diluting the gastric emulsion 2 fold in the intestinal fluid (130 mM NaCl, 1.6 mM $CaCl_2.(H_2O)_2$, pH 7.0) containing 0.2 mg mL^{-1} pancreatic lipase (L3126) and 20 mg mL^{-1} bile extract (B8631, about 50 wt% bile salts). FFA release was measured in duplicate with a pH-stat titrator at 37 °C (TitraLab 90, Radiometer, Denmark). The results are shown in the figure below.

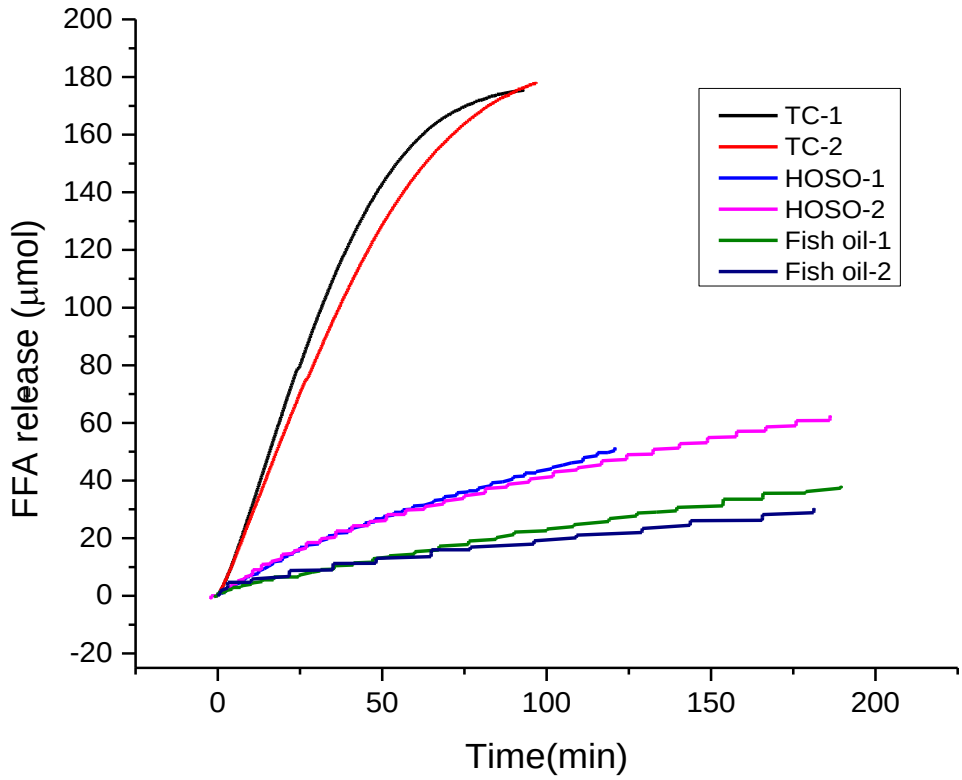

FFA release during intestinal digestion for different oils in emulsion, measured by the pH-stat method.

By fitting these data with eq. (9) of supplementary material S3, we obtained the FFA release rate per unit surface area, which we compared to the values obtained for the microfluidic experiments (table 1). The values for the pH-stat are in good agreement with our previous results (Marze, & Choimet, 2012), but much lower than those reported by Li and McClements (2010). This is likely related to the much lower concentrations of lipase and calcium we used compared to these authors. It is indeed known that the lipolysis rate is increased by both lipase and calcuim concentrations. The pH-stat values are also much lower than the microfluidic values. As already discussed, this can be due to a coalescence process for emulsions, but it is unlikely to explain alone such a large difference.

Table 1: FFA release rate per unit surface area of the oil droplets.

Oil	FFA release rate by the pH-stat method (µmol s^{-1} m^{-2})	FFA release rate by the microfluidic method (µmol s^{-1} m^{-2})
TC	$68\times10^{-3} \pm 7\times10^{-3}$	41.2 ± 1.4
HOSO	$10.5\times10^{-3} \pm 0.8\times10^{-3}$	13.2 ± 0.2
Fish oil	$5.1\times10^{-3} \pm 0.8\times10^{-3}$	3.08 ± 0.01

The pH-stat data were also fitted with eq. (11) of supplementary material S3 to evaluate the effect of the total reaction volume. The FFA release rate per unit specific surface area are compared in table 2 with the values fitted for the microfluidic experiments using eq. (10). The values are now much closer (related by a factor 2.4, or in the same range for HOSO). It is thus clear that the total reaction volume is an essential parameter to compare experiments at different scales.

Table 2: FFA release rate per unit specific surface area of the oil droplets.

Oil	FFA release rate by the pH-stat method (µmol µL s^{-1} m^{-2})	FFA release rate by the microfluidic method (µmol µL s^{-1} m^{-2})
TC	544 ± 56	226.6 ± 7.7
HOSO	84.0 ± 6.4	72.6 ± 1.1
Fish oil	40.8 ± 6.4	16.94 ± 0.06

Finally, we analyzed the pH-stat data by the standard enzyme activity calculation, using the initial maximal slope (µmol min^{-1}) of the FFA release curve, normalized by the mass of lipase in the reaction volume (µmol FFA min^{-1} mg^{-1} lipase, usually abbreviated to U mg^{-1}). The value of 0.84 U mg^{-1} for HOSO is about 2 fold lower than the minimal value reported by the manufacturer for olive oil. This result is nevertheless reasonable as the protocol of the manufacturer (Sigma) is unknown except for the pH which is 7.7, but overall should be similar.
Knowing the total number of moles of TG in the reaction volume, we also calculated a maximal molar percentage (% min^{-1}) of FFA release from the initial maximal slope. To compare with the microfluidic data, we derived an equation based on the same assumption:

$$\frac{dN_{FFA}}{dt} = kN_{FFA,total} = -2\frac{dN_{TG}}{dt} = -2kN_{TG,total} \quad (1)$$

As $N_{TG,total} = \frac{V_0 \rho}{M_W}$, then we have:

$$\frac{dV}{dt} = kV_0 \quad (2)$$

which we can integrate to find:

$$V(t) = V_0(1 - kt) \quad (3)$$

where *k* is the FFA release rate (in min^{-1}). Eq. (3) was used to fit the maximal slope in the decrease of the normalized droplet volume, multiplied by 100 to obtain the value in % min^{-1}. The maximal BC release rate was also calculated by using the maximal slope of the normalized release curve, converted to % min^{-1}. The results are given in table 3, showing that this simple model, although not representing correctly the release curves that are not strictly linear, reconciles the data for both experiments. This means that the release rate in mol min^{-1} can be seen as driven by the total amount of TG, faster for a higher amount. The maximal BC release is also found to have similar values in % min^{-1}, not significantly different from those for FFA in the microfluidic experiments. Although the whole real-time kinetics of FFA and BC release were found to be distinct, using the maximal rate values confirms that some specific regimes obey the same kinetics.

Table 3: Maximal lipase activity and FFA release rate for the pH-stat experiments, FFA and BC release rates for the microfluidic experiments.

Oil	Maximal lipase activity by the pH-stat method (µmol FFA min^{-1} mg^{-1} lipase)	Maximal FFA release rate by the pH-stat method (% min^{-1})	Maximal FFA release rate by the microfluidic method (% min^{-1})	Maximal BC release rate by the microfluidic method (% min^{-1})
TC	3.7 ± 0.3	1.8 ± 0.2	2.8 ± 0.2	3.0 ± 0.4
HOSO	0.84 ± 0.01	0.71 ± 0.01	1.3 ± 0.2	1.42 ± 0.02
Fish oil	0.27 ± 0.03	0.38 ± 0.03	0.45 ± 0.07	0.55 ± 0.15

References

Li, Y., & Mcclements, D. J. (2010). New mathematical model for interpreting ph-stat digestion profiles: Impact of lipid droplet characteristics on in vitro digestibility. *Journal of Agricultural and Food Chemistry*, *58*(13), 8085–8092.

Marze, S., & Choimet, M. (2012). In vitro digestion of emulsions: Mechanistic and experimental models. *Soft Matter*, *8*(42), 10982–10993.

Chatzidaki, M. D., Mateos-Diaz, E., Leal-Calderon, F., Xenakis, A., & Carrière, F. (2016). Water-in-oil microemulsions versus emulsions as carriers of hydroxytyrosol: an in vitro gastrointestinal lipolysis study using the pHstat technique. *Food Funct.*, *7*(5), 2258–2269.

Mutsokoti, L., Panozzo, A., Pallares Pallares, A., Jaiswal, S., Van Loey, A., Grauwet, T., & Hendrickx, M. (2017). Carotenoid bioaccessibility and the relation to lipid digestion: A kinetic study. Food Chemistry, 232, 124–134.

4 ADDITIONAL PRELIMINARY RESULTS

4.1 Optimization of the junction for oil droplet size control

In the first microfluidic device design, oil droplets were generated by a single flow focusing junction (FFJ). 130 µm oil droplets were generated at a high W/O (water to oil) flow rate ratio of 300:2 µL min^{-1}. When the desired droplet size was achieved, oil droplets were guided to the trapping chamber by connecting the outlet of the FFJ chip to the inlet of the chamber chip using a PTFE tube as shown in fig. 4.1 (Marze et al., 2014). This design brought up several weaknesses:

- The generation of oil droplets at a high flow rate of the aqueous phase makes the system more susceptible to hydrodynamic resistance gradients. The connection of the PTFE tube increased the hydrodynamic resistance, breaking the flow equilibrium, especially at such a high flow rate. This equilibrium breaking could result in a polydisperse size distribution of the oil droplets (shown in fig. 4.2a).

- It was more likely to get air bubbles appearing inside the chamber due to manual disconnection/connection processes. The air bubbles could quickly develop during digestion and compromise the experiment (shown in fig. 4.2b).

In this PhD study, we wanted to generate oil droplets of a smaller size (≤ 100 µm) at a lower flow rate in order to serve several purposes:

- Smaller droplets allow more droplets to be observed in the same field of view.

- This allows the testing of the droplet size as a parameter.

- A lower flow rate stabilizes the oil droplet generation during the device operation.

However, due to the high viscosity of the oil compared to that of water, it was not an easy task to reduce the size of the oil droplets. Several methods for the reduction of the droplet size were tested, including increasing the water phase viscosity, adding a droplet splitting junction, and modifying the junction geometry. Besides these experimental approaches, device optimization was guided using numerical simulation with a commercial software suite (Comsol multiphisics v5.1). For the numerical simulation, the water phase parameters were taken from the library of the software. The parameters for the TC (C8:0) phase (density, dynamic viscosity) were estimated using the formula proposed by Goodrum et al. at 20 °C (Goodrum & Eiteman, 1996). The level set method was used for the simulation.

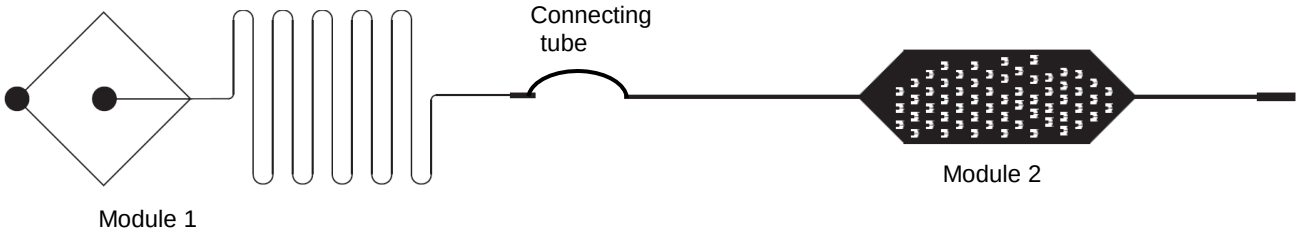

Fig. 4.1 Scheme design of the first model connecting the FFJ chip and the chamber chip.

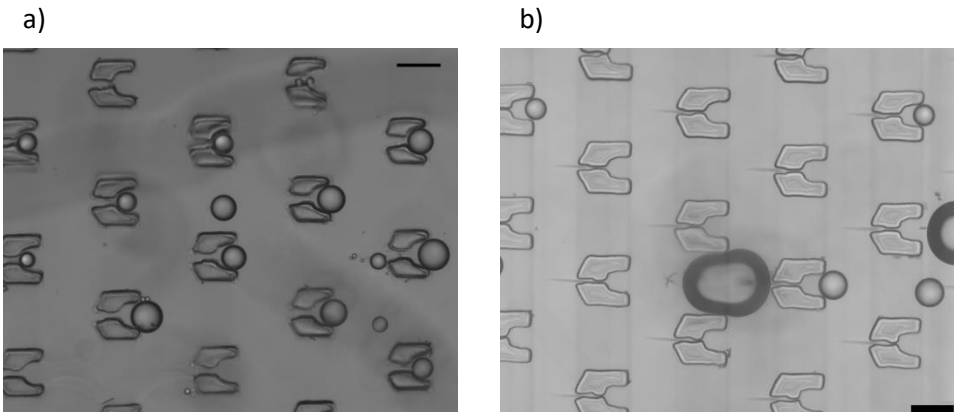

Fig. 4.2 a) Droplets trapped into the chamber, b) Air bubbles inside the chamber (the black bar scale is 200 µm).

4.1.1 Reducing droplet size by increasing the viscosity of the water phase

One of the reasons that make it so difficult to reduce the size of oil droplets is the much higher viscosity of the oil phase compared to that of the water phase. Thus, the oil droplet size should in principle be decreased by increasing the viscosity of the continuous water phase. Thus, glycerol was added to manipulate the viscosity of the continuous phase (Xu et al., 2006). Glycerol was added to pure water (dynamic viscosity of 1 mPa.s at 20 °C) to obtain a viscosity of the aqueous continuous phase of 6.1 mPa.s at 50 %wt glycerol in water. TC oil droplets were generated by the FFJ shown in fig. 4.3a. The oil droplet size was compared to the case of pure water. Fig. 4.3b shows the dependence of oil droplet size on the W/O flow rate ratio. In the first device, adding glycerol did not help reducing the size of the oil droplet. In the contrary, a slight increase of the droplet size was observed in the case of water with 50 %wt glycerol. The limited effect of the continuous phase viscosity could be explained by the breakup principle of the squeezing regime. In this work, the oil droplet was generated by the squeezing regime at small capillary number Ca. As the oil phase passes

through the “throat” region, the blockage of the continuous phase at the contraction part causes a large pressure upstream that pinches off an oil droplet. Thus, the droplet breakup is dominated by the pressure drop at the contraction. On the contrary, in the dripping regime at higher capillary number (normally in water in oil or air bubble in fluid generation or at high flow rate of the continuous phase), the shear stress dominates the breakup of the droplet. In this regime, the droplet size is smaller than the size of the contraction region, hence eliminating pressure drop involved in the droplet breakup. In the dripping regime, the droplet size is more influenced by the viscosity of the continuous phase (Jamalabadi et al., 2017).

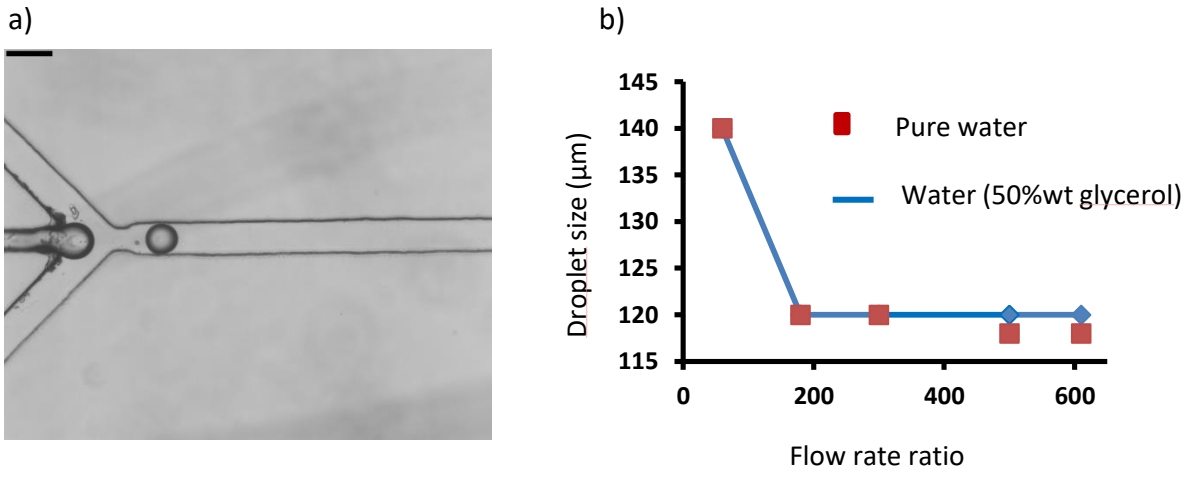

Fig. 4.3 a) FFJ geometry for TC droplet generation, the black scale bar is 200 µm, b) dependence of the droplet size on the W/O flow rate ratio of continuous phase to dispersed phase in the cases of glycerol in water or pure water.

4.1.2 Reducing droplet size using a dividing branch junction

Another way to reduce the size of the droplet is to use a droplet splitting junction (Abate & Weitz, 2011). A splitting junction was added after the FFJ in order to divide one oil droplet into two smaller droplets. Fig. 4.4 shows the numerical simulation of oil droplets split into smaller droplets at a splitting junction. The original oil droplet generated by a FFJ compresses as it enters a smaller channel and is finally divided into two identical smaller droplets.

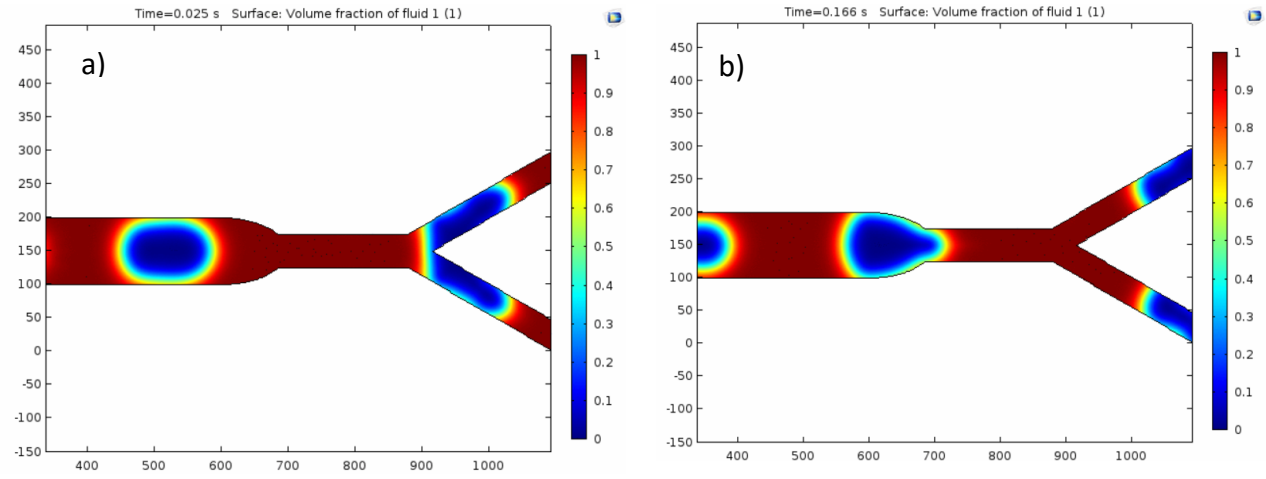

Fig. 4.4 Simulation of TC oil droplet splitting at a dividing branch junction: a) original oil droplet before the dividing junction and droplet split at the junction, b) original oil droplet compressed by a smaller channel to enhance subsequent splitting and two identical smaller droplets out of the junction.

Fig. 4.5 shows the experimental results of TC oil droplets splitting by a PDMS splitting junction. TC oil droplets of 130 µm were generated by setting flow rates of the oil dispersed phase and of the continuous phase to 0.5 µL min^{-1} and 100 µL min^{-1}, respectively. After forming at the FFJ (fig. 4.5a), TC droplets were compressed (fig. 4.5b) and deformed at the splitting junction (fig. 4.5c). Fig. 4.5d shows the original droplet was split into two smaller droplets by the junction edge. Unlike the simulation results, the split oil droplets were different in size. This can be explained by the small difference in hydrodynamic resistance of the two branches caused by imperfection of the channel geometry and of the hydrophilic treatment. Another issue of the splitting junction is that one branch could get stuck during the hydrophilic treatment. In the case of one single channel the dirt and fabrication residues can easily be washed out by the flow. However, in the case of two smaller branches, if one channel gets stuck, flow will choose the other way to go, leaving one channel untreated. The results show that inserting a splitting junction is not an optimal solution to the problem.

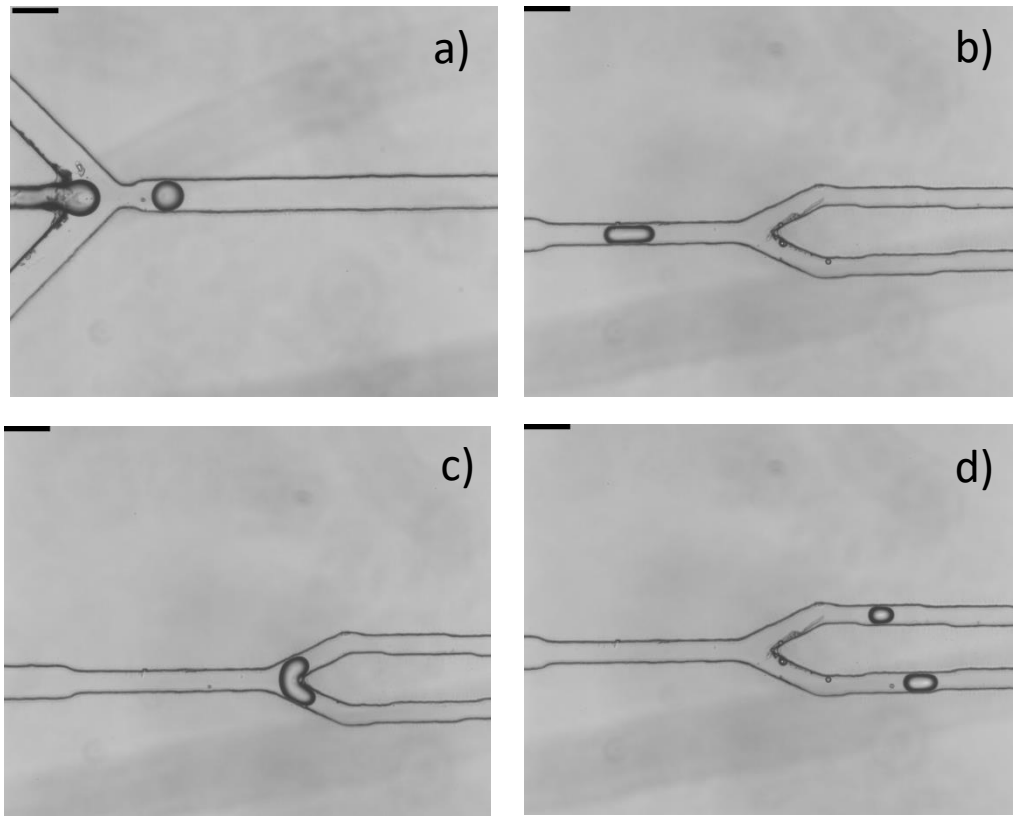

Fig. 4.5 Experimental results for the division of oil droplets at a splitting junction: a) large droplets generated at the FFJ, b) large droplets compressed in a smaller channel, c) droplets squeezed at the splitting junction, d) smaller droplets formed in each branch after the splitting. The black scale bar is 200 µm.

4.1.3 Reducing droplet size by modifying the geometry of the FFJ

Formation of droplets depends on the geometric parameters of the FFJ. Several geometric parameters including the size of the middle channel, the size of the constricted part (fig. 4.6b) after the FFJ, and the angle between the continuous phase and the dispersed phase channels ("squeezing angle" or junction angle) were tested. Flow rates of TC oil and water were set to 0.5 and 90 µL min^{-1}, respectively. It was observed that reducing the size of the constricted part (throat region) did not reduce the size of the oil droplet (fig. 4.6a, b). Moreover, fig. 4.6c shows that reducing the size of the center channel also did not help reducing the size of the oil droplet. In this case, droplets were cut at the end of the center channel instead of at the throat region, resulting in the formation of larger oil droplets.

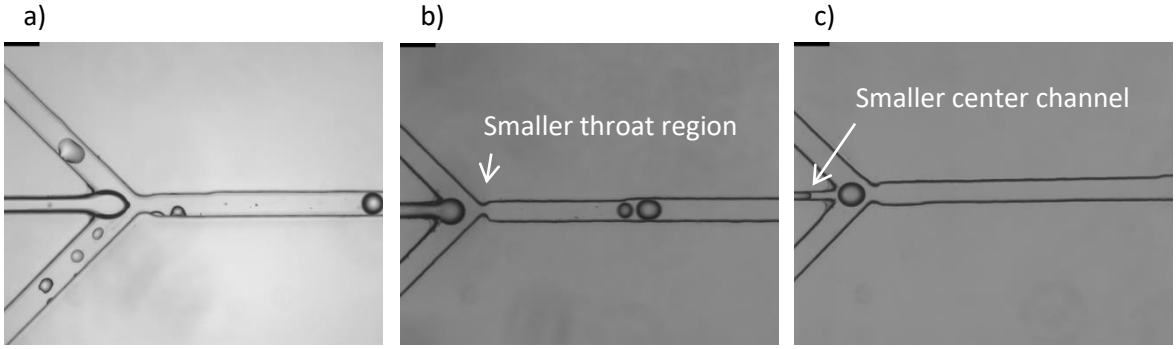

Fig. 4.6 TC droplet generated at a FFJ with different geometric parameters. Droplet size varies: a) 125 µm, b) 140 µm, c) 160 µm. The black scale bar is 200 µm.

In a FFJ junction, the oil droplet is formed by squeezing the oil dispersed phase by two lateral flows of continuous phase. Thus, it is expected that increasing the angle between the continuous phase and the dispersed phase will help reducing the size of the oil droplets. Several designs of the FFJ with increasing junction angle were tested (fig. 4.7). Fig. 4.8 shows that by increasing the junction angle, smaller droplet size (≤100µm) can be generated with smaller W/O flow rate ratio. One thing needs to be noted that, the FFJ geometry shown in fig. 4.7c, in addition to the increased junction angle of 90°, the geometrical size of channel was also reduced, hence contribution to the decrease of droplet size.

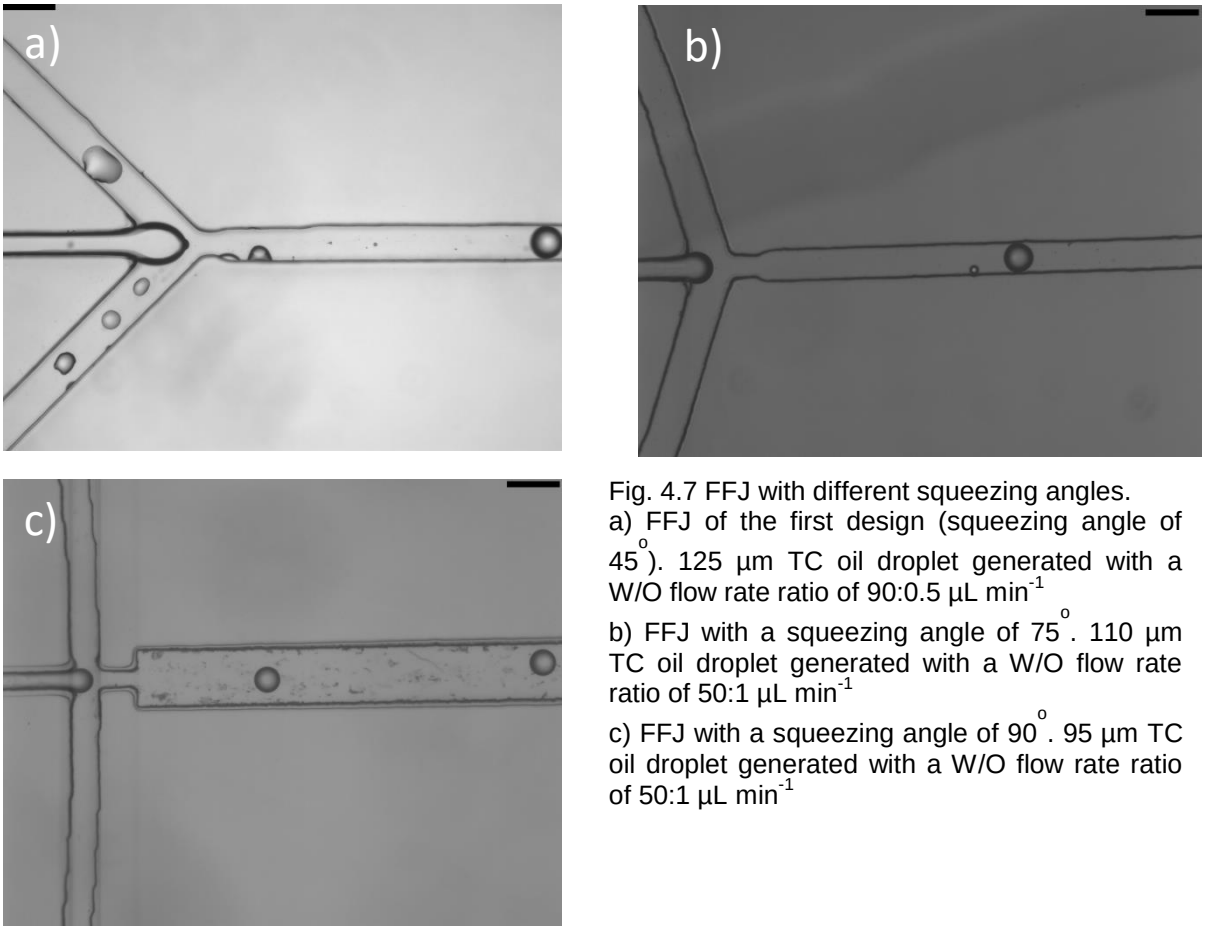

Fig. 4.7 FFJ with different squeezing angles.
a) FFJ of the first design (squeezing angle of 45^{o}). 125 µm TC oil droplet generated with a W/O flow rate ratio of 90:0.5 µL min^{-1}
b) FFJ with a squeezing angle of 75^{o}. 110 µm TC oil droplet generated with a W/O flow rate ratio of 50:1 µL min^{-1}
c) FFJ with a squeezing angle of 90^{o}. 95 µm TC oil droplet generated with a W/O flow rate ratio of 50:1 µL min^{-1}

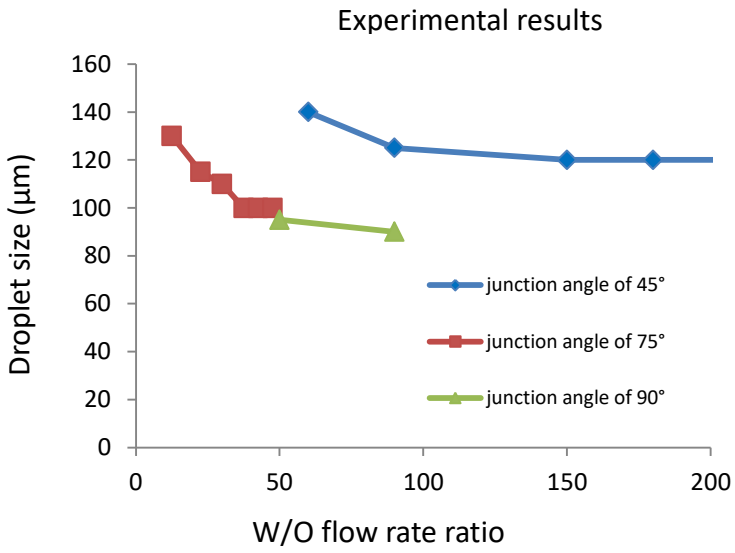

Fig. 4.8 Oil droplet size depending on the flow rate ratio W/O obtained in FFJ geometries with increasing value of the junction angle.

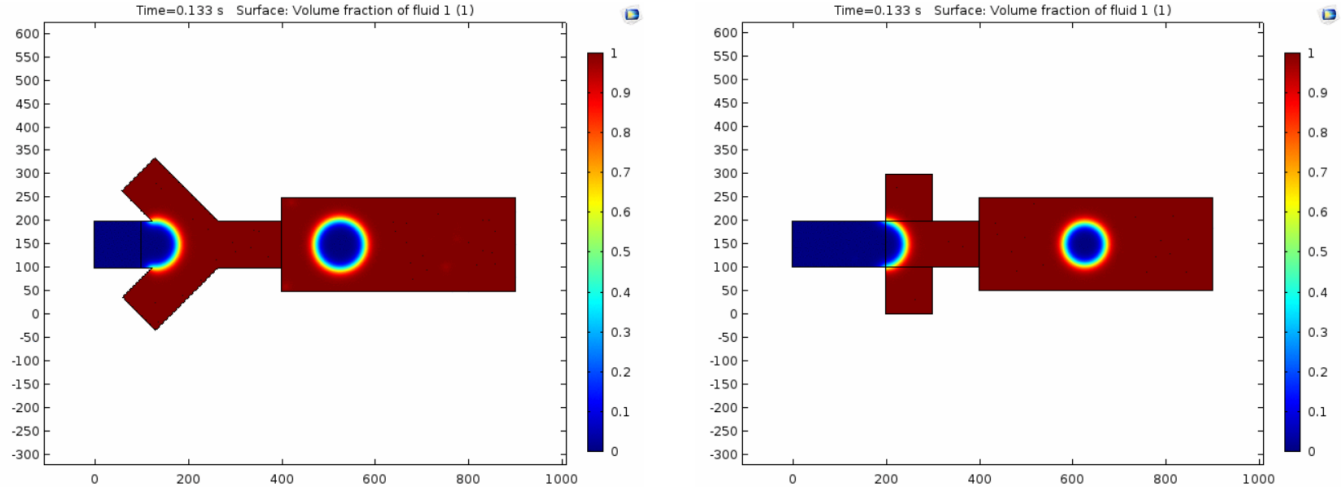

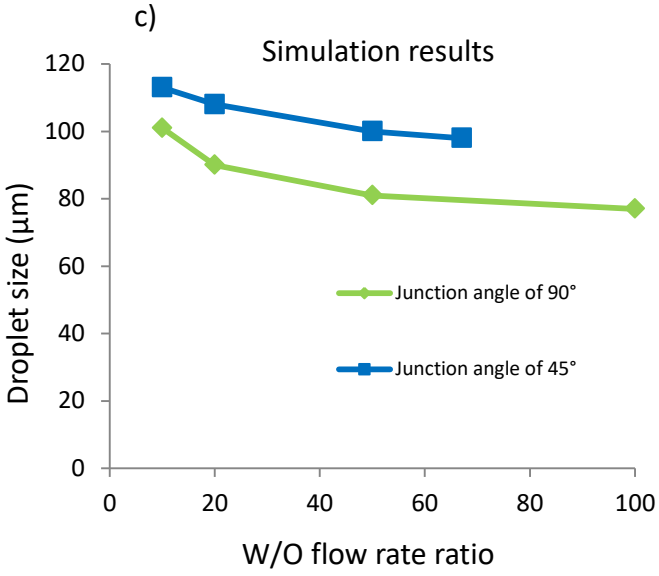

Fig. 4.9 Simulation of oil droplet-generation at a W/O flow rate ratio of 50:1 at a FFJ with different junction angles a) 45°, b) 90°, c) evolution of the oil droplet size with the W/O flow rate ratio for two junction angles.

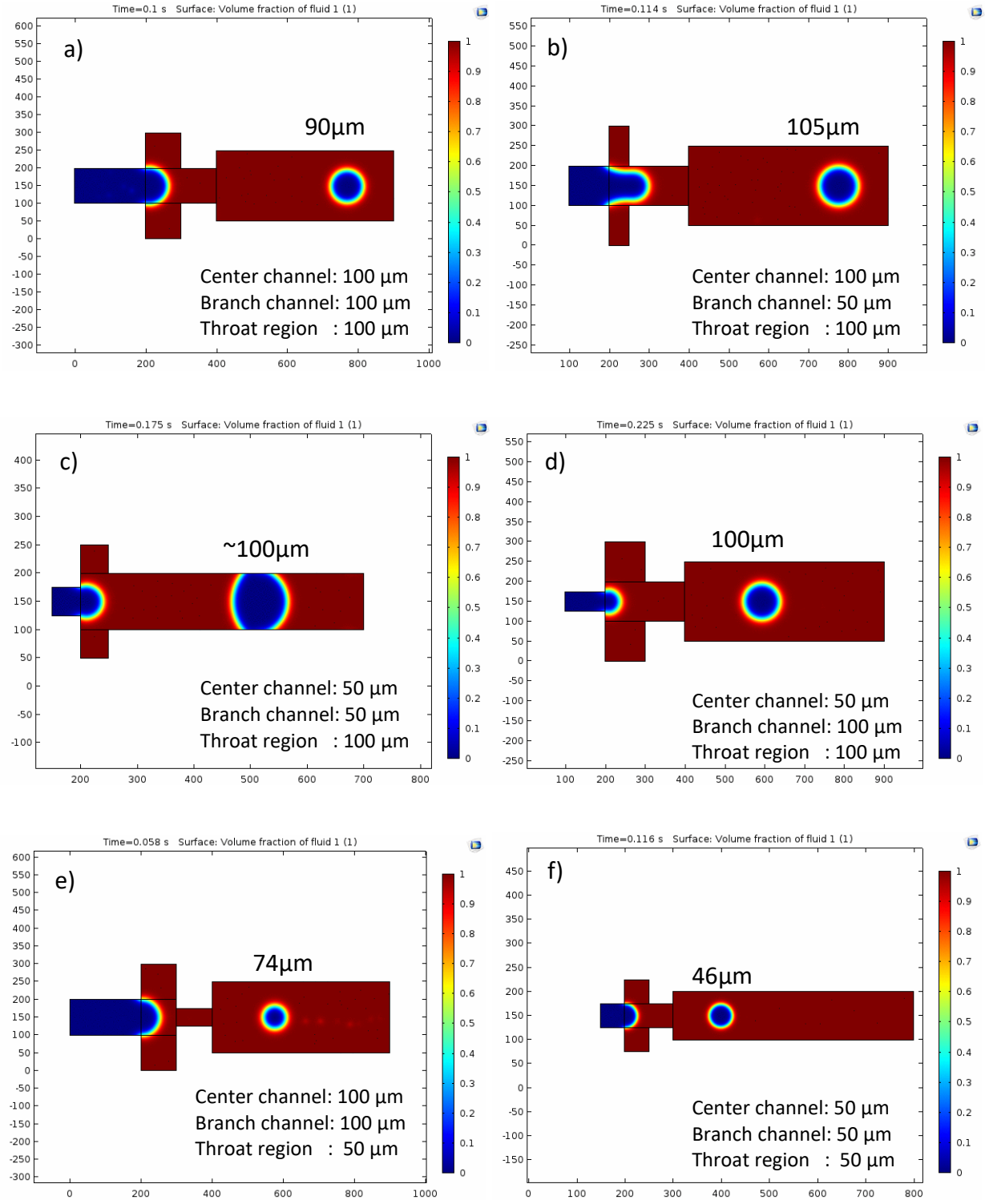

Fig. 4.10 Effect of the FFJ geometry on the oil droplet size simulated using comsol multiphysics. The W/O flow rate ratio used for all cases is 20:1.

The simulation results also confirm the decrease of TC droplet size with the increase of the junction angle to 90°, as shown in fig. 4.9. The effect of the junction angle was reported by several simulation studies in the literature (Jamalabadi et al., 2017; Ngo et al., 2016).The increase of the junction angle results in the reduction of the active area for droplet formation, forming smaller droplet at the same flow rate values of both continuous and dispersed phases.

In order to further characterize the effect of the FFJ geometry on the droplet size, simulations of TC oil droplet generation with various size of the center channel, branch channel and throat region were carried out. The simulation results are shown in figs. 4.10. Comparing fig. 4.10b,c,d to fig. 4.10a shows that a reduced size for either the continuous phase channel or the dispersed phase channel (or both) results in the formation of larger oil droplets. As the velocity of inlet was a constant, reduction of the size of the continuous phase channel resulted in a decrease of shear force acting on the disperse phase, thus, lager droplet formed Fig. 4.10e reveals the effect of the throat size on the droplet size. The droplet diameter was reduced to 74 µm with a throat size of 50 µm. This result contradicts the experimental observation (fig. 4.6) in which the throat size had no effect on the reduction of the droplet size. Fig. 4.10f shows that a size reduction of the continuous phase channel, the dispersed phase channel and of the “throat” results in the formation of smaller oil droplets. Other works in the literature also show a decreased droplet size with a reduced size of the throat region (Li et al., 2008). In the squeezing regime, the pressure drop at the contraction part dominates the oil droplet breakup, explaining the role of the “throat” region size on the oil droplet size (Lee, Walker, & Anna, 2009).

4.1.4 Tests of T-Junction geometry

One of the issues of the FFJ geometry is its potential to block at one branch channel during the hydrophilic treatment (small PDMS piece, dirt, etc…). As the FFJ contains two branch channels for the continuous phase, if one of them gets blocked, all the flow deviates to the other branch channel, thus leaving no pressure to remove the blocking residues. This problem can be solved by using a T-junction geometry.

T-junctions with different channel sizes were tested. TC oil was used as the dispersed phase. The experimental results are shown in fig. 4.11. It was observed that the size of the water channel (horizontal one) is the main factor determining the size of the oil droplets. Although the branch channel size of sample S1 (40 µm) was slightly larger than that of sample S4 (30 µm), the droplet size in the S1 case was smaller than that in the S4 case, as the main channel size for S1 (50 µm) is smaller than that for S4 (100 µm). The simulation

results also confirm that the oil droplet size depends mainly on the size of the main channel rather than on that of the side channel (fig. 4.12). Those results are also in agreement with the work of Garstecki et al. which reported the crucial role of the main channel size on the droplet size in the squeezing regime (Garstecki et al., 2006). Similar to the case of FFJ, in the squeezing regime of the T-junction, the tip of the dispersed phase blocks the cross-section of the main channel, thus the breakup due to pressure drop dominates the generation of the droplet rather than the shear stress on the droplet (Jamalabadi et al., 2017). Thus, the droplet size was mostly related to the size of the cross-section of the main channel. Indeed, in the squeezing regime in a T-junction, the droplet size was larger than the size of the main channel and decreased with the reduction of the main channel cross-section.

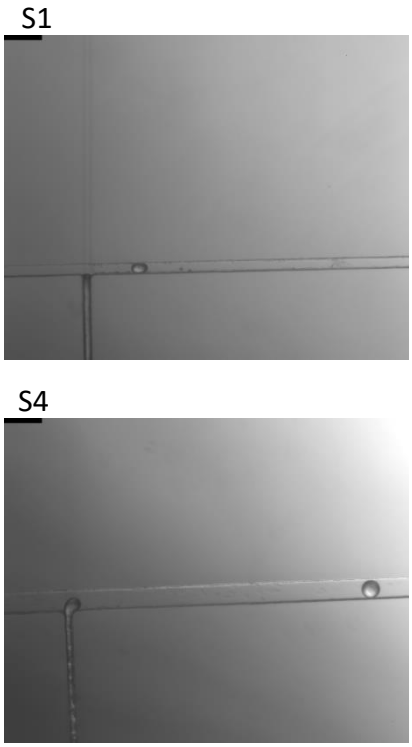

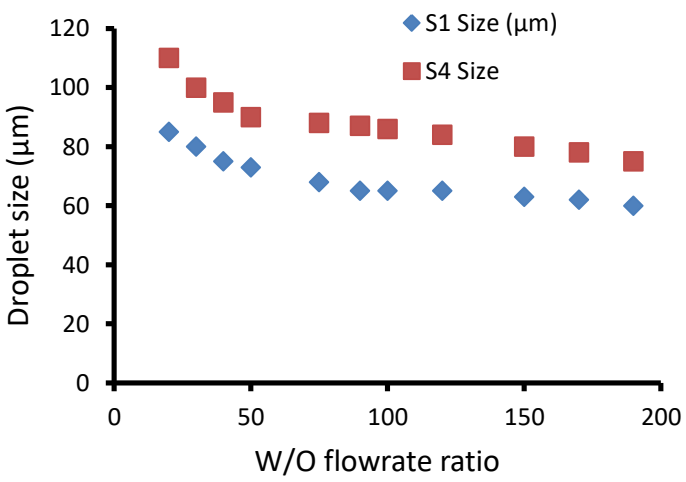

Fig. 4.11 Dependence of the oil droplet size on W/O ratio with two T-junctions of different channel sizes. The black scale bar is 200 µm.

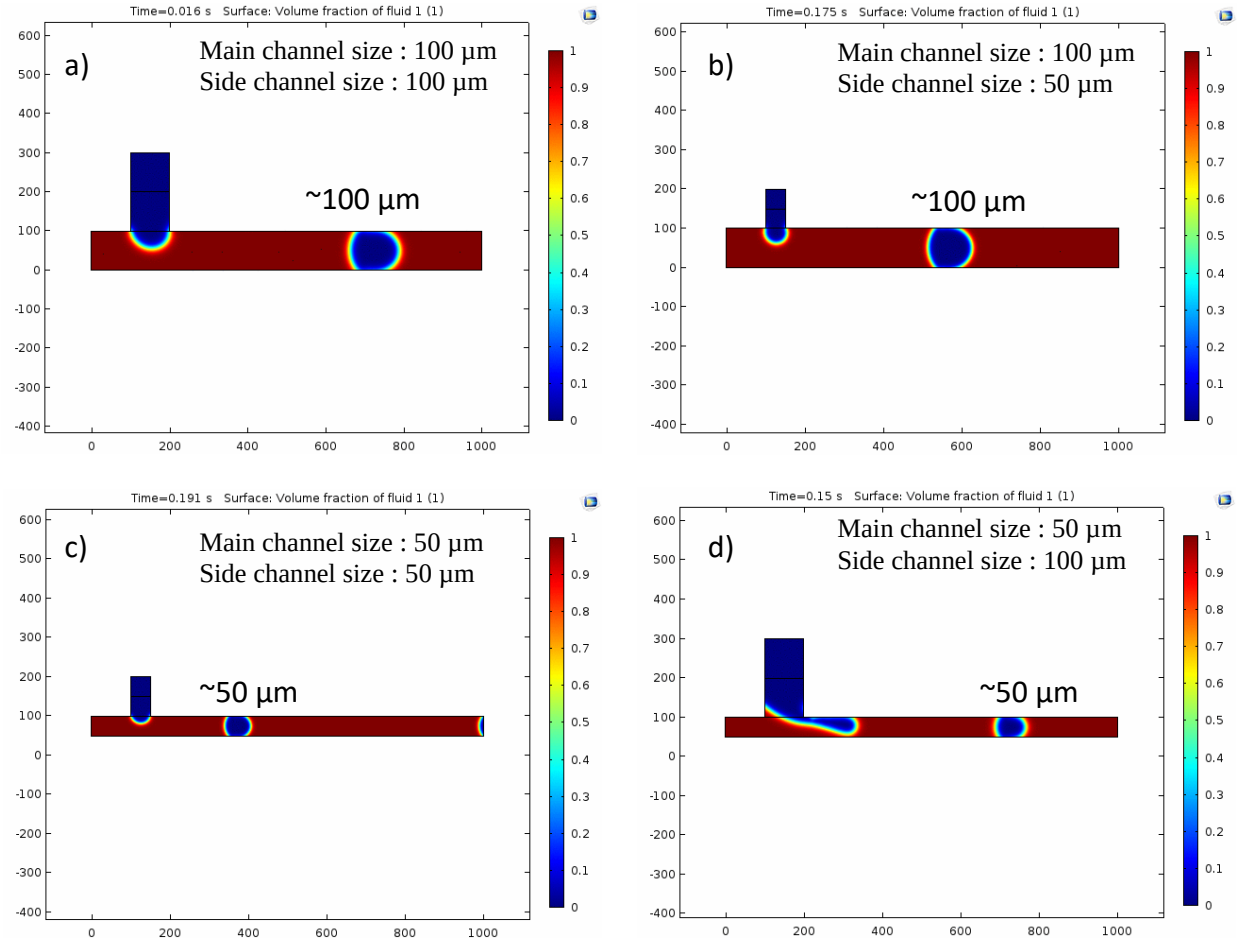

Fig. 4.12 Simulation of oil droplet generation at T-junctions of different geometries.

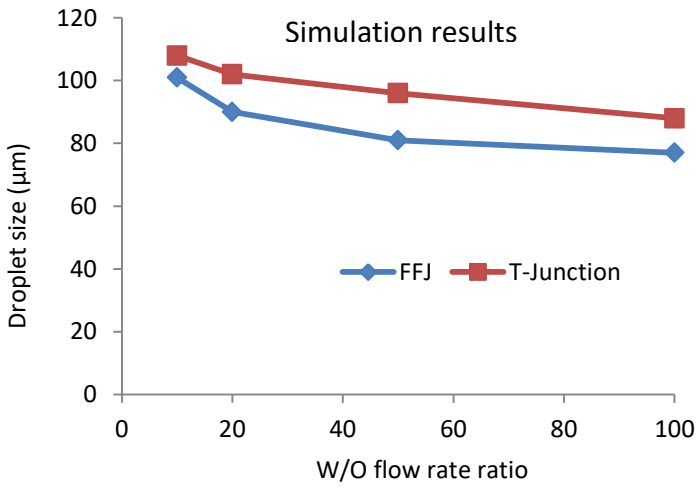

Fig. 4.13 Evolution of TC oil droplet size as a function of W/O flow rate ratio for FFJ or T-junction simulated by Comsol multiphisics.

The simulation also shows the difference of the TC droplet size generated by FFJ and T-Junction. For the comparison, the geometry parameter of both FFJ and T-junction were set to be identical. The size of middle, branch channel and throat region (for FFJ) and of main and side channel (for T-junction) were set to be 100 µm. Angle junction in both FFJ and T-junction were set of 90°. The simulation results show that the FFJ structure is more efficient in reducing the oil droplet size than T-junction (fig. 4.13).

4.1.5 Effect of oil phase viscosity on the oil droplet size

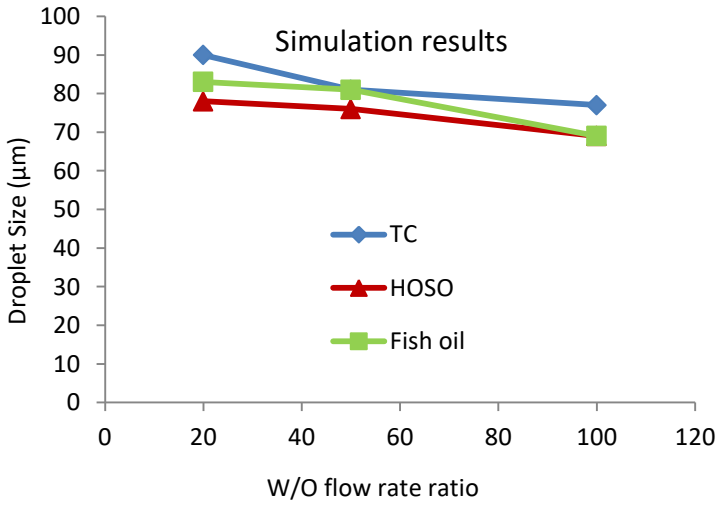

Fig. 4.14 Effect of the oil phase viscosity on the oil droplet size generated by FFJ (simulated by comsol multiphysics).

The effect of the oil phase viscosity on the oil droplet size was evaluated by using Comsol multiphysics simulation. The dynamic viscosity (at 20 °C) of TC, HOSO, fish oil was set to be of 23, 107, 68 mPa.s, respectively. Those chosen values were estimated using formulas proposed in several works (Aksoy, Yabanova, & Bayrakçeken, 2011; Goodrum & Eiteman, 1996; Yin & Sathivel, 2010). The oil droplets were generated by FFJ shown in fig. 4.9b. Despite of various O/W viscosity ratio for those three oils, the droplet size were of the same range (fig. 4.14). The limited effect of oil phase viscosity on the droplet size was confirmed by the results obtained experimentally. A T-junction device was used to generate oil droplets for different types of oil. Three types of oil of different viscosity (TC, HOSO, fish oil) were used. The flow rate of the oil phase was set to 1 µL min^{-1} for all types of oil. Fig. 4.15 shows that the same range of droplet size (≤ 100 µm) can be reached with oils of different viscosity. The small effect of the oil viscosity on the droplet size confirms that in the squeezing regime of oil droplet generation, the oil droplet formation is dominated by the geometry of the channel

(size of the channel, junction angle) rather than viscosity ratio between the oil phase to the aqueous phase.

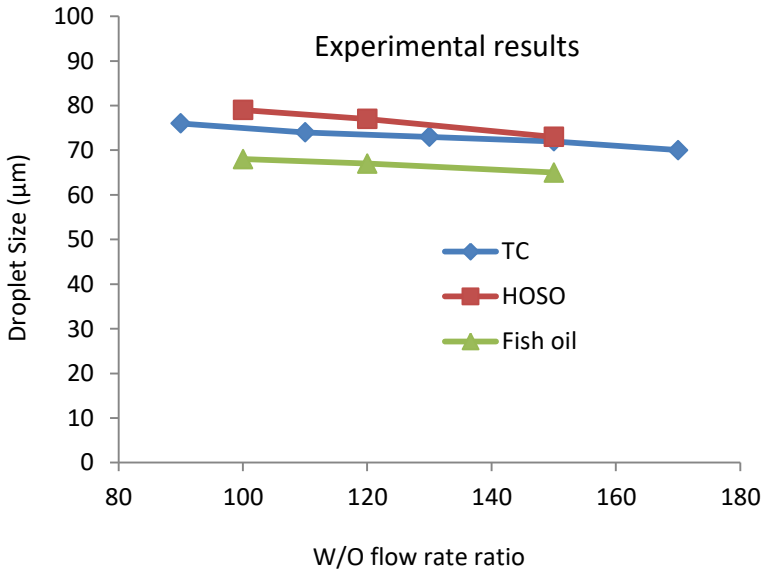

Fig. 4.15 Dependence of the droplet size on the flow rate ratio (W/O) for three oils (TC, HOSO, fish oil).

In summary, by using both simulation results and experimental results, several parameters involved in the oil droplet generation were addressed. In this work, the oil droplet was generated by FFJ and T-Junction in the squeezing regime at small capillary number Ca. In this regime, the pressure drop at the "throat" region dominates the oil droplet breakup over the shear stress of the continuous phase. Thus, the oil droplet size was closely related to the size of the channel (especially the size of the throat region of the FFJ or the main channel of T-junction). On the contrary, water in oil droplet or air bubble in fluid are normally generated at dripping regime at higher capillary number, in which, the shear stress dominates the droplet breakup. Thus, for those cases, the droplet size is controlled by the viscosity ratio of the two phases and the surface tension.

4.2 Effect of digestive juice composition on the kinetics of lipid digestion

Fig. 4.16 shows the effect of different bile salts on the digestion of TC and HOSO oil droplets (initial size of 100 µm). Digestive juice containing either 10 mg mL^{-1} bile extract or 5 mg mL^{-1} single bile salt (sodium glycodeoxycholate) was used for the digestion. The release rate constant of the FA (k_s) was calculated using the Zeroth order kinetics model (Marze &

Choimet, 2012). For the case of HOSO oil, change of bile salts had almost no effect on the digestion. In the contrary, for TC oil, the use of the bile extract yielded faster kinetics of lipid digestion (k_s=66.3±3.9 µmol. s^{-1}. m^{-2}) compared to single bile salt (k_s=41.2±1.4 µmol. s^{-1}. m^{-2}). The results suggest that the digestion of the medium chain length TG is more susceptible to the change of bile salts.

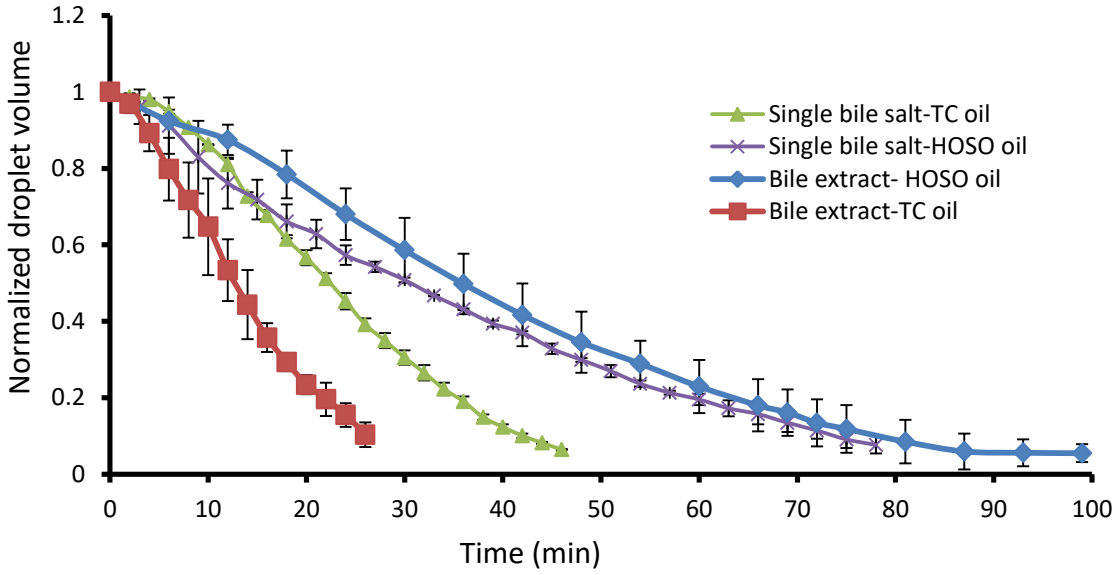

Fig. 4.16 Time evolution of the normalized droplet volume during digestion of TC and HOSO by different digestive fluid compositions (containing a single bile salt or a bile extract).

4.3 Effect of the droplet size on the kinetics of lipid digestion

Digestion of TC oil droplets with 33 µm radius was carried out. Bile extract was used for this experiment. The kinetics of digestion for those smaller droplets was compared with that for larger ones (52 µm radius) in similar digestion conditions, and shown in fig. 4.17. Similar k_S values were found in both cases. The results show that the kinetics of lipid digestion normalized by the surface area is independent of the initial size of the oil droplets, thus validating the Zeroth order kinetics model in the digestion of oil droplets. By normalizing with total initial amount of oil, the relative FFA release per unit time (%.min^{-1}) k(%) were calculated to be of 5.4 (%.min^{-1}) for smaller droplets and 3.9 (%.min^{-1}) for larger ones. Higher relative FFA release rate explains faster digestion for the case of smaller oil droplets.

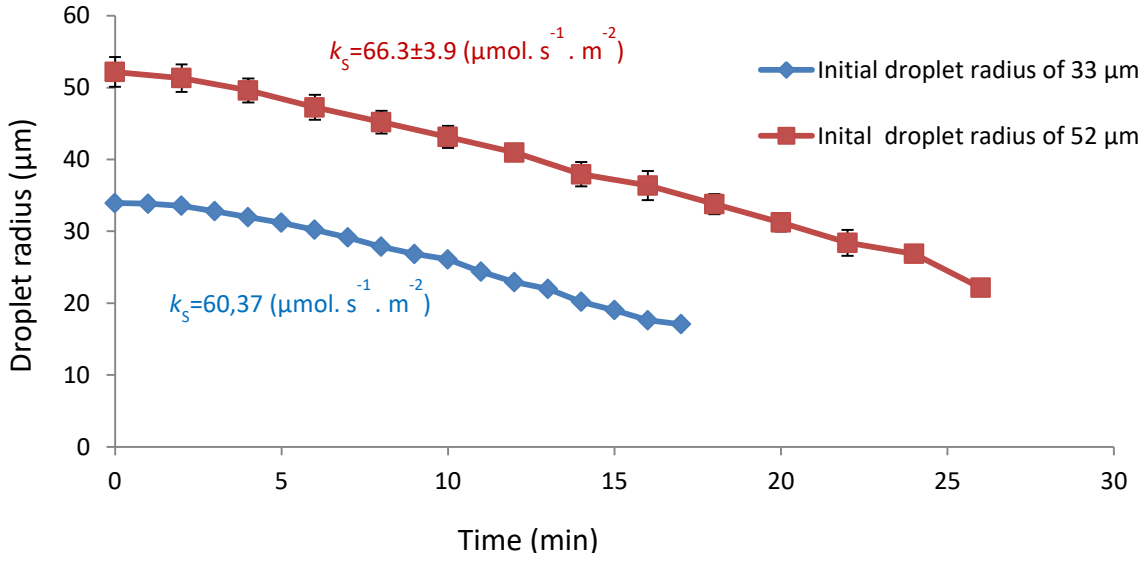

Fig. 4.17 Kinetics of lipid digestion for oil droplets with different initial sizes.

4.4 Effect of digestive juice flow vs. static

Here we tested the effect of flow rate of digestive juice (containing sodium glycodeoxycholate) on the digestion of TC oil. Two different flow profiles were used for this experiment. In the flow profile A, at the beginning, as soon as the digestive juice filled the chamber, the flow was stopped to achieve a static digestion condition for 1 hour before the flow rate (50µl/min) was started again. In the flow profile B, the digestive juice was continuously flowed (50µl/min) into the digestion chamber during 16 min, then the flow was stopped until the end of the digestion. Fig. 4.18a shows the evolution of the oil droplets size in both static and non-static digestion regimes of the flow profile A. In the static regime, after the flow was stopped, the amount of digestive juice inside the chamber trigger the hydrolysis of lipid thus the oil droplet size is initially reduced. Then, the hydrolysis is quickly stopped, the droplet size remaining the same. As soon as the flow was started again, the digestion continued normally. The smaller hydrolysis of lipid at the beginning and quick stop of hydrolysis during the static regimes could be explained by the lack of bile salt due to the adsorption of bile salt to the PDMS device channel. The SAXS data (shown in fig. 4.21) showed that the single bile salt adsorbed to the PDMS channel and this absorption reached saturation after 8 min of flow. That could also explain the continuous digestion after the flow was stopped at 16 min in the flow profile B (shown in fig. 4.18b). As the flow was stopped at 16 min, the remaining bile salt was abundant (due to not being adsorbed to the PDMS surface) for lipid digestion.

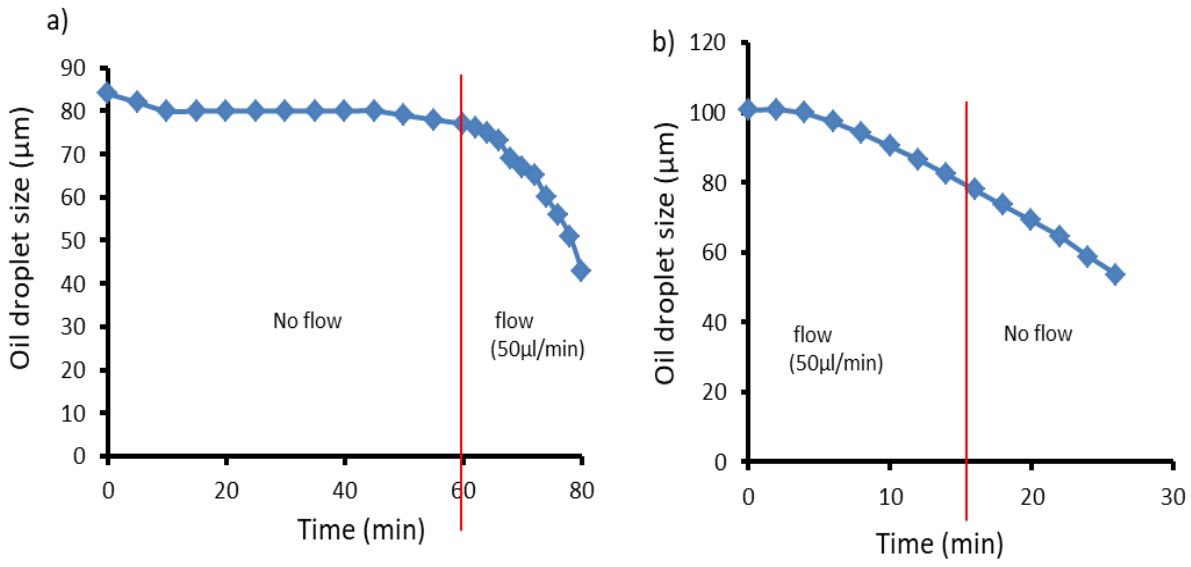

Fig. 4.18 Evolution of oil droplet size as the function of time in static and non-static digestion condition.

4.5 The roles of the lipase and bile salt on the BC release

In this experiment, either lipase or bile salt was removed from the intestinal juice that was flowed into the chamber. TC droplets (100 µm in size) containing 0.2% of BC were used for the digestion. The BC release of both cases was compared with the curve of the standard TC digestion obtained by intestinal juice containing both lipase and bile salt (shown in fig. 4.20).

In the case of removal of lipase, the lipase-free intestinal juice contained only the single bile salt (sodium glycodeoxycholate). As no lipase was present in the juice, no digestion of TC was observed during 150 min of juice flowing (shown in fig. 4.19). However, a decrease of BC concentration was observed, thus suggesting the transfer of BC from oil droplet to the micellar phase of simple bile salt micelles, even without the presence of lipase. The solubilization of lipophilic molecules in simple micellar phase has been reported in the literature (Mithani, Bakatselou, TenHoor, & Dressman, 1996; O'Reilly, Corrigan, & O'Driscoll, 1994; Rosoff & Serajuddin, 1980). Even though, the release rate of BC from the oil droplet per unit droplet surface area in the case without lipase (k_s=0.0013 µmol s^{-1} m^{-2}) is much smaller than that obtained in the standard digestion with the presence of both the lipase and bile salt (k_s=0.57 ± 0.04 µmol s^{-1} m^{-2}). The lipid digestion products generated by lipolysis are known to associate with bile salts to form mixed micelles. Those mixed micelles were found to provide a much higher solubilization capacity for lipophilic bioactive molecules compared to the case of simple micelles formed from bile salt alone in the case without lipase (Kossena, Boyd, Porter, & Charman, 2003; Kossena et al., 2004). The enhanced solubility of

lipophilic bioactive molecules in the mixed micellar phase could partly explain the higher BC release rates in the standard case with both lipase and bile salt.

In the case of bile salt removal, TC digestion was observed due to a significant solubility of the medium carbon chain FA (caprylic acid) in the aqueous phase, that is able to form micelles. The release rate of BC from the oil droplet per unit droplet surface area was measured to be of k_s=0.3321 µmol s^{-1} m^{-2}. This value is smaller than that of the standard digestion with both lipase and bile salt due to the absence of bile salt, however, this is still much larger than in the case of bile salt alone. These results once again validate the role of lipid digestion on the BC release.

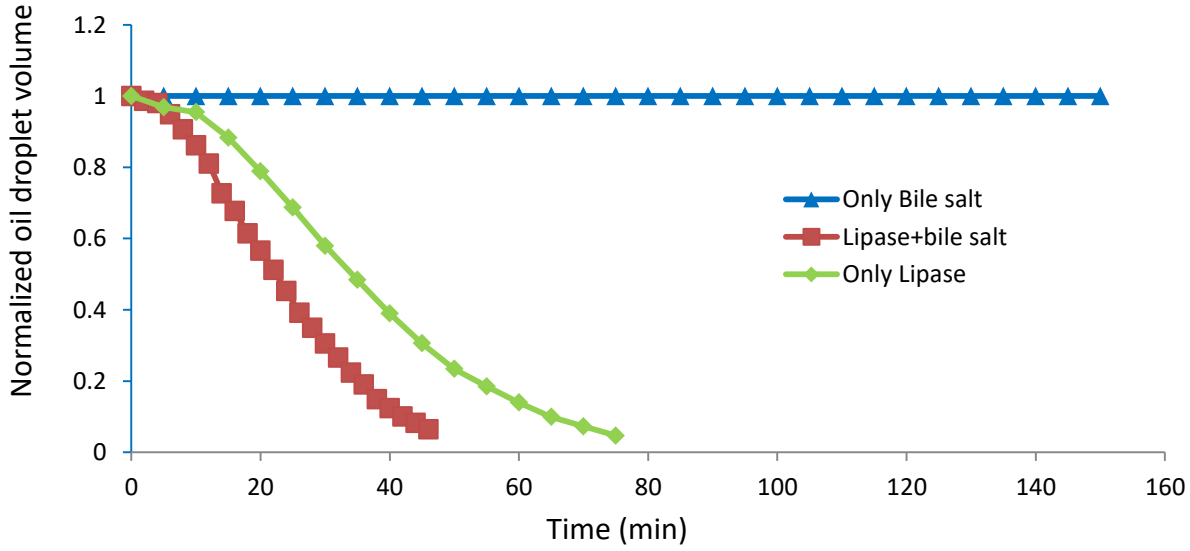

Fig. 4.19 The role of lipase on the lipid digestion.

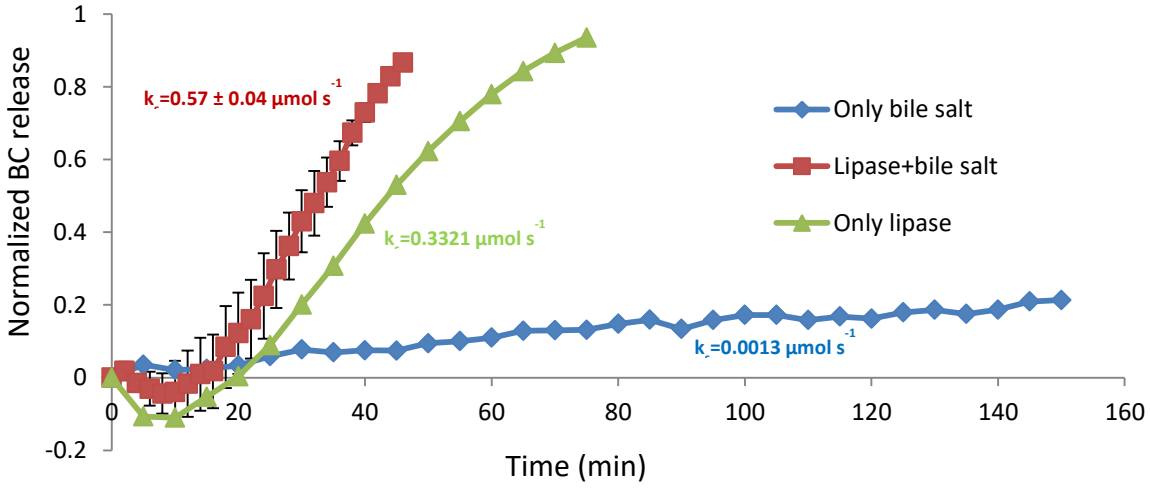

Fig. 4.20 The role of the lipase on the BC release.

4.6 Structural characterization of sodium glycodeoxycholate assembiles and their association with pancreatic enzymes

In this part, the structural characterization of bile salt assemblies in the absence or presence of pancratic enzymes is presented. The assemblies of a single bile salt (sodium glycodeoxycholate) and their association with pancreatic enzymes (lipases, proteases, and amylase) were characterized using synchrotron SAXS (small angle X-ray scatering), DLS (dynamic light scattering), and TEM (transmission electron microscopy).

4.6.1 Materials and methods

Lipase from porcine pancreas type II (L3126), sodium glycodeoxycholate (NaGDC, G9910, 97% purity), sodium dihydrogen phosphate (NaH_2PO_4) were purchased from Sigma-Aldrich. The lipase from porcine pancreas was estimated to contain 2% lipase-colipase, 7% amylase, and 15% proteases by weight. The sample were prepared by mixing /stirring (for one hour) NaGDC and/or pancreatin and a buffer stock solution (100 mM NaH_2PO_4, pH 7.0). The mixture was then centrifugated at 1000g for 15min at room temperature to remove large residues. All the samples were analysed within six hours.

4.6.2 Synchrotron SAXS

The SAXS measurements were carried out at the SWING beamline of the Synchrotron SOLEIL (Saint-Aubin, France). The wave vector q ranged from 0.006 $Å^{-1}$ to 0.6 $Å^{-1}$. The X-ray energy was 12 keV. The distance between the sample and detector was fixed to 1.935 m. The background intensity was obtained by measuring the scattering intensity from the 2 mm quartz measurement capillary containing only the buffer solution. The absolute scattering intensity was obtained by subtracting background from the total scattering intensity. Scattering patterns were acquired for 25 min with an interval of 6 s (except for the first 20 s). The data acquisition and conversion of 2D patterns to 1D curves were done by a homemade program (FOXTROT).

The sample solutions were flowed through the PDMS microfluidic device (containing no droplet) before it flowed through the measurement capillary at a continuous flow rate of 50 $\mu L.min^{-1}$. The temperature inside the microfluidic device and measurement capillary was maintained to 37 °C.

The structural properties of the assemblies were deduced by fitting the intensity scattering curve I(q) by using software SasView v4.1.2. All the curves were fitted with various models (including the stacked discs one).

4.6.3 Dynamic light scattering

The structural features of the assembillies were also characterized (at 37 °C) by Zetasizer Nano ZS (Malvern Instruments Ltd., Worcestershire, UK) equipped with a 4 mW He–Ne laser at 633 nm. The measured scattering angle (the angle between the laser beam and the detector) is 173°. The refractive index of the aqueous phase, samples of NaGDC, pancreatin and mixture of both NaGDC, pancreatin were set to 1.33, 1.55, 1.49, and 1.52, respectively. The absorption was set to 0.001 for all samples. Stable measurement was acquired during 30 s. At least ten measurent repetitions were used to deduce the number-based hydrodynamic diameter.

4.6.4 TEM (transmission electron microscopy)

15 µL drop of sample solution was placed on a carbon-coated TEM copper grid (Quantifoil, Germany) which is previously submitted to a glow-discharge for hydrophilicity. Then, for better image contrast, the sample was negatively stained with 15 µL of a 2 % aqueous solution of uranyl acetate (Merck, Germany). The sample was dried in room condition before the TEM measurement. The TEM equipment was a JEM-1230 microscope (Jeol, Japan) operated at an acceleration voltage of 120kV. The images were recorded on a 1.35 K x 1.04 K x 12 bit ES500W erlangshen CCD camera (Gatan, USA).

4.6.5 Results and discussion

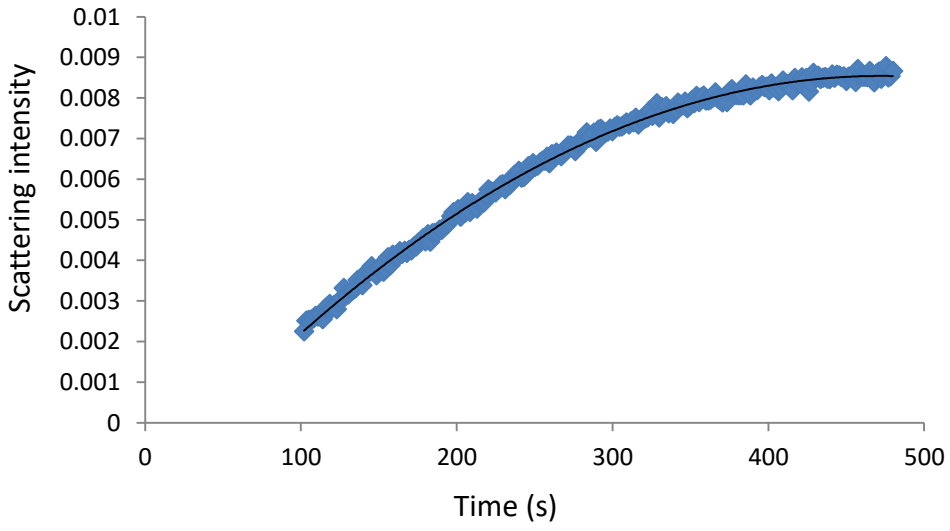

Fig. 4.21 Time evolution of scattering intensity in the presence of NaGDC.

It was found in the presence of NaGDC that the scattering intensity always increased during the first 8 min of the measurement before reaching a constant value (fig. 4.21). This increase kinetics was attributed to the adsorption of NaGDC on the PDMS surfaces that was previously addressed in the part 4.4 (see fig. 4.18).

As shown in the fig. 4.22, the sample of 5 $mg.mL^{-1}$ NaGDC alone yield a similar scattering intensity curve to the sample of 5 $mg.mL^{-1}$ NaGDC with the presence of 0.1 $mg.mL^{-1}$ pancreatin (representing pancreatic insufficiency), suggesting no change of the bile salt assembly due to pancreatin in the pancreatic insufficiency state. In contrary, the scattering intensity curve for the sample of 5 mg. mL^{-1} NaGDC and 4 $mg.mL^{-1}$ pancreatin (normal fed state) was significantly different from the others. The scattering profile for the sample of 4 $mg.mL^{-1}$ pancreatin alone is shown in fig. 4.23. This curve with a log-log steep slope at low q is different from other curves shown in fig. 4.22 with the log-log steep slope at high q.

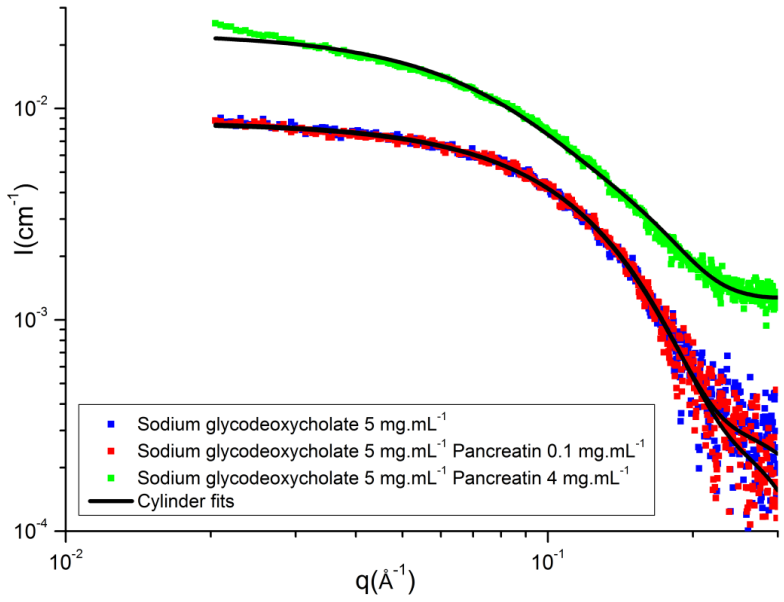

Fig. 4.22 SAXS intensity curves (Background subtracted) fitted by the cylinder model for different systems (see legend).

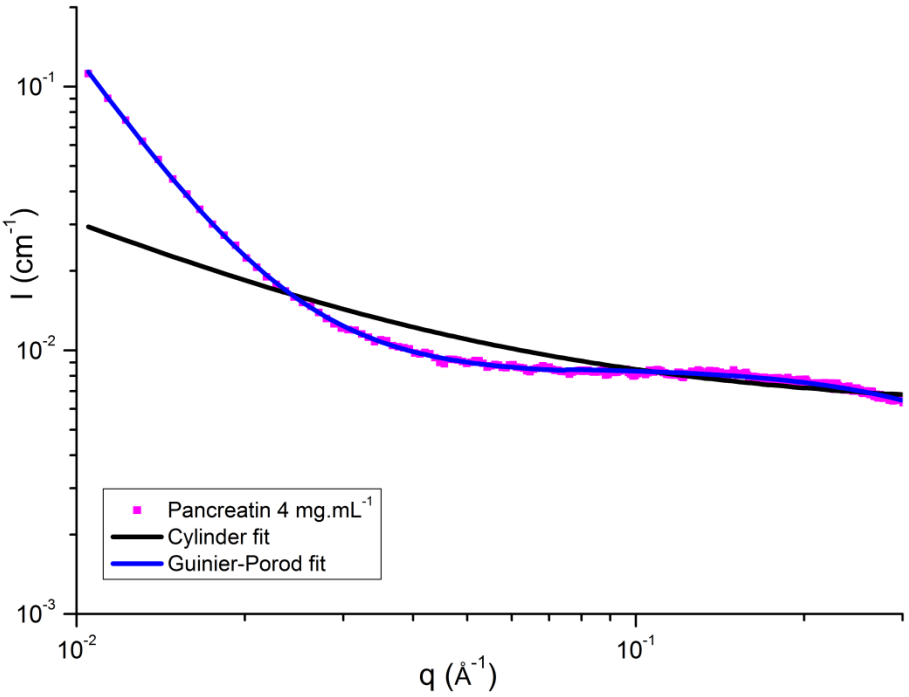

Fig. 4.23 Background subtracted SAXS intensity curve for pancreatin fitted by the cylinder model or the Guinier-Porod model.

For all those curves, shape-dependent Cylinder model and the shape-independent guinier-Porod model (presented in the previous part) provide the best fitting. Except for the case of 4 mg.mL^{-1} pancreatin alone, the cylinder-model was not suitable to describe the curve at low q region (fig. 4.23). In the cylinder model, the structure factor S(q) is neglected due to the low dispersion concentrations of the sample. The scattering length densities ρ of the solvent and of the particles were calculated using the SasView SLD calculator. For the case of pancreatin, the scattering length density was estimated using the Protein Scattering Length Calculator (psldc.isis.rl.ac.uk/Psldc). The form factor P(q) and the volume of one particle V_p (cm^3) are only related to the length parameters of the model geometry (R_c and L_c for cylinder). Thus, the only fitted parameters were the two length parameters of the particles and the volume fraction ϕ_p that can be roughly estimated from the mass fraction $Ø_ϑ$. For the Guinier-Porod model, all the parameters were fitted.

Table 4.1 presents main length parameters from the curve fitting with cylinder models (D_c and L_c) and the Guinier-Porod models (D_g and d), and from DLS measurements (D_h). For the Guinier-Porod models, the Porod exponent d of the 5 mg.mL^{-1} NaGDC alone or in the

presence of 0.1 mg.mL^{-1} pancreatin is close to 4, reveiling smooth-surface 3D particles. In the case of normal fed state with the presence of 4 mg. mL^{-1} pancreatin, the Porod exponent d is 2.0, indicating 2-dimentional structure (polymer chains). For the case of 4 mg.mL^{-1} pancreatin alone, the Porod exponent d is close to 3.0, indicating rough surface of mass fractals of aggregated polymer chains (Hammouda, 2010). For all cases, the Guinier exponent s is close to 0.0, indicating the 3D particles rather than rod-like or platelets-like structure. The diameter of gyration D_g (=2R_g) is found to increase in the presence of 4 mg.mL^{-1} pancreatin (3.0 nm compared to 2.4 nm of 5 mg.mL^{-1} NaGDC alone). For the case of 4 mg.mL^{-1} pancreatin, the diameter of gyration D_g is high (79nm), consistent with the size scale of the aggregated polymer chains. These diameter of gyration D_g values are also consistent with those measured by DLS (D_h) with the relation D_h= D_g/0.7530 (except for pancreatin alone). The factor 0.7530 is close to the theoretical one 0.7746 for a sphere (Hammouda, 2010). This factor comes from the different particle size probed by different scattering methods. Although the factor 0.7530 can not be applied for the case of pancreatin alone mostly due to larger error for this case, the similar trends are observed for both SAXS and DLS methods. The presence of 4 mg.mL^{-1} pancreatin causes the slightly increase in size of bile assemblies (~1nm) and pancreatin not being aggregated. In contrary, for the case of pancreatin alone, the large aggregated proteins cause significantly increase in size of the assembly (more than one order of magniture) and a rough surface (Porod exponent d is close to 3.0). The results are in agreement with literature. Several articles reported the aggregation of purified enzymes α-amylase, lipase of *Bacillus thermocatenulatus* as well as the disaggregation of *Bacillus thermocatenulatus* with the addition of bile salt (H. L. Liu, Chen, & Chou, 2003; Luisa Rúa, Schmidt-Dannert, Wahl, Sprauer, & Schmid, 1997).

The cylinder model shows the disc-like assemblies formed in the case of NaGDC alone or with the low pancreatin concentration with diameter and height of the cylinder are of 3.9 and 1.8 nm, respectively. Those values are close to the ones reported for sodium taurodeoxycholate with 3.6 nm and 1.2 nm in diameter and height, respectively (Charles et al., 1980).

The elongated cylinders assembilies formed in the case of NaGDC with high pancreatin concentration (4 mg. mL^{-1}) have diameter and height of 2.7 nm and 6.2 nm, respectively. Those values are close to the reported ones of a cylinder for sodium taurodeoxycholate-pancreatic colipase with 2.9 nm and 6.1 nm in diameter and height, respectively (Charles et al., 1980).

	D_h	D_g	m	D_c	L_c
Bile 5 $g.L^{-1}$ (+ lipase 0.1 $g.L^{-1}$)	3.1 ± 0.3	2.4 ± 0.2	3.9 ± 0.3	3.9 ± 0.1	1.8 ± 0.1
Bile 5 $g.L^{-1}$ + lipase 4 $g.L^{-1}$	4.1 ± 0.3	3.0 ± 0.1	2.0 ± 0.1	2.7 ± 0.1	6.2 ± 0.3
Lipase 4 $g.L^{-1}$	90 ± 20	31 ± 1	2.7 ± 0.2	a	a

Table 4.1 Length parameters (in nm) from DLS measurements (D_h) and from the fitting of SAXS intensity curves with the Guinier-Porod (D_g and m) and the cylinder (D_c and L_c) models. The error is the standard deviation. The cylinder model could not describe well the SAXS data for pancreatin.

The visual appearance of those assemblies was provided by TEM. Fig. 4.24a shows the TEM image of many assemblies forming a large network for the case of NaGDC alone. The assemblies are mostly found in spherical shape with the apparent size in the range 10-30 nm. Smaller assemblies with the size around 5 nm are seen on the edges of the network (zoomed image of fig. 4.24a). For the case of pancreatin alone, two large homogeneous spheroidal assemblies of 70 and 130 nm are observed, expected to be protein aggregates (fig. 4.24b). A few smaller individual assemblies of 10nm can be observed. Fig. 4.24c shows the well-dispersed individual assemblies (with the size range of 10-40 nm) for the NaGDC pancreatin mixture. Only a few of them forms networks compared to the case of NaGDC alone. The TEM results confirm the aggregation for the pancreatin alone and the disaggregation with the addition of NaGDC. However, the TEM resolution was insufficient to detect assemblies smaller than 5 nm, thus not providing the structural characterization of individual assemblies as delivered by other techniques.

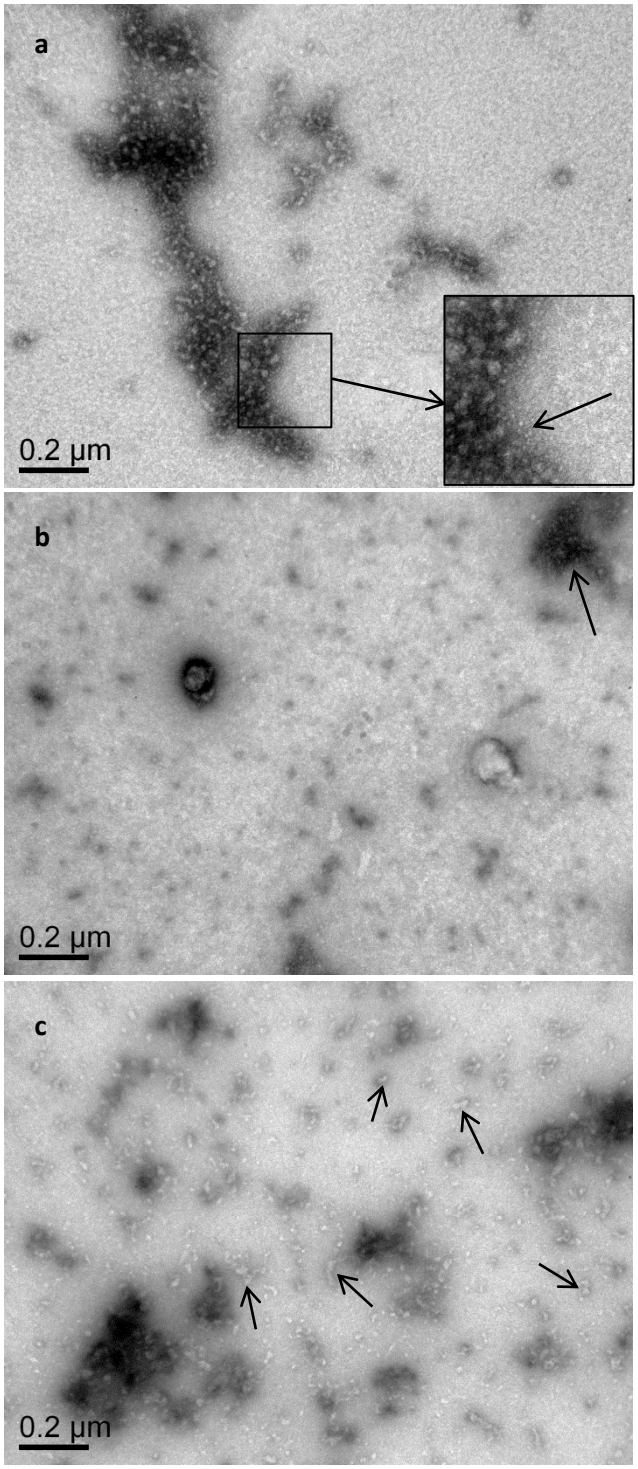

Fig. 4.24 Representative TEM micrographs of A) NaGDC 5 mg.mL^{-1} (inset is a 2x zoom showing the smallest assemblies), B) pancreatin 4 mg.mL^{-1} (arrow shows a region of individual assemblies), C) NaGDC 5 mg.mL^{-1} + pancreatin 4 mg.mL^{-1} (arrows show elongated assemblies resembling aggregated dimers).

References

Abate, A. R., & Weitz, D. A. (2011). Faster multiple emulsification with drop splitting. Lab on a Chip, 11(11), 1911–1915.

Aksoy, F., Yabanova, I., & Bayrakçeken, H. (2011). Estimation of dynamic viscosities of vegetable oils using artificial neural networks.

Charles, M., Riva, M. G. M., & Chabre, M. (1980). Small-angle Neutron Scattering Study of the Association between Porcine Pancreatic Colipase and Taurodeoxycholate Micelles, 297–317.

Garstecki, P., Fuerstman, M. J., Stone, A., & Whitesides, G. M. (2006). Formation of droplets and bubbles in a microfluidic T-junction — scaling and mechanism of break-up, 437–446.

Goodrum, J. W., & Eiteman, M. A. (1996). Physical properties of low molecular weight triglycerides for the development of bio-diesel fuel models. Bioresource Technology, 56(1), 55–60.

Hammouda, B. (2010). A new Guinier – Porod model A new Guinier – Porod model, 716–719.

Jamalabadi, M. Y. A., DaqiqShirazi, M., Kosar, A., & Shadloo, M. S. (2017). Effect of injection angle, density ratio, and viscosity on droplet formation in a microfluidic T-junction. Theoretical and Applied Mechanics Letters, 7(4), 243–251.

Kossena, G. A., Boyd, B. J., Porter, C. J. H., & Charman, W. N. (2003). Separation and characterization of the colloidal phases produced on digestion of common formulation lipids and assessment of their impact on the apparent solubility of selected poorly water-soluble drugs. Journal of Pharmaceutical Sciences, 92(3), 634–648.

Kossena, G. A., Charman, W. N., Boyd, B. J., Dunstan, D. E., & Porter, C. J. H. (2004). Probing Drug Solubilization Patterns in the Gastrointestinal Tract after Administration of Lipid-Based Delivery Systems: A Phase Diagram Approach. Journal of Pharmaceutical Sciences, 93(2), 332–348.

Lee, W., Walker, L. M., & Anna, S. L. (2009). Role of geometry and fluid properties in droplet and thread formation processes in planar flow focusing. Physics of Fluids, 21(3).

Liu, H. L., Chen, W. J., & Chou, S. N. (2003). Mechanisms of aggregation of alpha- and beta-amylases in aqueous dispersions. Colloids and Surfaces B: Biointerfaces, 28(2–3), 215–225.

Luisa Rúa, M., Schmidt-Dannert, C., Wahl, S., Sprauer, A., & Schmid, R. D. (1997). Thermoalkalophilic lipase of Bacillus thermocatenulatus. Journal of Biotechnology, 56(2), 89–102.

Marze, S., Algaba, H., & Marquis, M. (2014). A microfluidic device to study the digestion of trapped lipid droplets. Food Funct., 5(7), 1481–1488.

Marze, S., & Choimet, M. (2012). In vitro digestion of emulsions: Mechanistic and experimental models. Soft Matter, 8(42), 10982–10993.

Minekus, M., Alminger, M., Alvito, P., Ballance, S., Bohn, T., Bourlieu, C., … Brodkorb, A. (2014). A standardised static in vitro digestion method suitable for food-an international consensus. Food and Function, 5(6), 1113–1124.

Mithani, S. D., Bakatselou, V., TenHoor, C. N., & Dressman, J. B. (1996). Estimation of the increase in solubility of drugs as a function of bile salt concentration. Pharmaceutical Research, 13(1), 163–167.

Ngo, I.-L., Woo Joo, S., & Byon, C. (2016). Effects of Junction Angle and Viscosity Ratio on Droplet Formation in Microfluidic Cross-Junction. Journal of Fluids Engineering, 138(5), 051202.

O'Reilly, J. R., Corrigan, O. I., & O'Driscoll, C. M. (1994). The effect of simple micellar systems on the solubility and intestinal absorption of clofazimine (B663) in the anaesthetised rat. International Journal of Pharmaceutics, 105(2), 137–146.

Rosoff, M., & Serajuddin, A. T. M. (1980). Solubilization of diazepam in bile salts and in sodium cholate-lecithin-water phases. International Journal of Pharmaceutics, 6(2), 137–146.

Xu, J. H., Li, S. W., Tan, J., Wang, Y. J., & Luo, G. S. (2006). Preparation of highly monodisperse droplet in a T-junction microfluidic device. AIChE Journal, 52(9), 3005–3010.

Yin, H., & Sathivel, S. (2010). Physical properties and oxidation rates of unrefined menhaden oil (brevoortia patronus). Journal of Food Science, 75(3), 163–168.

5 CONCLUSION AND PERSPECTIVE

In this PhD thesis work, the interplay between the lipid digestion and micellar solubilization of lipophilic micronutrients (bioaccessibility) was studied by using microfluidic tools.

The first stage of this PhD work shows that the real-time kinetics of lipophilic bioactive molecules can be monitored and quantitatively analyzed using microfluidics and confocal microscopy. The real-time kinetics is needed to provide better understanding of the fate of micronutrients in the gastrointestinal tract, towards improvement of their bioaccessibility. The work also proposes a novel approach based on microfluidics for *in vitro* lipid digestion study.

The microfluidic device was constructed and optimized to obtain a channel surface with a long-termed hydrophilicity for the generation and manipulation of oil droplets in aqueous phase. In proper storage conditions (the device channel was filled with water at pH 11 and stored at 4^0C), the channel surface of the device remained hydrophilic for months. The geometry of the junction for droplet generation was optimized through experiments with the aid of simulation data using Comsol multiphysics software. Geometrical parameters of the junction that affect the droplet formation were tested. For the case of the FFJ, the oil droplet size decreases with an increase of the junction angle from 45° to 90° and with the simultaneous reduction in size of all the channels (branch channel, middle channel, throat region). For the T-junction, the oil droplet size mainly decreases with the size of the main channel. The results were in agreement with the literature. By using an optimized junction geometry, oil droplet with a size < 100 µm were obtained, allowing simultaneous monitoring of seven oil droplets within the field of view of the confocal microscope objective. The issue of flow instabilities during the oil droplet trapping was solved by the implementation of an open-close procedure of the oultets that allows the generation and trapping of the oil droplets in a single device. The stability of the flow was also enhanced by the lower flow rate of the continuous phase as well as by eliminating differences of hydrodynamic resistance of the two pathways (leading to the waste container and leading to the digestion chamber).

A systematic digestion study of 3 different oils: tricaprylin (TC), high oleic sunflower seed oil (HOSO), or fish oil was carried out in the second stage of the PhD works. Beta-carotene (BC) or retinyl palmitate (RP) was systematically added to the oils. Different digestion kinetics were obtained for the different oils. This difference was expected from the literature, in which higher lipase activities for oil with shorter FA and higher micellar solubilization capacity for shorter-chain lipolytic products (FFA, MG) result into faster lipid digestion kinetics. The results showed an increasing trend for both BC and RP concentration inside the oil droplet during triglyceride digestion. The accumulation effect of lipophilic micronutrients was due to their slower release rate compared to that of the lipolyitc products.The results

also revealed a non-linear kinetic relation between the lipid digestion and the release of micronutrients (bioaccessibility), in contrast to the linear relation usually shown in the literature due to a lack of data points. The release kinetics of both BC and RP depended on the type of oil. Slowly digested oil with long polyunsaturated fatty acid chain (fish oil) provided a higher release efficiency for BC than the quickly digested oil with medium saturated fatty acid (TC). In the case of faster lipid digestion (TC, HOSO), the BC must compete with more lipolytic products to incorporate into mixed micelles. Moreover, shorter carbon chain lipolytic products form smaller mixed micelles resulting in a decreased solubilization capacity for BC. The effect of the gastric phase added before the intestinal phase was also studied. During that gastric phase, due to the absence of bile salt, only digestion of TC oil was observed due to a sufficiently high aqueous solubility of medium carbon chain fatty acid (caprylic acid). The results revealed that the effect of the gastric phase on the intestinal phase increased with the decrease of the chain length of the fatty acid.

Intestinal juices with different compositions were also tested. Digestive juice with the bile extract yielded a faster kinetics of lipid digestion of oil with medium chain length (TC) than with the single bile salt. In addition, a low concentration of lipase resulted in a longer time needed for the saturation of the lipase concentration at the oil droplet surface. After the lipase saturated the oil droplet surface, the kinetics of lipid digestion was independent of the lipase concentration in the digestive fluid. A transfer of BC from TC oil droplet to simple bile salt or caprylic acid micelles was observed in the presence of lipase alone or bile salt alone, respectively.

The effect of the initial droplet size on the lipid digestion was also tested. The results revealed that the kinetics of lipid digestion (normalized by the surface area) is independent of the initial size of the TC oil droplets. A test with two different flow profiles of the intestinal juice revealed the adsorption of single bile salts to the PDMS device channel. The adsorption of single bile salt to the PDMS surface during the first 8 min of flow was also observed with the SAXS data. The SAXS data revealed the association of single bile salt with pancreatic enzymes. The disaggregation of pancreatic enzymes in the presence of bile salts was observed as well.

As lipid digestion is a surface dependent reaction, both the surface area and the nature of the oil-water interface are expected to affect the lipid digestion kinetics, hence the kinetics of lipophilic micronutrients solubilization as well. The surface area is influenced by the droplet size, the coalescence factor. The nature of the droplet interface is affected by surfactants, digestive juice molecules... Thus, in perspective, further works could be carried out to study the role of the coalescence process on the lipid digestion as well as on the release of

lipophilic bioactives. Physicochemical parameters such as droplet size, interfacial properties of the oil droplets (various surfactants, emulsifiers, proteins), composition of the gastrointestinal digestive juices could be further investigated with different types of oils and more lipophilic bioactive molecules.

6 ACKNOWLEDGEMENTS

This thesis is carried out at the ISD (Interfaces et Systèmes Dispersés) and Nano team research group, BIA (Biopolymères Interactions Assemblages), INRA (French National Institute for Agricultural Research), Nantes, France. First of all, I would like to express special thanks to my two supervisors, Mr. Marc ANTON and Mr. Sebastien MARZE for their all concern, instruction, advices, and as well as great patience for my thesis work during three years.

Secondly, I am deeply grateful for all the guidance and support in microfluidics from my advisor Mrs. Melanie MARQUIS.

My sincere thanks to the member of my “comité de suivi de these”, Mr. Jean-Christophe GALAS and Mr. Steven LE-FEUNTEUN for all their scientific and personal consults.

I want to thank all the members of my PhD defense jury for their time and concern, thank Mrs. Stéphanie DESCROIX and Mrs. Maud CANSELL for being the reviewers of the thesis defense, thank Mrs. Jullien MARIE-CAROLINE and Mr. Jack LEGRAND for their acceptance to be in the jury.

Furthermore, I want to thank Joelle, Alex of Nano team for their great support and helps.

Thanks to all the members of ISD team and Nano team for their support, kindness and patience during my time working here.

7 APPENDIX

1. Composition of the fish oil

EPAX 1050 TG

	moyenne	e-t		moyenne	e-t
% 14:0	0.27	0.04	% 14:0 corr	0.25	0.03
% 15:0	0.09	0.01	% 15:0 corr	0.08	0.01
% 16:0	3.19	0.10	% 16:0 corr	2.97	0.09
% 18:0	3.24	0.14	% 18:0 corr	3.07	0.14
% 20:0	0.72	0.03	% 20:0 corr	0.70	0.03
Somme	7.51				
% 16:1 n-9	0.00	0.00	% 16:1 n-9 co	0.00	0.00
% 16:1 n-7	0.83	0.01	% 16:1 n-7 co	0.78	0.01
% 17:1	0.00	0.00	% 17:1 corr	0.00	0.00
% 18:1 n-9	7.26	0.11	% 18:1 n-9 co	6.94	0.08
% 18:1 n-7	1.19	0.15	% 18:1 n-7 co	1.15	0.14
% 20:1	2.67	0.07	% 20:1 corr	2.62	0.07
somme	**11.95**		**somme**	**11.50**	
% 16:2 n-4	0.00	0.00	% 16:2 n-4 co	0.00	0.00
% 18:2 n-6	1.31	0.04	% 18:2 n-6 co	1.26	0.04
% 20:2 n-6	0.42	0.05	% 20:2 n-6 co	0.41	0.05
somme	**1.73**		**somme**	**1.67**	
% 18:3 n-6	0.00	0.00	% 18:3 n-6 co	0.00	0.00
% 18:3 n-3	0.00	0.00	% 18:3 n-3 co	0.00	0.00
somme	**0.00**		**somme**	**0.00**	
% 20:4 n-6	1.96	0.10	% 20:4 n-6 co	1.94	0.09
% 18:4 n-3	0.82	0.04	% 18:4 n-3 co	0.80	0.01
% 20:4 n-3	0.83		% 20:4 n-3 co	0.82	0.04
somme	**3.62**		**somme**	**3.56**	
% 20:5 n-3	15.29	0.09	% 20:5 n-3 co	15.36	0.09
% 22:5 n-3	3.12	0.19	% 22:5 n-3 co	3.13	0.19
somme	**18.41**		**somme**	**18.49**	
% 22:6 n-3	56.77	0.23	% 22:6 n-3 co	57.71	0.23

2. Composition of the high oleic sunflower seed oil

FA composition	%
8:0	0.00
10:0	0.00
12:0	0.00
13:0	0.00
14:0	0.05
15:0	0.02
16:0	3.77
18:0	3.19
20:0	0.00
SAT	**7.07**
14:1	0.00
16:1 n-9	0.04
16:1 n-7	0.11
18:1 n-9	85.17
18:1 n-7	0.00
20:1	0.25
22:1	0.13
MONO	**85.68**
18:2 n-6	6.92
20:2 n-6	0.22
20:3 n-6	0.00
20:4 n-6	0.00
n-6	**7.12**
18:3 n-3	0.13
20:4 n-3	0.00
20:5 n-3	0.00
22:5 n-3	0.00
22:6 n-3	0.00
n-3	**0.13**

UNIVERSITE ECOLOGIE BRETAGNE GEOSCIENCES LOIRE AGRONOMIE ALIMENTATION

UNIVERSITÉ DE NANTES

Titre : Etude de la relation entre la digestion de triglycérides et la bioaccessibilité de micronutriments lipophiles en temps réel par microfluidique à gouttes

Mots clés : triglycérides, micronutriments lipophiles, bioaccessibilité, digestion, microfluidique à gouttes, microscopie confocale de fluorescence

Résumé : Une bonne absorption des micronutriments lipophiles est importante pour maintenir la santé et prévenir certaines maladies chroniques. Cependant, leur assimilation est très variable, dépendante de facteurs liés aux aliments et à l'hôte. L'hypothèse principale de cette étude est que la cinétique de digestion des triglycérides contrôle la cinétique de bioaccessibilité des micronutriments lipophiles, étape majeure avant leur absorption. Pour tester cette hypothèse, la digestion de différents triglycérides et la solubilisation de différents micronutriments lipophiles en micelles biliaires ont été suivies simultanément in vitro en conditions intestinales et/ou gastriques. Pour contrôler finement les caractéristiques des gouttes d'huile et les conditions de digestion semi-dynamique, un dispositif microfluidique a été développé. Les cinétiques ont été suivies en temps réel par microscopie confocale de fluorescence. La diffusion des rayons X aux petits angles (SAXS) a également été utilisée pour caractériser les dynamiques de création/transformation des micelles mixtes. Les résultats de microfluidique révèlent une relation non linéaire entre la solubilisation micellaire des micronutriments et des produits de digestion des triglycérides, leur cinétique contrôlant la bioaccessibilité des micronutriments. D'autre part, l'étape gastrique influence la digestion intestinale en fonction du type de triglycérides, et induit une dégradation du micronutriment. Les résultats de SAXS ont révélé que la pancréatine change la structure du micelle biliaire. Ces résultats peuvent servir à rationaliser la formulation d'aliments pour optimiser l'absorption de micronutriments lipophiles.

Title: Studying the real-time interplay between triglyceride digestion and lipophilic micronutrient bioaccessibility using droplet microfluidics

Keywords: triglyceride, lipophilic micronutrients, bioaccessibility, digestion, droplet microfluidics, confocal fluorescence microscopy

Abstract: A high absorption of lipophilic micronutrients is important to maintain health and prevent several chronic diseases. However, their assimilation is quite variable, due to food related and host related factors. The main hypothesis of this study is that the kinetics of triglyceride digestion controls the kinetics of lipophilic micronutrient bioaccessibility, which is a major step before absorption. To test this hypothesis, the digestion of different triglyceride oils and the solubilization of different lipophilic micronutrients in bile micelles were simultaneously monitored in vitro in intestinal and/or gastric conditions. To allow a full control of the oil droplet characteristics and of the semi-dynamic digestion conditions, a droplet microfluidic device was developed. Digestion kinetics of lipids and micronutrients were monitored in real time using confocal fluorescence microscopy. In addition, small angle X-ray scattering (SAXS) was used to characterize the dynamics of creation/transformation of mixed micelles. The microfluidic results reveal a non-linear relation between the micellar solubilization of lipophilic micronutrient and of triglyceride lipolysis products, their kinetics controlling micronutrient bioaccessibility. Moreover, the gastric phase influences the intestinal digestion depending on the type of triglyceride, and induces a degradation of the micronutrient. The SAXS results reveal that pancreatin changes the structure of the bile salt micelle. These results might be applied to rationalize the formulation of foods in order to optimize the absorption of lipophilic micronutrients.